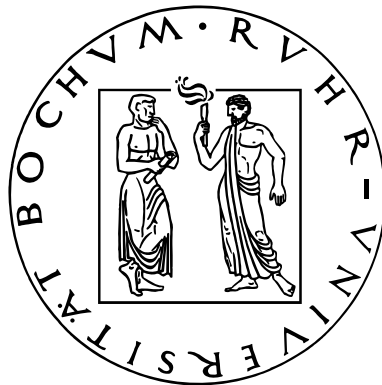# Low Surface Brightness Galaxies

and their Environments

Dissertation

zur

Erlangung des Grades
"Doktor der Naturwissenschaften"
der Fakultät für Physik und Astronomie
an der Ruhr-Universität Bochum

vorgelegt von

Dominik Rosenbaum

Bochum, Januar 2006

Contents

IV

List of Figures

List of Tables

Chapter 1

Introduction

Low Surface Brightness (LSB) galaxies produce less light per area element than High Surface Brightness (HSB) galaxies. This is caused by the fact that LSBs possess a much lower stellar surface density than HSB galaxies. Thus, these galaxies are fainter in surface brightness than those called "normal", the HSB galaxies. It is also known that LSBs are blue galaxies (e.g.: McGaugh & Bothun 1994, de Blok et al. 1995, van den Hoek et al. 2000) with low metallicities (e.g.: McGaugh 1994). Following McGaugh & Bothun (1994) and O'Neil (2000b), it can be excluded that they could be simply faded remnants of galaxies which had their starburst or their major star forming event at high redshifts. If LSBs were faded remnants of HSB galaxies, this would mean that they are very old, and were dimmed out due to the evolution of the stars which were formed during the major star forming event. Such objects would possess red colors, much redder than the known color values in LSB galaxies. It is also known since the early 80s that LSBs have ~ 2.4 times higher H I mass to light ratios than HSBs (first reported by Romanishin et al. 1982). Therefore, LSBs are believed not to be faded objects but galaxies which for unknown reasons did not form as much stars over their lifetime as HSBs.

The present dissertation examines this special class of galaxies. Since these objects are hard to detect, the realization of their presence and their importance for the cosmological understanding increased with the development in sensitivity of modern telescopes and detectors over the last two decades.

1.1   Historical Overview

Understanding galaxy formation and evolution is one of the most late-breaking fields of research in modern astrophysics. One contribution to the scenarios of galaxy formation and evolution comes from the faint end of the surface brightness distribution, namely the Low Surface Brightness galaxies. Due to their higher frequency, these galaxies play a more important role than thought some years ago.

The history of discovering LSB galaxies comes along with the struggle for understanding the selection effects of our telescopes, instruments, and the resulting surveys. Edwin Hubble

(1936) already mentioned the problems of selection effects in the search for extragalactic objects. Furthermore, he made first presumptions on these effects that absolutely faint galaxies will be detected towards much lower distances than intrinsically bright galaxies. Thus, as a consequence, faint galaxies seem to be distributed through a much smaller volume than absolutely bright galaxies. This statement forms a first naive definition of the so-called search volume, which was defined (see e.g.: McGaugh et al. 1995a) as the apparent volume corresponding to a maximum distance up to which one is able to find a galaxy of a certain surface brightness. This implies that the search volume of LSBs is smaller than that of HSBs galaxies due to selection effects. As the night sky is never dark due to scattered moonlight and light pollution produced by our rising civilization, it is hard to detect those extremely faint extragalactic objects. Additionally, the sky is illuminated by celestial objects itself like galactic stars and bright extragalactic objects. These light sources set down the contrast and make the faint end of the surface brightness distribution invisible to us especially at some regions of the sky. Furthermore, our telescopes and detectors also contribute to the bias in our observational understanding of the universe towards objects with higher surface brightnesses. This is due to the non-flatness of the image produced by non-perfect optics of the telescopes. Also noise of the detecting electronics and amplifiers contributes to the bias. In addition to the illumination of the night sky, catalogs of galaxies are usually isophotal diameter limited or magnitude limited or both.

Two years after Hubble's predictions concerning a possible existence of LSB galaxies, two of these intrinsically faint galaxies were discovered by Harlow Shapley (1938). They reported on the Local Group members Fornax and Sculptor dwarf galaxies, which are faint in total luminosity as well as in surface brightness. These two objects were considered to be exceptions in an universe which was thought to be dominated by large and luminous spiral and elliptical galaxies at that time. In the following, the possibility that the observed luminosity function was biased towards large and bright galaxies was mentioned several times (e.g.: Reaves 1956, Arp 1965). Subsequently, more and more faint objects were found. However, the opinion that galaxies populate only a very narrow range of surface brightness was kept for a long time. This culminated in the publication submitted by Freeman (1970) who found 28 of a sample of 36 spiral and S0 galaxies to form a peaked Gaussian-like surface brightness distribution. He found this distribution to have a maximum at 21.65 B-mag/arcsec^2 and a full width at half maximum of σ=0.3 B-mag/arcsec^2 (see Fig. 1.1). This seemed to be analogous to the surface brightness distribution of ellipticals which had been found before by Fish (1964). If this was true, it would imply that galaxy formation with its different conditions in gas surface density, mass, star formation history and angular momentum generally ends up in producing galaxies with a typical surface brightness. Another loophole could be, that the Freeman-sample was biased towards bright galaxies due to selection effects.

Six years later, after a continued debate on the results of Freeman, Disney (1976) discussed the selection effects as described before extensively and consulted them in order to explain the Freeman distribution. Furthermore, he also predicted a lot of galaxies of both low and (redshifted) high surface brightness type to be overwhelmed by the background brightness of the night sky. Therefore, they became invisible to us. He argued, that if we
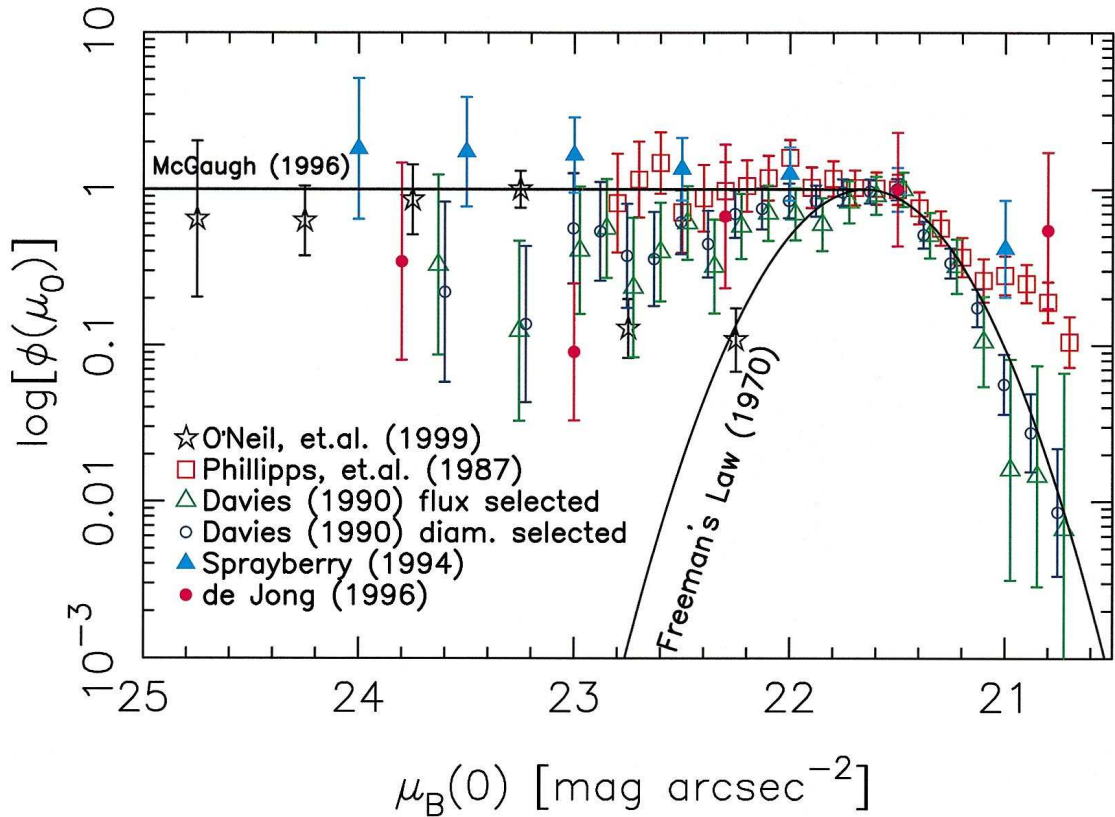
Figure 1.1: From O'Neil & Bothun (2000): Volume corrected surface brightness distribution of several data sets. Black asterisks correspond to the distribution obtained in O'Neil & Bothun (2000). The distributions found by Phillipps et al. (1987) (red squares), Davies (1990) (green triangles, black circles), Sprayberry (1994) (blue filled triangles) and de Jong (1996) (red dots) are plotted for comparison.

were living in a giant elliptical galaxy, we as optical astronomers would be blinded to most of the universe due to the surface brightness of our host galaxy. Therefore, the fact that we reside in a spiral galaxy must also have a (less dramatic) influence to the bias of what we see from the universe. These thoughts of Disney (1976) were soon proved by observational studies. Fisher & Tully (1981) published H I observations of a large galaxy sample and compared their detections to the Catalogue of Galaxies and Clusters of Galaxies (CGCG, Zwicky et al. 1968). They found that numerous LSBs fell below the magnitude cutoff in the CGCG. Later, it was realized (e.g.: Romanishin et al. 1982) and became more popular that a distinct class of LSB galaxies with different properties exists apart from the class of the normal High Surface Brightness galaxies. These HSBs were thought to form the dominant galaxy population of the universe.

In 1987 an extremely large and H I rich low surface brightness galaxy with a central disk surface brightness of $\sim 25.5\, B$-mag/arcsec^2, was discovered by chance. It shows

a prominent bulge with a central surface brightness of $\sim 20\,B$-mag/arcsec^2 and a disk
scale length of $\sim 55\,$kpc. This galaxy was found by using the technique of photographic
amplification (Malin 1978). The discoverers (Bothun et al. 1987), who christened it
Malin 1, first thought this object to be an apparent superposition of a dwarf Virgo cluster
galaxy and a background emission-line galaxy. However, this case was ruled out by H I
observations at several redshifts from the Arecibo radio telescope in Puerto Rico. It
became clear, that Malin 1 was a very extraordinary disk galaxy at redshift z=0.083
(Impey & Bothun 1989) with an extremely large LSB disk and a bulge component of
larger extent. It has a lower central surface brightness than S0 galaxies, comparable to
that of ellipticals. Furthermore, it was stated that the H I gas content is five times higher
in mass than measured in normal spirals and the gas-mass to light ratio is with a value
of $M_{H\,I}/L_B \simeq 5$ one of the highest values known overall. From their spectroscopy the
discoverers realized that Malin 1 possesses a low-level Active Galactic Nucleus (AGN).
This meant in conjunction with the presence of mostly neutral gas a conflict with the
established AGN explanations. These explanations predict Seyfert AGNs to possess a
prominent bulge, as well as spiral structure in the disk and a high H I density around the
nucleus. The prominent bulge is seen in Malin 1 but the spiral structure of the disk and
the high H I density are not present in this galaxy. Additionally, the authors claim this
galaxy to be an example of inefficient disk formation. They mention that it has a line
width and column density similar to the damped Lyman-α absorption systems discussed
by Wolfe et al. (1986). These objects are seen in the spectra of high redshift quasars
as foreground absorption and they were thought to be progenitors of present day disk
galaxies. A more detailed study of Malin 1 was then performed by Impey & Bothun (1989)
and the first results and conclusions presented by Bothun et al. (1987) were confirmed.
With the discovery of Malin 1 and the subsequently started search for Malin-like galaxies
which succeeded in the discovery of a second (Bothun et al. 1990), a third (Sprayberry
et al. 1993) and finally a whole class of so called Malin-Cousin galaxies (e.g.: Schombert
& Bothun 1988, Sprayberry et al. 1995), it became clear that LSB galaxies are not only
dwarf galaxies. Furthermore it was shown that they can also exceed the mass of the
largest HSB galaxies (see Fig. 1.4).

When calculating the search volumes of such large galaxies like Malin 1, it became clear,
that the probability to find such an object in the sky is very low due to selection effects.
Bothun et al. (1997) discussed the search volumes of LSBs with different surface bright-
nesses and scale lengths and they concluded that it is very unlikely to discover Malin 1-like
galaxies even if the universe would be overwhelmed by them. Furthermore, Impey &
Bothun (1997) stated that if one places Malin 1 at a distance from us similar to the dis-
tance to M 31, we would directly look through its disk (which would extend to 20° in
angular size at the sky) without noticing it. Hence, it became obvious that these objects
are not only individual cases and that the space density of these large, but LSB, galaxies is
not negligible (Bothun et al. 1990). Therefore, one can consider the discovery of Malin 1,
which was pure luck as Bothun et al. (1987) emphasize several times, to be a milestone in
the research field of LSB galaxies. After that, a lot of work was done in this field which

contributed to the puzzle of LSBs as well as to the understanding of galaxy formation and evolution in general. During the last 20 years, since the discovery of Malin 1, the ideas we got about LSBs have been solidified concerning the observational properties. However, the cause of the existence of such a class of galaxies with its high gas contents, but no significant past or current star formation, is still ambiguous. One important survey on LSB galaxies was performed by Impey et al. (1996). They fed the UK Schmidt survey to an automated plate scanning machine in order to search for LSBs and found a number of ~ 700 local ($z \leq 0.1$) LSB galaxies within a sky area of ~ 780 square degrees. This means that nearly one LSB per square degree can be found in the local universe. The discovered LSB sample consisted of mostly late-type spirals and most of the sample galaxies were gas rich.

Nowadays, we know that Freeman (1970) was biased due to selection effects, but our surveys today are still biased, too. Although a lot was found out about LSBs during the last two decades, we cannot fully understand the formation and evolution of galaxies and the structure of the universe, as long as we are so strongly biased towards the HSB part of the galaxy population. The intensity of this bias is not yet foreseeable. Actually, there are hints that the damped Lyman-α absorbers which are seen as foreground absorption in spectra of distant quasars might likely be LSB galaxies (e.g.: O'Neil 2002, Bowen et al. 2001, Turnshek et al. 2001). Additionally there is an actual discovery of a first H I galaxy in the Virgo cluster (named VIRGOHI21, Minchin et al. 2005) without any optical counterpart. Therefore, a broad spectrum of star formation efficiency is present in the universe which has yet to be discovered over its full range. It seems to be ranging from pure H I galaxies without stars over LSB galaxies, which might lay in between H I galaxies and HSBs, up to extremely starbursting HSB galaxies.

1.2 Properties of Low Surface Brightness Galaxies

At the beginning, the introduction of low surface brightness as a special class of galaxies was a working hypothesis. This was introduced in order to probe if LSBs are only at 1% appearance with respect to HSBs as predicted by the Freeman (1970) law, or if they exist much more frequently than thought before. This means that at the outset each working group participating in "LSB business" had its own imagination about what low surface brightness means. Therefore, one can find several definitions of low surface brightness. Different techniques to determine the central surface brightness of galaxies exist in the literature. Hence, one has to be careful when talking about LSB galaxies, in order not to mix up LSB galaxies of different definitions and to compare apples to oranges.

In the following section, the perception of LSB galaxies is defined as it is used in the present PhD thesis. Furthermore, the properties of LSBs from observations as well as from theory of galaxy formation are assorted. The section closes with the motivation for the research work this dissertation is based on.

1.2.1   Definition of Low Surface Brightness

Galaxies are known to be extended objects in a first and historical-observational definition. This is in contrast to stars which are initially point sources smeared out by atmospherical and optical effects called "seeing". For stars only the total flux within a certain bandpass (which has to be corrected for the seeing for instance by fitting point spread functions) is important, but for galaxies also the areal distribution of the flux across the objects has to be taken into account. Thus, for galaxies not only the total magnitude is an important observable, but also the flux within a certain region normalized by the area of the region. This quantity is called surface brightness. It is typically measured among several locations within the light distribution of a galaxy, which is then referred to as local surface brightness. On scales in the range of the size of the local universe, where relativistic effects can be neglected, surface brightness does not decrease with increasing distance of the objects (as it is the case for apparent magnitude). This is due to the fact that the flux f of an object scales with its distance d as $f \sim 1/d^2$ but the area A on which the object is imaged, also scales with $A \sim 1/d^2$. Since surface brightness is defined as f/A the distance is cancelled down.

On cosmological scales another effect called cosmological dimming or Tolman dimming (Tolman 1934) influences the surface brightness and sets it into a dependence on redshift z. The flux is proportional to $f \sim 1/(1+z)^4$ which means that Tolman dimming is negligible small for nearby galaxies and the local universe ($z \lesssim 0.1$), but for higher redshifts its influence increases rapidly. For example, galaxies with a redshift of $z = 0.2$ are dimmed by 0.8 mag, those with a redshift of z=2 by 4.7 mag. This corresponds to a factor of $\simeq 1/50$ in linear flux between these two redshift examples.

LSB galaxies are galaxies with a central, cosmological undimmed surface brightness $\mu(r = 0) =: \mu(0)$ fainter than a certain value several sigma beyond the Freeman (1970) value $\mu(0) = 21.6 \pm 0.3 \, \text{mag/arcsec}^2$ (in Johnson-B filter, henceforth indicated with B). In this equation r is the radius along the the major axis of the galaxy. Since this is at first a working hypothesis for the distinction of two classes of galaxies, HSB and LSB, the border where low surface brightness begins varies in literature from $\mu_B(0)$=22.0 mag/arcsec^2 (e.g.: McGaugh et al. 1995a, i.e. 1.33σ beyond the Freeman value) up to $\mu_B(0)$=23.0 mag/arcsec^2 (as used for instance in Impey & Bothun 1997, i.e. 4.66σ beyond the Freeman value). One possible value for the border between LSBs and HSBs is $\mu_B(0)$=22.5 mag/arcsec^2 (e.g.: used in de Blok et al. 1995, Morshidi-Esslinger et al. 1999, Meusinger et al. 1999, Rosenbaum & Bomans 2004). This value lies 3σ beyond the Freeman value.

Several techniques measuring the surface brightness can be found in literature. One possibility is to measure the azimuthally symmetric radial surface brightness profile in dependence on the effective radius of the annuli over which the surface brightness was averaged. Although the light distribution in galaxies is not completely described by such profiles, it is reasonably approximated by them (McGaugh et al. 1995a). Another technique is to measure the average surface brightness within areas along isophotes.

The measured surface brightness profiles of most LSB galaxies are well fitted by an exponential law (e.g.: Davies et al. 1990, McGaugh & Bothun 1994, McGaugh et al. 1995a,

Dalcanton et al. 1997a):

$$\mu(r) \;=\; \mu(0) + 1.086 \cdot \frac{r}{\alpha_l} \qquad\qquad (1.1)$$

with $\mu(r)$ the surface brightness, r the radius of the galaxy, $\mu(0)$ the central surface brightness and α_l its scale length. O'Neil et al. (1997a) examined 127 LSB disks of a central surface brightness of $\mu_B(0) \geq 22.0\,\mathrm{mag/arcsec^2}$ in the Cancer and Pegasus cluster. They found that 80% of the sample galaxies could be well fitted by exponential radial surface brightness profiles, whereas 17% were best fitted by King (1962) profiles, and 3% could not be fitted by either model.

1.2.2 Known Properties from Observations

Since the surface brightness distribution derived by Freeman (1970) was known to be biased at the faint end due to selection effects, it soon became clear that LSBs are not only a phenomenon which appears with an relative frequency of less than 2% (which would be the probability corresponding to 2σ of the Freeman distribution). A lot of work on the number density of the faint end surface brightness distribution was done (e.g. by: McGaugh et al. 1995a, Dalcanton et al. 1997a, O'Neil & Bothun 2000, O'Neil et al. 2003, see also Fig. 1.1). This was performed in order to disprove the opinion that the number density of the LSB phenomenon was negligible small, which was still but sporadic present until the mid 90s (e.g.: Roukema & Peterson 1995). After that, these objects were taken seriously by the general community and an enormous progress in the research field on LSBs occurred and is still going on. The properties of this special class of galaxies were studied in detail over the last 20 years and a lot of differences were found compared to HSBs.

As mentioned before, LSB galaxies are not only dwarf galaxies, but their extent can also reach dimensions of large HSB spirals and even exceed them. For example, Malin 1 is the largest galaxy known in the universe with regard to the scale length. The discovery of more Malin 1-like giant LSBs (Schombert & Bothun 1988, Sprayberry et al. 1995) proved that this special galaxy is not an extraordinary phenomenon, but a more common event than expected. Schombert et al. (1992) compared the morphology of their LSB galaxy sample obtained from a visual search of the Second Palomar Sky Survey (Reid et al. 1991) and from the Virgo Galaxy Catalog (Sandage & Binggeli 1984) to the Upsalla Galaxy Catalog (UGC, Nilson 1973). LSB galaxies were found to be distributed over all Hubble types (Fig. 1.2, see also Fig. 1.4) with a slight tendency to appear more frequently at later types. This tendency is also found by McGaugh et al. (1995b). These facts support the importance of LSBs for our understanding of galaxy formation and evolution, since low surface brightness plays a role in all morphological types of galaxies. Especially the nature of the large, Malin-like LSB galaxies remains enigmatic for the following reasons:

Large, Malin-like LSB galaxies are gas rich in general. Pickering et al. (1997) examined four giant LSB galaxies in H I and found that the total gas mass of each object amounts of $\sim 10^{10}\,\mathrm{M_\odot}$. Evidence for a large amount in total mass of neutral hydrogen is also found for instance by Matthews et al. (2001a), O'Neil (2002), and O'Neil et al. (2004). McGaugh &
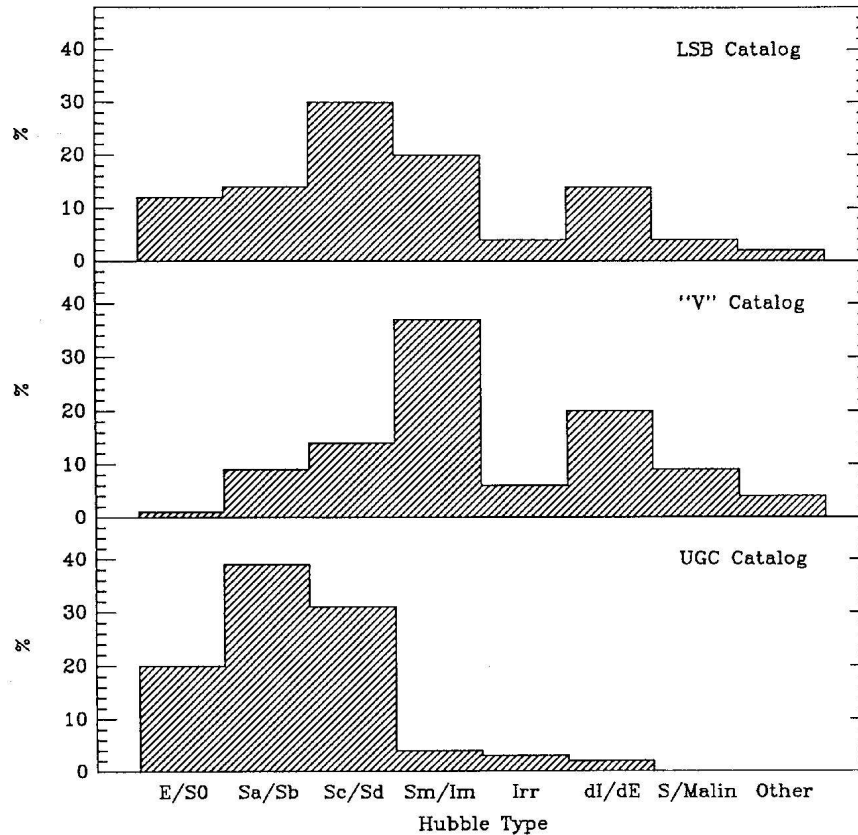
Figure 1.2: From Schombert et al. (1992): The Figure shows the distribution of the sample LSB galaxies over Hubble types. It was found by a visual search based on the Second Palomar Sky Survey (Reid et al. 1991) (top panel) and in the Virgo catalog compiled by Sandage & Binggeli (1984) (middle panel). The LSB catalog is dominated by late type galaxies. This is due to the fact that the catalog is diameter limited. Hence, there is a selection against elliptical galaxies, which possess steep profiles. The authors state that only a handful of ellipticals are in the catalog due to the diameter limit, and only these ellipticals which are surrounded by faint halos were selected. Further on, they report that 14% of the sample objects are early type spirals and the majority of LSBs falls into the Sc, Sm and Im Hubble classes. By comparing the LSB sample to the galaxy distribution in the UGC (bottom panel) one can see, as the authors claim, that the mean type found in the LSB search is considerably a later Hubble type. One can conclude from this study that LSB galaxies are found in all Hubble types.

de Blok (1997) examined the gas mass fraction of spiral galaxies in the context of surface brightness. They found this fraction to be significantly higher in LSB spirals than in HSB disks. The gas mass fraction is defined as $f_g = M_g/(M_g + M_*)$ (with M_g the total gas mass and M_* that in stars). It describes the fraction of gas mass which is not yet converted into
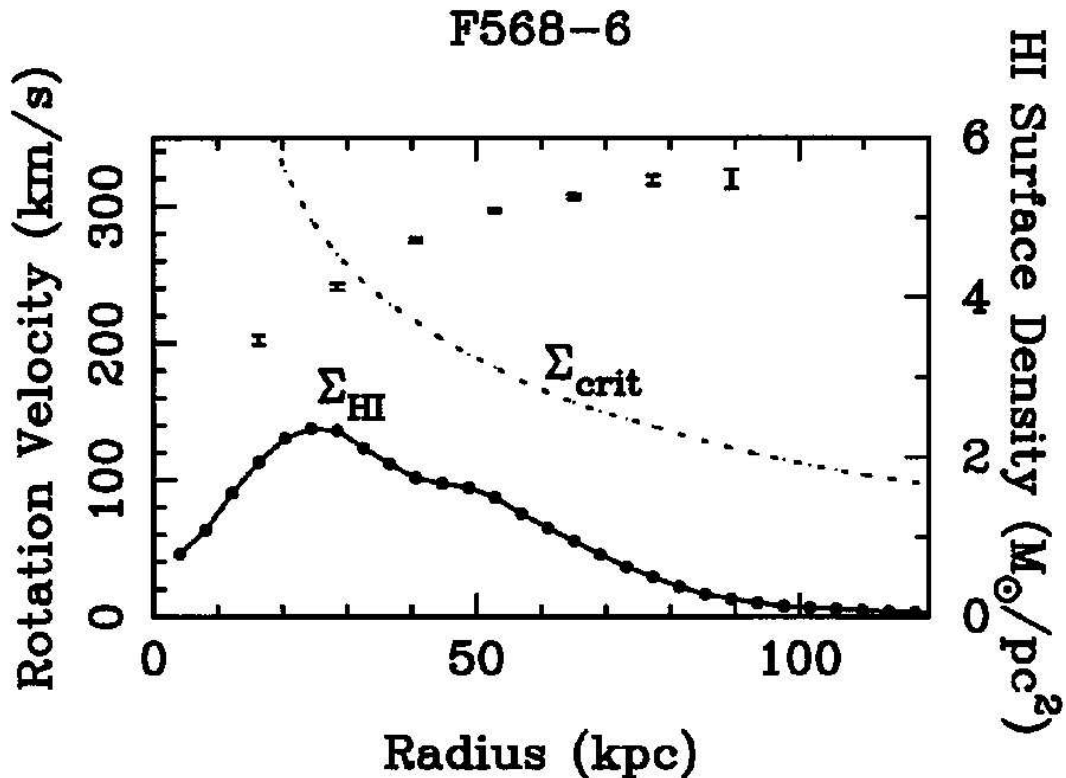
Figure 1.3: From Pickering et al. (1997): The rotation curve of Malin 2 (left scale, dots with error bars) and the HI surface density (right scale, dots connected with line) are drawn against the radius along the major axis. The dashed line shows the critical surface density for the formation of star forming giant molecular clouds (Kennicutt (1989) criterion). Note that the HI surface density stays below this critical value at all radii. The rotation curve is typical for a Dark Matter dominated galaxy, since it does not show a maximum in the inner few ten pc and increases also at higher radii.

stars. This also contributes to the image of LSB galaxies being equipped with enough gas to form as much stars as HSBs, but they did not. One important clue to the nature of such LSB galaxies is the fact that the gas surface density of these LSBs is generally low in comparison to HSBs. As found by Pickering et al. (1997), the surface density of the large LSBs of their sample is systematically below the critical density for the formation of molecular, star forming clouds (see also Fig. 1.3). This critical density is known as the Kennicutt (1989) criterion.

Large LSBs are thought to produce less stars than HSB galaxies due to this low gas surface density. Thus, the key to the understanding of these LSB galaxies rests in the answer to the question what kept the surface density to stay below this critical value. One

clue to this question comes from studies of the environment. If LSBs would have no galaxy neighbours on small and intermediate scales, this absence of a gravitational trigger could keep the gas to stay in a stationary situation. This mode would be without much turbulence and hence without density perturbations which cause gas clouds to collapse and to initiate sufficient star formation (see also section 1.4). A lack of nearby neighbours on small scales below 2 Mpc is seen by Bothun et al. (1993), who examined the spatial distribution of LSB galaxies in the Center for Astrophysics redshift survey (CfA, Huchra et al. 1993). They performed galaxy number countings within cones of a mean projected radius of 0.5 Mpc and a velocity range of $500 \, \mathrm{km s^{-1}}$. These results were validated by Mo et al. (1994) who studied the spatial distribution of LSBs by calculating the cross correlation functions of LSBs with HSBs of the CfA and IRAS sample (Rowan-Robinson et al. 1991). The fact, that nearby ($r \leq 0.5$ Mpc) companions of LSB galaxies are missing was also detected by Zaritsky & Lorrimer (1993). The idea, that a lack of tidal interaction in LSB disks causes a suppression of star formation and keeps the system static, fits also to the results of theoretical models of tidally triggered galaxy formation (e.g.: Lacey & Silk 1991).

Another hint to the theory of LSB galaxies growing up in a less dense environment than HSB galaxies comes from color and metallicity studies. Most LSBs are found to be blue. Their $(B - V)$ color index shows an average value of $(B - V) \simeq 0.44$ mag (McGaugh 1994, Romanishin et al. 1983). This is not an effect of the initial mass function (IMF) of LSBs. The idea of galaxies having a smaller amount of massive ($M > 60 M_\odot$) (red) stars or a higher amount of low mass (blue) stars than HSBs, which means a bottom heavy IMF, is known to be not the only possible explanation (Lee et al. 2004). They performed stellar population synthesis modelling on seven LSBs of the sample of LSB galaxies obtained from Fuchs (2002). They found the IMF to be steep with a power law index of $\alpha = 3.85$ (the Salpeter (1955) value is $\alpha = 2.35$). This could explain the high mass to light ratio and the blue colors. However, from their modelling followed that not only the IMF but also a rather recent star formation could be responsible for it. If it is not caused by the IMF, this would imply that the blue color of LSBs can be due to a lower metallicity or a younger age or both. Indeed, the metallicity in LSBs is found to be low ($Z < \frac{1}{3} Z_\odot$, McGaugh 1994). However, it seems to be rather an effect of age of the dominant stellar population (Haberzettl 2005) than an effect of metallicity, since there is no correlation between the oxygen abundance and the color of the galaxies (McGaugh 1994). Moreover, Pickering & Impey (1995) found most of the Malin-like LSBs of a sample of 10 objects to possess metallicities of $Z = Z_\odot$. Zackrisson et al. (2005) found the age determination of LSBs by fitting stellar population synthesis to spectra of LSBs to be still uncertain. Therefore, the origin of LSBs is still an open question.

As galaxy formation first took place in the overdense regions of the initial universe and later in the less dense areas, the hint that the dominant stellar population in LSBs seems to be generally younger than the one in HSBs also fits to a scenario in which LSBs were formed in low density regions. By the way, there exists a class of remarkable red LSBs with $(B - V > 1)$ (O'Neil et al. 1997b, O'Neil 2000a, 2001) that seems to have another formation and evolution history than the blue ones. LSB galaxies are also known to have a small amount of molecular gas, low CO abundances and low dust contents (e.g.: Matthews &

Wood 2001, Matthews et al. 2001b). First trials to detect CO in LSBs during the 90s were unsuccessful (Schombert et al. 1990, Knezek 1993, de Blok & van der Hulst 1998, Braine et al. 2000). First, CO was successfully detected in edge-on LSB systems (Matthews & Gao 2001) and later in a red LSB galaxy (O'Neil et al. 2000). However, the latter one was doubted by Cabanela et al. (2001) who claimed a non-detection on that object.

A very important issue are the rotation curves of LSBs which are Dark Matter dominated not only at radii of the outer disk like it is the case for HSB disk galaxies but also in the inward radii. Hence, LSB galaxies show generally very flat rotation curves. This can be seen in the diagram in Figure 1.3, where the rotation velocity of the LSB galaxy 586-6 (also known as Malin 2) is plotted versus the radius (points with error bars). The rotation curves of LSBs were studied in detail for instance by Bothun et al. (1997), de Blok & McGaugh (1997), McGaugh et al. (2001), de Blok et al. (2001) and de Blok & Bosma (2002). The latter two studies established the observational fact that the mass density profiles of LSBs show a steep decreasing outer slope and a more shallow inner component. These profiles are called core profiles, whereas profiles without a nearly constant inner component are called cusps. In de Blok & Bosma (2002), high resolution spectra of a total of 26 LSB galaxies were examined and it was concluded that most LSB galaxies show a core mass-density profile. This contradicts the current Cold Dark Matter (CDM) simulations which generally predict those galaxies to possess a cusp mass-density profile (Navarro et al. 1996). Similar observational results were also found for instance by Swaters et al. (2004) based on H I and Hα long-slit observations. In McGaugh et al. (2003) the consequences of these observational facts are discussed, since there is a discrepancy with common CDM cosmology theory, which comes from structure formation simulations and predicts the density profiles of Dark Matter halos to be generally cuspy (e.g.: Navarro et al. 1996, 1997).

1.2.3 Theoretical Clues to LSBs

As described before, a discrepancy between theory and observational constraints on LSB galaxies is found concerning their Dark Matter halos (see also de Blok 2004). This is the object of an extensive debate today, since the importance of LSB galaxies to the total galaxy population is increased due to the awareness that we still miss a lot of LSBs in our surveys caused by selection effects and that the real amount of LSBs is higher (e.g.: O'Neil & Bothun 2000, see also Fig. 1.1). There is another discrepancy between theory and observational issues. Some observations imply, that LSBs are more isolated on scales below 2 Mpc. It is argued that the LSB phenomenon is due to the low galaxy density in the environment of LSBs (see subsection 1.2.2). However, some possible constraints on the nature of LSB galaxies come from simulations of disk galaxy formation scenarios (e.g.: Dalcanton et al. 1997b, Boissier et al. 2003). In these simulations, the dark matter halos of LSB disks were found to have a higher spin parameter than that of HSB spirals. The spin parameter λ is a dimensionless quantity defined as $\lambda = J_{tot}|E|^{1/2}G^{-1}M^{-5/2}$, with total angular momentum J_{tot}, system energy —E—, mass M, and gravitational constant G (Peebles 1969, Dalcanton et al. 1997b). In the study by Boissier et al. (2003) the

spin parameter of LSBs with $\mu_B(0) > 22.0\,\mathrm{mag/arcsec^2}$ exceeded values of $\lambda = 0.06$. The higher spin parameter of the LSB Dark Matter halos implies that more angular momentum is contained in the disk which naturally results in higher scale lengths of LSB disks. This means that the total amount of gas (which is similar in mass to that of HSBs) is distributed on larger scale lengths than in HSBs. This scenario would explain the low gas surface densities, which cause the galaxies to be LSBs due to the nature of their dark matter halos and stays in competition with the scenario that LSBs formed in low density environments. Hence, the question remains if LSB galaxies result from nature or nurture.

The study by Boissier et al. (2003) also found hints that the dark matter halos of LSB galaxies are less dense than the halos of their HSB counterparts. This is also seen by Bailin et al. (2005), who found the concentration index of the Dark Matter halos and the spin factors to be anti-correlated. This results in higher spin factors and lower concentration indices for LSB Dark Matter halos than in halos of HSBs. Avila-Reese et al. (2005) analyzed the properties of galaxy-size dark halos of void, field and cluster environments in their ΛCDM cosmological N-body simulations. They found halos in clusters to have a median spin parameter ~ 1.3 times lower, a minor-to-major axial ratio ~ 1.2 times lower (more spherical), and less aligned internal angular momentum than halos in voids and the field. With the obtained halo parameters, they calculated semi-numerical models of disk galaxy evolution. These simulations result in the trends that the disk galaxies which formed in low-λ and highly concentrated halos, with a gas infall history truncated early (cluster environment), are preferentially of earlier morphological types. Furthermore they are redder, have higher surface brightnesses, smaller scale lengths, and lower gas fractions than disk galaxies formed in high-λ and low-concentration halos (void environment). Given this is true, it proves possible to unite observational results and theoretical predictions of ΛCDM theory for the formation of LSBs. Therefore, one may assume the higher spin factor of LSB Dark Matter halos to be due to a possible lower density in the vicinity of these galaxies. Presumed that, LSBs grew up in a low density environment, their low surface brightness may be due to a combination of nature and nurture.

1.3   LSB Galaxies and Active Galactic Nuclei Activity

LSBs are not thought to be common Active Galactic Nuclei (AGN) hosts, because they generally possess low gas surface densities, a weak spiral structure, and mostly small or absent bulges. Thus, only a few references to this topic exist in literature. Analyzing the spectra of Malin 1, Bothun et al. (1987) and Impey & Bothun (1989) found low-level AGN activity in this giant LSB galaxy. The emission lines turned out to be typical for a Seyfert 1 galaxy, although the steep Balmer gradient and the large $H\alpha/H\beta$ are more typical for a broad line radio galaxy than a Seyfert galaxy. The puniness of the AGN is ascribed to a low feeding rate. Other giant LSB galaxies also show evidence for AGN activity. In Malin 2 and 1226+0105 also weak AGNs of type Seyfert 1 (Bothun et al. 1990, Sprayberry et al. 1993) are seen. Sprayberry et al. (1995) found AGN activity within three of a sample of eight giant LSBs (including 1226+0105), two of them of type Seyfert 1

and one Seyfert 2. From this low number statistics (including Malin 1 and 2) the authors tentatively conclude that AGNs are actually more common in giant LSB disk galaxies than in higher surface brightness disk galaxies. These results were confirmed by a systematic study of AGN activity in giant LSBs performed by Schombert (1998). He performed a spectroscopic survey of nuclei of 34 giant LSBs and 9 giant HSBs and found out, that 17 out of 34 LSBs have active cores. By comparing the results to those of HSBs, which have completely different global disk properties (like current and past SFR, disk kinematics, their morphological appearance, mass-to-light and gas ratios etc.), he concluded that the AGN mechanism is decoupled from the disk properties of a galaxy. The conformity found between these two classes of objects were bulges. 17 of 32 bulges (both LSB and HSB) galaxies showed AGN activity (55%), but the fraction of AGNs without bulges was 3 of 11 (27%). Similar results were also found by Knezek & Schombert (1993).

A relation exists between the mass of the central black hole of an AGN and the luminosity of its bulge (Magorrian et al. 1998). With increasing bulge luminosity the black hole mass also increases. Another important relation is the connection between the stellar velocity dispersion within the half light radius and the black hole mass (Gebhardt et al. 2000). These relations have not yet been applied to AGNs in LSBs. This application could give important clues to the understanding of LSB AGNs. Although the AGN activity in LSBs as well as in HSBs seems to be strongly related to the presence of a bulge, the exact AGN feeding mechanisms in LSBs still remain enigmatic due to their low gas and star surface densities.

1.4 Motivation for the present Dissertation

Beside the theoretical formation scenario concerning the higher spin parameters of the Dark Matter halos of Low Surface Brightness galaxies (section 1.2.3), there exists another possible formation scenario, also supported by observational evidence. This scenario describes that LSB galaxies were formed in low density regions of the universe (e.g.: Bothun et al. 1997, Rosenbaum & Bomans 2004), where they evolved very quietly and undisturbed due to the absence of neighbouring galaxies or nearby companions. Hence, no perturbation of the potential trapping the gas occurred by tidal forces due to close neighbours. Therefore, no starbursts which would have gradually brightened their disks, could have been initiated and their gas density remained at low surface density. Also the infall of massive gas clouds, which could have disturbed the potential and could have initiated sufficient star formation, was improbable at such low density locations. As mentioned above, studies on the environment of LSB galaxies were done before by Bothun et al. (1993) and Mo et al. (1994), but no examinations on larger scales (>2 Mpc) exist. Thus, it is known that LSB galaxies have less neighbours on scales below 2 Mpc. Therefore, the theory of these galaxies being LSBs due to the absence of tidal triggers could be true. However, no conclusions of the location of LSBs in the context of the Large Scale Structure (LSS) can be drawn, since structure formation takes place on larger scales.

For the present dissertation the properties of the SDSS survey as a catalog for LSB

galaxies were explored. After that, the galaxy density in the environment of LSB galaxies was examined on scales beyond 2 Mpc, which had not been studied before. Additionally, the results obtained for the clustering properties of LSBs on scales below 2 Mpc (e.g.: Zaritsky & Lorrimer 1993, Bothun et al. 1993) were checked. The aim of this part of the thesis is to verify or falsify the formation scenario of LSBs as described in the paragraph before. The verification of this scenario will not only contribute to the understanding of the formation and evolution of LSB galaxies, but also give clues to the structure formation in the universe also at the bright end of the luminosity distribution.

In addition, an uncommon phenomenon in LSB galaxies, the AGN activity in LSB galaxies is studied. As said before, these galaxies are not expected to be good candidates for hosting AGNs. Nevertheless, a few studies in literature found some LSB galaxies showing weak AGN activity. Using the spectroscopic data of the SDSS public releases it was planned to search for AGN candidates (using emission line diagnostic diagrams following Osterbrock 1989) within the LSB sample compiled for the environment studies. The primary purpose is to find out how common the AGN phenomenon really is in LSB galaxies. Additionally, the examination of structural properties like surface brightness, bulge luminosity, color, and emission line fluxes as well as a comparison of the sample to AGNs in HSBs was intended. From that we will learn a lot about black hole masses and their feeding mechanisms in AGNs, which are hosted by LSB galaxies. Finally, the AGN study is set into a context of the environment studies in order to look for a possible link between AGN activity and galaxy density environment of LSBs which host AGNs.

The present dissertation is organized as follows. In Chapter 2 the characteristics of the dataset public released in different stages of the Sloan Digital Sky Survey (SDSS) are shown, which is the basic data set for this dissertation, as well as for the environment studies and the search for AGN activity of LSB galaxies. Chapter 3 deals with the selection function of the SDSS spectroscopic main galaxy sample. It probes the properties of the SDSS as a LSB survey. Furthermore, the selection effects have to be examined in order to understand its influences on the results concerning the environment studies, which are presented in Chapter 4. A project aiming on measuring the current star formation rate of LSB galaxies in different environments and its preliminary results are presented in Chapter 5.2. The results of the search for AGN activity in LSBs can be found in Chapter 6. In Chapter 7, all results are discussed and put into a context to existing results from literature. Chapter 8 gives a brief summary, whereas in Chapter 9 the work still ahead is listed in an outlook.
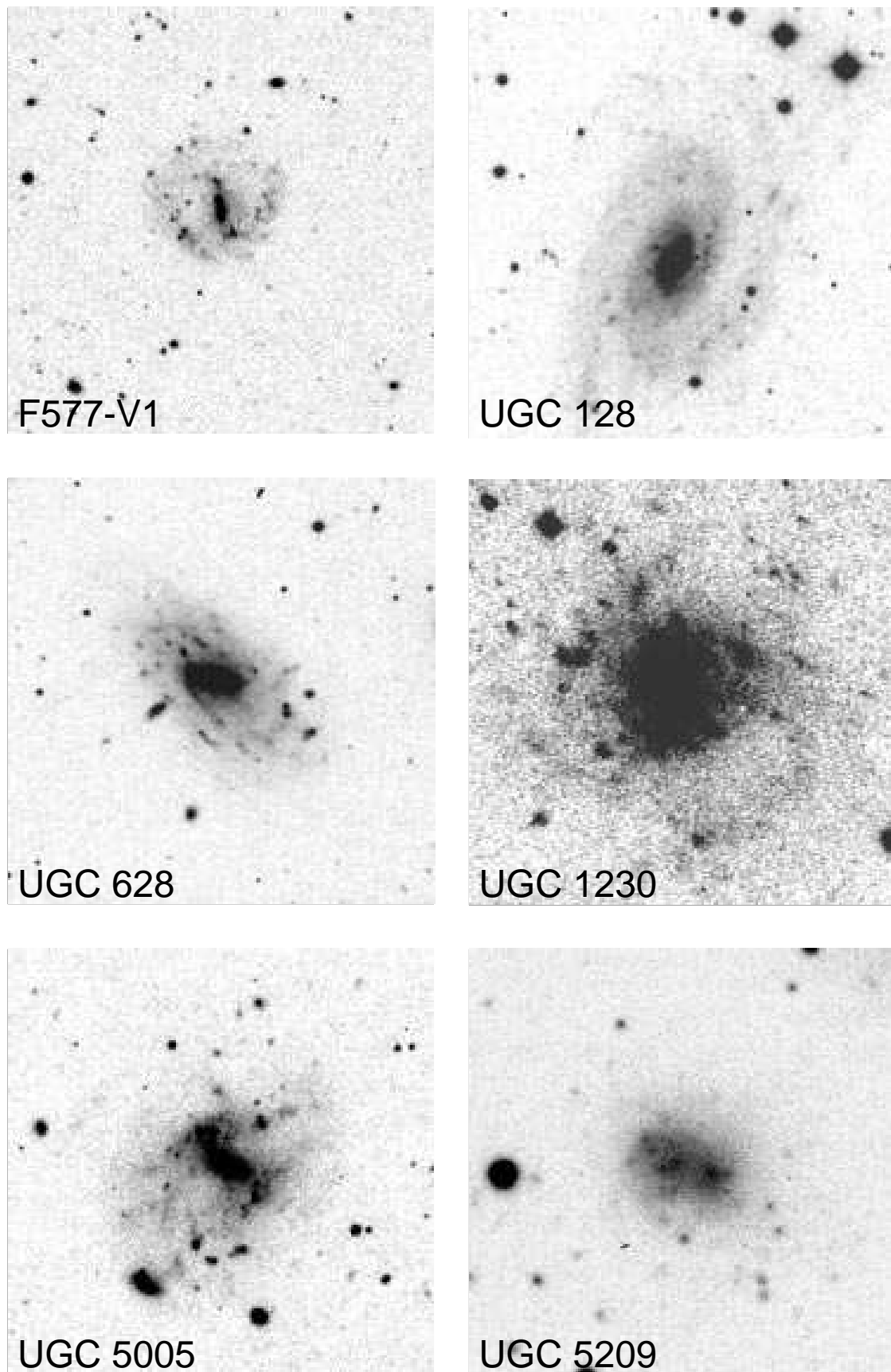
Figure 1.4: From de Blok et al. (1995): R-images of six typical Low Surface Brightness galaxies. The size of each image is $2.3' \times 2.3'$. North is at the right, east is at the top.

Chapter 2

Characteristics of the Sloan Digital Sky Survey

In this Chapter the characteristic properties of the data set collected in the Sloan Digital Sky Survey are presented. Moreover, the technical features of the survey telescope and its imaging camera and spectrographs are summarized. Finally, the different Public Releases of the Sloan Digital Sky Survey are introduced and described in detail.

2.1 The Sloan Digital Sky Survey

The Sloan Digital Sky Survey (SDSS, York et al. 2000) is an imaging and spectroscopic survey which is planned to cover approximately one quarter of the whole sky. The survey area of around 10,000 deg^2 is mainly distributed in the North Galactic Cap. Additionally, three stripes are located in the South Galactic Cap.

The emphasis in scientific goals is placed on galaxies and quasars. The standard operations for surveying have started in April 2000 and were finished during summer 2005. With the completion of the survey, it has collected spectra of $\sim 10^6$ galaxies, $\sim 100,000$ quasars and $\sim 30,000$ stars.

The survey uses a f/5 telescope of 2.5 m main mirror diameter with a wide field optimized Ritchey-Chrétien optical design (Waddell et al. 1998). The diameter of the secondary mirror is 1.08 m, and it provides an obscuration of 27% of the incoming beam to the f/2.25 primary mirror. The central hole in the primary mirror is 1.17 m in diameter. The telescope is located at the Apache Point Observatory in the Sacramento Mountains near Sunspot, New Mexico (see also Fig. 2.1). The geographical coordinates of the telescope are ϕ=32°46' 50" N and λ=105°49' 12" W. Its elevation is 2788 m. The telescope is enclosed by a removable hut and it is not mounted within a dome in order to avoid aggravation of the seeing due to dome seeing effects. Since the telescope is completely exposed to the wind and light sources, a sophisticated wind and light baffle, consisting of an outer and an inner baffle, was necessarily mounted onto the telescope using a self-supporting architecture.

Figure 2.1: The image shows a view of the SDSS telescope site, the Apache Point Observatory, New Mexico / USA (from www.sdss.org). On the left one can see the 2.5 m SDSS telescope with its removable hut. The light path of the telescope is covered by a wind and light baffle. Near the hut in the foreground, the dome of the photometric telescope is imaged. In the background, the 3.5 m telescope of the Astrophysical Research Consortium can be seen.

The inner light blind baffles both the primary and secondary mirror.

The telescope is pivoted using an altitude-azimuth mounting and its optical design is of a scale and focal ratio which is well adapted to both the size of fibers for a multi-fiber spectrograph and the pixel scale of available large-format CCDs for a time-delay-and-integrate (TDI) imaging survey (Waddell et al. 1998). In the imaging runs, telescope and camera operate in the drift scan (also called TDI) mode. In this mode, the celestial image drifts over the camera due to the telluric rotation, since the telescope is not tracking a fixed sky position. Due to the altitude-azimuth mounting, the rotation of the field of view of the camera has to be compensated depending on which location of the sky the telescope points. Therefore, the camera is pivoted at the telescope and is spinned by a de-rotation

unit before scans so that the alignment of the CCD chips is perpendicular to the drift scan direction. Since the telescope is not tracking during exposures due to TDI mode, the de-rotation device does not rotate the camera while performing drift scans. However, in spectroscopic mode, the de-rotation device is used during exposures because the telescope is tracking in this specific mode.

Two instruments are used at this telescope. For the imaging mode a complex camera containing 30 charge-coupled devices (CCDs) of $2\,k\times2\,k$ SITe/Tektronix chips with a pixel size of $24\,\mu$m (which corresponds to an angular size of 0.396") is mounted onto the telescope. Additionally, the device possesses a set of 22 astrometric CCDs. With this camera it is possible to obtain images nearly simultaneously in the modified Gunn-bandpasses u, g, r, i, z (the photometric system is described in detail by Fukugita et al. 1996) in drift scan mode (see also Fig. 2.2).

Due to this special operation mode and the architecture of the CCD camera, one gets exposure times of around $54\,$s in each filter. The field size is $2.5°$ in elevation, in azimuth it is limited to the duration of the scan (usually $15°$). The photometric calibration to the images is done using an auxiliary $0.5\,$m so called Photometric Telescope (PT) which is located near the survey telescope. The flux calibration is performed using standard-star fields at $15°$ intervals along the different scans. Thereby, the atmospheric extinction is determined using the PT. In photometric moonless nights with good seeing conditions imaging is performed, whereas nights with suboptimal conditions are used for spectroscopic operations.

For spectroscopy a pair of two channel fiber optics spectrographs, which are able to take spectra of 640 objects simultaneously, is operated at the survey telescope. Each spectrograph possesses 320 fibers and two channels, one red covering the wavelength range of 5800-9200 $\mathring{A}$ and the other one blue with a coverage of 3800-6150 $\mathring{A}$. This wavelength range is divided between two cameras by a dichroic at $\lambda \simeq 6150\mathring{A}$. Thus, there are four CCD chips of the same type as used in the imaging camera.

The spectrographs provide a typical resolution of $\lambda/\Delta\lambda \simeq 1800$, which translates to a value of $167\,$km/s in velocity resolution. The pixel size in velocity space is $69\,$km/s. The fiber diameter corresponds to an angular size of 3". Spectroscopy is undertaken with guided exposures of overlapping tiles which are called plates. Each plate has a projected diameter of $3°$. All spectroscopic fields are obtained with a total integration time of 45 minutes and more, distributed uniformly over at least three exposures. This results in a signal-to-noise ratio of $(S/N)^2$=4.5 pixel^{-1} for an object with a magnitude of 20.2 in the g band. Additionally to the spectroscopic science frames, a smear image of 4 minutes integration time is taken, at which the telescope is moved. The effective aperture which is then covered by the fiber contains 5"$\times$8", aligned with the parallactic angle. With this exposure, the light of the objects, which is excluded from the fiber due to the seeing and atmospheric refracture, is covered. Thus, a more accurate flux calibration is possible.

A series of interlocking pipeline tasks processes the data automatically. Routines for astrometric and photometric calibrations, detection of the objects, measuring of their properties, and the selection of the objects for the spectroscopic follow up observations are the main
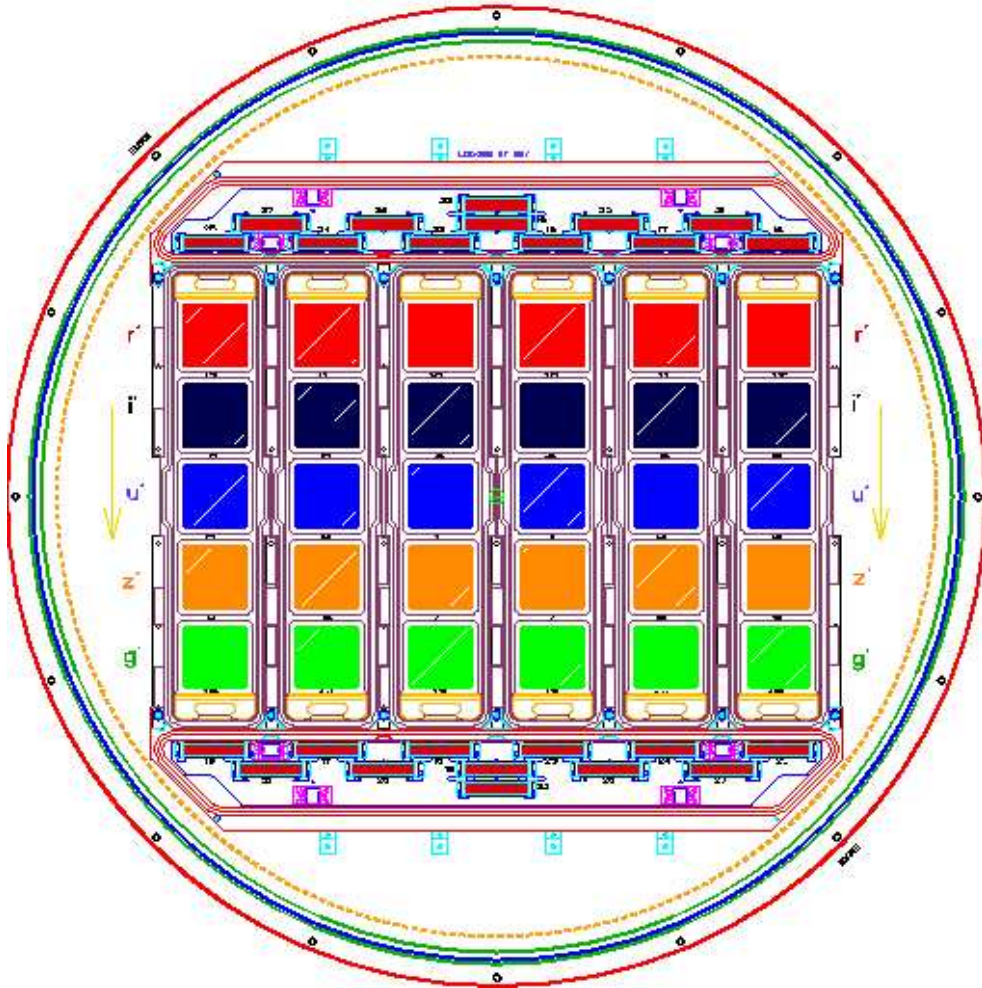
Figure 2.2: The field of the SDSS Camera from Gunn et al. (1998). The photometric CCDs are arranged in six identical columns of five 2048×2048 chips, each with one of the five primary filter bands u, g, r, i, z. The yellow arrows beside the CCD columns indicate the drift scan direction. Leading and trailing these columns are arrays of twelve 2048×400 chips for astrometric calibration and focussing purposes. One stripe of the survey is composed of two "time-delay and integrate" drift scans, each one centered on different columns.

tasks of the pipeline. Furthermore, the reduction of the spectroscopic data is also performed automatically by the pipeline including the measurements of the emission and absorption lines of each object, the correlations with other line measurements or template spectra and the determination of the redshifts. Since the characteristic properties of the pipeline vary a bit between the different public releases due to developments and improvements, a detailed description of the pipeline is given in the following sections concerning the specific data releases.

2.2 The Public Releases of the SDSS

The data of the SDSS are published in several steps to the general astronomical community, each step timely separated by about one year from the others. Each outcoming data release contains a larger covering area, some bug fixes and other improvements compared to its antecessor. However, each subsequent release has incorporated all the data included in the predecessor, but this subset data was reprocessed by the new version of the pipeline.

2.2.1 The Early Data Release of the SDSS

In June 2001, the SDSS consortium released a preliminary data set to the public community. The so called Early Data Release (EDR, Stoughton et al. 2002) of the SDSS covers $462 \, \deg^2$ of imaging data and 54,000 spectra mainly from scans in two equatorial stripes and from two regions off the equator, which have an overlap with the formerly called SIRTF (now Spitzer) First Look Survey (Condon et al. 2003). Since the data of the EDR were taken during commissioning runs, which were performed for hardware and software evaluation, not necessarily all of the scientific requirements concerning the image quality, target selection or photometric calibration, were satisfied.

The data containing imaging and spectroscopic frames from the 2.5 m telescope and photometric data from the PT are transferred from the Apache Point Observatory to Fermilab for reduction and calibration. Before processing, the drift scan data of each photometric CCD is broken into several frames containing 1361 lines. Then the 128 rows of the next frame are added onto the top of each frame, so that the input image size for the pipelines is 2048×1489 pixels. The line overlap of 128 pixels is exactly the same as the column overlap of two contiguous scans.

Imaging data are processed by the following pipelines. The astrometric pipeline corrects the pixel coordinates for the optical distorsion terms and astrometric solutions are calculated. Therefore, stars detected on the photometric CCDs in the r band are cross-linked to the positions of stars in the USNO CCD Astrograph Catalog (Zacharias et al. 2000). If this catalog does not cover the actual SDSS strip, bright stars detected with the astrometric CCDs are matched with the Tycho-2 Catalogue (Høg et al. 2000). With the matchings from the r band, a secondary catalog is produced in order to calculate the affine transformations in the u, g, i, z bands. Corrections for differential chromatic refraction are included, as soon as the colors of the object are known. The astrometric accuracy lies in the range of below 0.1" down to 0.02".

The Point Spread Function (PSF) and its behaviour in dependence of time and image location is measured by the postage-stamp pipeline. Additionally, this pipeline calculates a global sky for the field, the flat-field vector, and the bias level which are subtracted.

After that, the determined parameters are allocated to the frame pipeline which finds, deblends, and measures the properties of each object. Each frame has instrumental signatures removed by flat-field, bias, and bad column corrections. At the same time cosmics and the global sky are subtracted. Then bright objects with pixels of a value of 200σ above the sky noise are detected. After that, objects are found by smoothing the images with a

Gaussian fit to the PSF and by searching for 5σ peaks.

In the frame pipeline, images of galaxies are distinguished from stars by morphology. Therefore, the PSF magnitudes, the exponential fit magnitudes, de Vaucouleurs fit magnitudes, and the corresponding likelihoods are consulted. For extended objects (galaxies), the frame pipeline measures an azimuthally averaged radial surface brightness profile. In the catalog, this quantity is given as the average surface brightness in a series of 15 annuli with radii varying from 0.23" up to 263". The unit of this quantity is called "maggies" per square arcsec, which is a linear measure of the flux, whereas 1 maggie corresponds to an AB magnitude of 0. This parameter is used in the present work in order to determine the surface brightness of galaxies and to perform a separation between Low Surface Brightness and High Surface Brightness galaxies.

For spectroscopy, an automatic target selection is performed on the imaging data, searching for galaxy, quasar, and stellar targets. The galaxies which are selected for SDSS spectroscopy are called the "main galaxy sample". One selection criterion for galaxies is that they must be brighter than $r = 17.77$ mag using the Petrosian magnitude system (Petrosian 1976) which measures flux in apertures determined by the shape of the surface brightness system. Petrosian magnitudes in the case of the SDSS are integrated magnitudes over a radius of twice the Petrosian radius of the object, which is defined as that radius where the local surface brightness drops below a value of 20% of the main surface brightness within that radius. Additionally, an r-band Petrosian half-light surface brightness of $\mu_{50} \leq 24.5$ mag/arcsec^2 is demanded as selection criterion for the main galaxy sample.

Moreover, selection for spectroscopic galaxy targeting requires the object to have a difference between PSF magnitude and model magnitude in r of greater than 0.3 mag. With these cuts, about 90 galaxy targets per square degree with a mean redshift of $\overline{z} = 0.104$ are selected. The fraction of galaxies eliminated by the surface brightness cut is with 0.1% very small, whereas nearly all stellar contamination is removed (Strauss et al. 2002).

Quasars are also selected for spectroscopy by using their distinctive colors and by analyzing radio observations in the VLA FIRST survey catalog (Becker et al. 1995).

For the spectroscopic data reduction, the spectro2d pipeline is used. These programs work in two stages. First, each 15 min-exposure from each CCD chip is reduced separately and then, the results are combined. Thereby, bias and flat-field spectra as well as superflats are used for corrections. Next, flux-calibration is performed by matching the spectra of the spectrophotometric and reddening standards of the observed plate to the synthetic composite F8 subdwarf spectrum from Pickles (1998).

The redshift of galaxies and quasars in the SDSS EDR is determined either by the emission line or the cross-correlation method, depending on which method delivers the higher confidence level. Emission lines are obtained from a wavelet transform of the continuum-subtracted spectrum. The outcoming list of emission lines of each object is matched against a list of common galaxy and quasar emission lines, and each significant peak which is found by the wavelet is fit with a Gaussian, assigned to a trial line identification and an associated trial redshift. The confidence level is the sum over the weights of the detected lines divided by the sum over the weights of the expected lines. As resulting emission line redshift that

one with the highest confidence level is chosen.

The other method which is used to determine redshifts in the SDSS pipeline is the cross-correlation of the (continuum-subtracted) spectra following a method of Tonry & Davis (1979) with stellar, emission line galaxy or quasar template spectra. By cross-correlating a measured spectrum with stellar spectra, the emission lines are masked out so that only absorption lines are relevant for the redshift. The measured spectrum is Fourier-transformed and convolved with a transform of each template spectrum. The three highest peaks of the cross-correlation functions, which are found in each template, are fitted with parabolic functions, whereas the confidence level is determined by the width of the peak. In the case of high differences between the confidence levels of the three peaks, the pipeline extends the analysis to lower wavenumbers including the continuum. Then, the redshift of the template which provides a better match to the continuum shape of the object is used and the object is flagged to be restudied later manually.

All the properties concerning EDR were consolidated using the informations given in Stoughton et al. (2002). In that publication, a deep and detailed presentation of the EDR can be found.

2.2.2   The SDSS Data Releases 1 & 2

The Data Release 1 (DR1, Abazajian et al. 2003) is the first major data release and became available in March, 2003. It covers an area of $2099\,\text{deg}^2$ in imaging and $1360\,\text{deg}^2$ in spectroscopy. The spectroscopic subsample consists of data of 134,000 galaxies, 18,680 quasars and 17,600 stars. The data are taken from runs in two areas at the celestial equator and in one northern cap area. The coverage of the EDR is a subset of the DR1 regions.

The improvement in the data quality of the DR1 with respect to the EDR was mainly achieved by changes in the photometric part of the pipeline. The photometric equations have been reformulated, problems with scattered light of the EDR were solved here. In DR1 the photometric pipeline was modified so that the problems in following rapid variations of the point-spread function, which appeared in EDR, were solved. A correction algorithm for a small nonlinearity in the response of the photometric CCDs was also newly implemented into the pipelines of the DR1 and improvements with respect to the deblending algorithm of the EDR were attained. Additionally, the original cosmic ray correction algorithm was replaced with an enhanced algorithm as described in Fan et al. (2001).

The spectroscopic pipeline was upgraded concerning bias subtraction, flat fielding, bad pixel and bad column correction. The corrections for absorption lines in the earth atmosphere and the flux calibration have also improved. In the end the continuum and line fitting codes were enhanced, too. Further details concerning the improvements in the DR1 with respect to the EDR can be found in Abazajian et al. (2003).

On March 15, 2004 the second data release (DR2, Abazajian et al. 2004) was published. Its footprint area covers in imaging about $3300\,\text{deg}^2$ whereas the spectroscopic area amounts over $2600\,\text{deg}^2$. The spectroscopic sample in the DR2 contains about 260,000 galaxies and

36,000 quasars. The main improvement concerning the reduction pipelines with respect to the DR1 is a bug fix in determining and calculating model magnitudes which led to a systematic overestimation of 0.2 mag caused by a bug in aperture correction of DR1 and EDR. Other changes to the imaging pipelines were a further improvement of the deblending algorithm, the PSF determination due to errors in the sky level and the missing of stars in the target detection due to an undersampling of the PSF in good observational conditions with a seeing better than 0.9".

2.2.3   The Data Release 3

The third data release of the SDSS includes imaging data over $5282 \deg^2$ and covers an area of $4188 \deg^2$ in spectroscopy. It was published on September 27 in 2004, shortly after DR2. This is due to the fact that the quality of the data output produced with the pipeline version used in DR2 was satisfactory and, thus the pipeline versions analyzing both images and spectroscopy were retained for DR3. Nevertheless, its coverage has been improved to a factor of 1.6 in area for both imaging and spectroscopy since it contains data taken up to June 2003. Although the reduction and data processing pipelines were kept in the version which was already used for DR2, there are some innovations in DR3. All objects which were unclassified after automatic processing were updated manually concerning the classification and the redshift was determined. This affected 477 objects, mainly with a low signal-to-noise ratio, including 377 objects of DR2. Further on, for quality assurance reasons, each of the $10' \times 13'$ subfields of the DR3 was tagged with a quality flag which is based on four attributes, namely the seeing in r-band, the mean offset between the 7" aperture magnitude and the PSF magnitude for bright stars, systematic offsets of the location of stars in color space and problems during data processing of the scrutinized subfield.

2.2.4   The Data Release 4

The fourth data release is the last but one of the SDSS data releases. It includes imaging data over $6670 \deg^2$ and covers an area of $4783 \deg^2$ in spectroscopy. It became public on July 29 in 2005. There are no published differences in the data processing between DR3 and DR4. This means that the reduction and data processing pipelines were kept in the version which was already used for DR3. However, the coverage of DR4 has been improved to a factor of 5/4 in imaging area with respect to DR3. For spectroscopy the progress in sky area is 14%.

For this PhD thesis, the Data Release 4 (DR4, Adelman-McCarthy et al. 2005) is the main data source. Nearly all results concerning SDSS presented in this thesis are based on DR4 except the results of LSB AGNs (chapter 6), which are partially produced from DR3. Previous data releases were used for the production of preliminary results during the last three years, which were partially published in Rosenbaum & Bomans (2004).

2.2.5 Future Plans for SDSS Data Releases

As described before, the actual data release is DR4 which was published in July 2005. It brought a progress in the survey area with respect to DR3, which amounts to a plus of $\sim 400 \deg^2$ (14%) in spectroscopy. The total covered area in imaging is $6170 \deg^2$ which means an improvement of $1388 \deg^2$ (25%) with respect to the DR3. However, no significant improvements concerning data processing were implemented in the DR4-pipelines which mainly base on a version already used for DR2.

The next data release after DR4, which is planned to be released in early 2006, will finish the series of public SDSS data releases. It will consist of data taken until July 2005. However, there will remain a substantial gap between the northern and southern pieces of the sky covered in the northern cap region, which can only be filled, if the SDSS collaboration will find funding in order to resume operations beyond summer 2005.

As stated in a press release from July 11, 2005, the project will be continued in the so called SDSS-II which now has a funding guaranteed until the end of the year 2008. Research is divided into three projects. At first the LEGACY project will complete the SDSS survey of the extragalactic universe. The SEGUE part (Newberg & Sloan Digital Sky Survey Collaboration 2003) of the SDSS-II has the challenge to map the structure and stellar makeup of the Milky Way Galaxy and the third part includes an intensive search for supernovae remnants (for further details and news check www.sdss.org).

Chapter 3

Properties of the SDSS as LSB survey

As described in Chapter 1, galaxy surveys are biased towards galaxies with higher surface brightnesses due to selection effects, so is the SDSS. Of course, one can only draw conclusions on objects which are observable. Hence, when dealing with galaxies at the edge of the detection limit, it is important to understand how complete the catalogue is and what kind of objects were missed. In the case of the SDSS, one has to understand which properties the galaxies have, which were chosen by its selection effects. Especially, when dealing with LSBs it is important to know how complete the surface brightness distribution is at the faint end. Therefore, it is important to understand the selection function of the spectroscopic main galaxy sample of the SDSS data releases.

In a nutshell, selection effects are due to the sky brightness of the telescope site including lunar phases, angular moon distances to the objects, the atmospheric conditions like seeing, and transparency, the optical properties of the telescope, flatfielding, the detector properties (like quantum efficiency, dark current and readout noise) and, last but not least, the sky brightness produced by our own galaxy and its absorption and extinction. All these effects bias our survey results towards a large number of HSB galaxies and only a sparse number of galaxies with low surface brightness. Additionally to this bias, there is a dimming effect of the surface brightness of the individual galaxy in dependence of redshift (Tolman 1934).

The search for galaxies within survey images is normally not performed by eye, today. Special algorithms investigate the data for galaxies by searching for signals above a certain noise deviation threshold and then applying diameter criterions or magnitude limits or both to the measured surface brightness profiles or total magnitudes. For automated spectroscopic surveys like the SDSS or the two-degree-Field Galaxy Redshift Survey (2dFGRS, Colless et al. 2001), there are routines which automatically find target galaxies within the survey images and then assign fibers to the chosen objects.

3.1   The SDSS spectroscopic Target Algorithm

In the automated reduction pipeline of the SDSS imaging data also an algorithm for spectroscopic target selection is implemented. This algorithm searches for galaxies, quasars and stars and selects them for spectroscopic follow-up observations. This is done by measuring the brightness of the detected objects. This algorithm as well as all magnitudes calculated by the SDSS pipeline are inverse hyperbolic sine magnitudes (*asinh*-magnitudes which are sometimes referred to informally as "luptitudes", for more informations see Lupton et al. 1999). The *asinh*-magnitude m is defined as:

$$m = -2.5/ln(10) \times [asinh(2bf/f0) + ln(b)], \tag{3.1}$$

with f the measured flux. The *asinh*-magnitude is characterized by a softening parameter b, which is the typical 1-sigma noise of the sky in a PSF aperture in 1" seeing. In this equation, $f0$ is given by the classical zero point of the magnitude scale (i.e. $f0$ is the flux of an object with a conventional magnitude of zero). Since the softening parameter b is measured relative to $f0$, it is dimensionless.

For each field of a size at the sky of $3°$ in diameter 640 fibers can be allocated (more details on the spectroscopic setup were given in chapter 2). The pipeline distinguishes between stars and galaxies by checking the following equation (from Stoughton et al. 2002):

$$\text{psfMag} - (\text{deV\_L} > \text{exp\_L})?\,\text{deVMag} : \text{expMag}) > 0.145, \tag{3.2}$$

with psfMag the obtained magnitude from PSF-fitting, deV_L the de Vaucouleurs fit logarithmic likelihood, exp_L the exponential disk fit logarithmic likelihood, deVMag the de Vaucouleurs magnitude fit and expMag the exponential magnitude fit. Equation 3.2 means that the difference between the psfMag and either the deVMag or the expMag, depending on which fits had the higher logarithmic likelihood (question mark), is used for the distinguishing between galaxies and point-like objects like stars and quasars. In the DR 2 and following data releases this criterion was used in a slightly changed version. The new equation is:

$$(\text{psfMag} - \text{cmodelMag}) > 0.145, \tag{3.3}$$

with psfMag again the obtained magnitude from PSF-fitting and cmodelMag the magnitude obtained from a linear combination of the best fit exponential and profiles. The composition is done in the measure of flux and not magnitudes. After the composition the magnitudes are calculated from the fluxes following equation 3.1. The cmodelMag magnitudes are in an excellent agreement with the Petrosian magnitudes for galaxies. For stars, cmodelMag and psfMag agree. This agreement is clearly improved in comparison to the former used better fit of expMag and deVMag.

At a first step, this criterion 3.3 (for DR2, DR3 and DR4) and equation 3.2 for EDR and DR1 respectively) is applied to the data in r-Band. If equation 3.3 is satisfied, the object type parameter for the r-Filter in the SDSS data is set to GALAXY, otherwise it

is set to STAR. Later, this criterion is again applied but this time to the summed fluxes over all bands, in which the object is detected. If true, the global object type parameter is set to GALAXY.

For spectroscopic galaxy target selection, Petrosian magnitudes in r-band are used as selection criterion. Petrosian magnitudes are a measure for the total magnitude of galaxies. The Petrosian flux in any band is the integrated flux within a certain number N_P (in the case of SDSS applies $N_P=2$) of the Petrosian radius r_P (Petrosian 1976):

$$F_P = \int_0^{N_P r_P} 2\pi r' dr' I(r'), \tag{3.4}$$

with $I(r')$ the azimuthally averaged surface brightness profile. The Petrosian radius r_P is the radius where the Petrosian ratio $\Re_P$, a measure for the local surface brightness with respect to the average surface brightness, drops to a certain value. In the case of the SDSS this certain value is $\Re_P=0.2$. Hence, at that radius where the following equation is satisfied, one obtains the Petrosian radius r_P:

$$\Re_P(r) = \frac{\int_{0.8r}^{1.25r} dr' 2\pi r' I(r')/[\pi(1.25^2 - 0.8^2)r^2]}{\int_0^r dr' 2\pi r' I(r')/(\pi r^2)} \overset{!}{=} 0.2 \tag{3.5}$$

A big advantage of the Petrosian magnitudes in comparison to isophotal magnitudes or similar total flux measures is that the metric apertures, within which the Petrosian fluxes are determined, are independent from sky brightness, foreground extinction, the galaxy central surface brightness and Tolman dimming (Strauss et al. 2002). Another important quantity is the mean surface brightness μ_{50} which is calculated from the flux within the Petrosian half-light radius r_{P50}. This means:

$$\int_0^{r_{P50}} I(r) r dr \overset{!}{=} \frac{1}{2} \int_0^{N_P r_P} I(r') r' dr'; \tag{3.6}$$

$$\implies \mu_{50} = m_P + 2.5 \cdot log(2\pi r_{P50}^2), \tag{3.7}$$

with m_P the Petrosian magnitude calculated from eqns. 3.4 and 3.1 ($N_P = 2$).

The spectroscopic target selection for galaxies chooses objects with an r-Petrosian magnitude brighter than $r \leq 17.77$ mag. Additionally to the Petrosian magnitude limit, an r-band Petrosian half light surface brightness of $\mu_{50} \leq 24.5$ mag/arcsec^2 is required. These cut criterions select about 90 galaxies per square degree for follow-up spectroscopy. The fraction of galaxies which were detected in the SDSS images but are not chosen as a spectroscopic target due to the surface brightness limit is very small (0.1%) (Strauss et al. 2002).

If the field is not very crowded and less than 640 objects are selected by applying the strict selection rules for galaxies and stars, these criterions are softened. Thus, also galaxies fainter than $r > 17.77$ mag or with a half light surface brightness fainter than $\mu_{50} > 24.5$ mag/arcsec^2 are selected. A third criterion is that the galaxies have to be larger than 5", which is reasonable, because the size of the fiber at the sky is 3". The

minimum distance for the placement of two adjacent fibers is 55" in projection at the sky which is due to the finite diameter of the fiber cladding. If there are two or more possible candidate objects for SDSS follow-up spectroscopy within a distance to each other of 55", not necessarily the brightest object is selected for spectroscopy. In Blanton et al. (2005) it is stated that, when two or more galaxies have a separation smaller than this distance, one member is chosen independently of its magnitude or surface brightness. It is a very important point for the environment studies (see Chapter 4) that in this case the selection is done by chance. This means that the environment studies are not biased against LSBs in dense environments.

The selection rules for total magnitude and surface brightness result in a completeness for galaxy targets of $\sim 99\%$. From that only 6% of the galaxies are lost due to fiber positioning constraints. In general, galaxies are not acquired due to this, but sometimes, preferably in dense environments like clusters this constraint applies. This means in a total that $\sim 93\%$ of the imaged galaxies are selected for spectroscopic follow-up observations with the SDSS telescope.

All these properties of the selection function do not directly apply selection criterions against LSB galaxies. First, this is due to the fact that if two (or more) adjacent target candidates are closer to each other than 55", the selection is done randomized and not necessarily the brightest object is selected. Second, as stated by Strauss et al. (2002), in the absence of noise, the Petrosian aperture is not affected by external effects like foreground extinction, the Tolman dimming and sky brightness. Thus, identical galaxies seen at two different (luminosity) distances have fluxes related exactly as the inverse square of distance (in the absence of K-corrections). They further argue, that one can therefore determine the maximum distance at which a galaxy would enter a flux-limited sample without knowing the galaxy's surface brightness profile (which would be needed for the equivalent calculation with eg. isophotal magnitudes). Hence they conclude that two galaxies which have the same surface brightness profile shape but different central surface brightnesses have the same fraction of their flux represented in the Petrosian magnitude, so there is no bias against the selection of low surface brightness galaxies of sufficiently bright Petrosian magnitude.

The whole amount of technical details on the star/galaxy separation and spectroscopic target selection would go beyond the scope of this work. All informations presented in this section were taken from York et al. (2000), Stoughton et al. (2002) and Strauss et al. (2002) which are referred to for further reading.

3.2 Resulting Constraints

It is obvious that the galaxy completeness number of 93% for spectroscopic target selection does not match the real galaxy population of the universe. It only refers to the ratio of galaxies, which were chosen for spectroscopic follow-up with respect to the number of galaxies which were detected in the SDSS images. Although the SDSS images provide a very good flat fielding due to the drift scan observation mode, the resulting exposure times

are short (54 sec, caused by the field of view and the time delay and integrate mode). Of course,this has impacts on the LSB galaxies which are detected with the SDSS.

Probing the environment of galaxies by using a spectroscopic survey, one can only give statements about the galaxies which were acquired by the survey. Therefore it is essential to understand the selection function in order to be able to explain for what kind of galaxies the resulting properties of such a test count. At a special interest is thereby the question how complete the LSB sample is. Therefore, first it must be defined, how the LSB galaxies were selected from the SDSS main galaxy sample.

3.2.1   The Division between LSB and HSB Galaxies

The data of all galaxies from the spectroscopic main galaxy sample with a redshift limited to $z < 0.11$ were copied from the SDSS DR4 server. The dataset contained for each galaxy an identifier, right ascension, declination, the azimuthally averaged surface brightness profile in the filters g and r, the redshift with errors and confidence, the Petrosian magnitudes of all bands, the Petrosian radius, the Petrosian half light radius, and the Petrosian radius containing 90% of the flux. Thereby a z-confidence greater than 90% was demanded additionally to the redshift limit. The z-confidence is a measure for the accordance of the redshifts from the different measurements of several emission or absorption lines of the scrutinized galaxy. The high confidence level was required in order to guarantee the redshift to be accurate which is important for the environment studies, since it is used as distance estimator. With this constraint, the SDSS reaches an accuracy in redshift space of ~ 30 km/s. Tests on the impact of the confidence level on the completeness of the galaxy sample showed that due to the z-confidence constraint (z-confidence$> 90\%$) only $\sim 0.2\%$ of the galaxies were not taken into account.

As the main galaxy sample was limited to a redshift of $z < 0.11$ for the present work, it still contains ~ 200000 galaxies. For each galaxy, the central surface brightness had to be determined by a feasible estimate to the surface brightness distribution. This was necessary, since it has to be known for the distinguishing between LSB and HSB as well as for the environment studies, which need the HSBs as a comparison sample. Therefore, it is currently impossible to perform the fits of each galaxy by a semiautomatic fitting routine, which can perform a bulge-disk decomposition. With actual hardware, a software like Galfit (Peng et al. 2002) needs about 30s per galaxy to perform such a fit. This would result in a total computing time of more than 70 days for the whole sample. Moreover, the obtained results all have to be checked by eye, and often fits have to be repeated. Therefore, another way had to be found.

The devision between LSB galaxies and HSBs was done using the azimuthally averaged surface brightness profiles of the SDSS data releases. For each galaxy of the spectroscopic main galaxy sample with a redshift of $z < 0.11$, the central disk surface brightness in g and r band was determined by fitting exponential disk profiles (equation 1.1) to the azimuthally averaged surface brightness profile provided by the SDSS data releases. Tests were performed for using the semiautomatic fitting routine nfit1d of the IRAF package "Space Telescope Science Data Analysis System" (STSDAS, Hanisch 1989). For that,

about 1000 LSB and HSB galaxies were fitted by IRAF while monitoring the fits by eye. During these extensive tests it turned out that the exponential fit following expression 1.1 applied to the first seven bins of the azimuthally averaged profile generally provides a good fit. Furthermore, it has the big advantage that it can be applied fully automatically. The use of the first six bins of the profile is due to the fact, that for most galaxies within this range the profile is not truncated towards outer radii. The truncation which normally appeared at the outer part beyond the 7th of the profile may be caused by reaching the detection limit or may be partially natural. The truncation of the profile due to different profiles within bulge and disk is not taken into account since only exponential fits are done. Fitting was performed for the azimuthally averaged surface brightness profiles in the filters g and r. The central surface brightnesses obtained from the fits in g and r were transformed into Johnson-B central surface brightnesses by using the following equation (Smith et al. 2002):

$$B = g + 0.47 \cdot (g - r) + 0.17. \tag{3.8}$$

After that the galaxies were distinguished between LSBs and HSBs by applying the Tolman dimming corrected surface brightness criterion:

$$\mu_B + 2.5 \cdot log \left(\frac{1}{(1+z)^4} \right) > 22.5, \tag{3.9}$$

with μ_B in mag/arcsec^2 as the central surface brightness obtained from exponential fitting as described before. If equation 3.9 was fulfilled, the object was designated as LSB galaxy, otherwise as HSB. Taking into account the Tolman dimming one avoids a contamination of the LSB sample by cosmological dimmed HSBs. For instance, a HSB with an undimmed central surface brightness of $\mu_B = 22.10$ mag/arcsec^2 and a redshift of z=0.1 would appear as a LSB with a central surface brightness of $\mu_B = 22.51$ mag/arcsec^2, if Tolman dimming were not taken into account. After the application of equation 3.9 to the galaxies from the SDSS DR4 spectroscopic main galaxy sample with a redshift of $z < 0.11$ and a z-confidence beyond 90%, a number of 1141 galaxies were identified as LSBs and 210702 galaxies were marked as HSBs.

3.2.2   The resulting LSB Sample

The properties of the imaging survey namely drift scan mode, the resulting high quality of the flatfield, exposure time, noise of CCD and amplifiers as well as the spectroscopic target algorithm (as described in section 3.1) have flown into the result that 1141 galaxies were recognized as LSBs (from DR4). To that preselected sample only the limiting of the redshift to $z < 0.11$ and the demanded z-confidence of greater than 90% were applied by the author of this thesis. As said before (section 3.2.1) the loss of galaxies due to the latter constraint is negligible. The redshift limit of $z < 0.11$ was applied in order to probe the local universe and to avoid bias onto the scientific results of the environment studies due to evolutionary effects. To the resulting sample the equation 3.9 was applied as the definition of low surface brightness in order to identify the LSB galaxies.
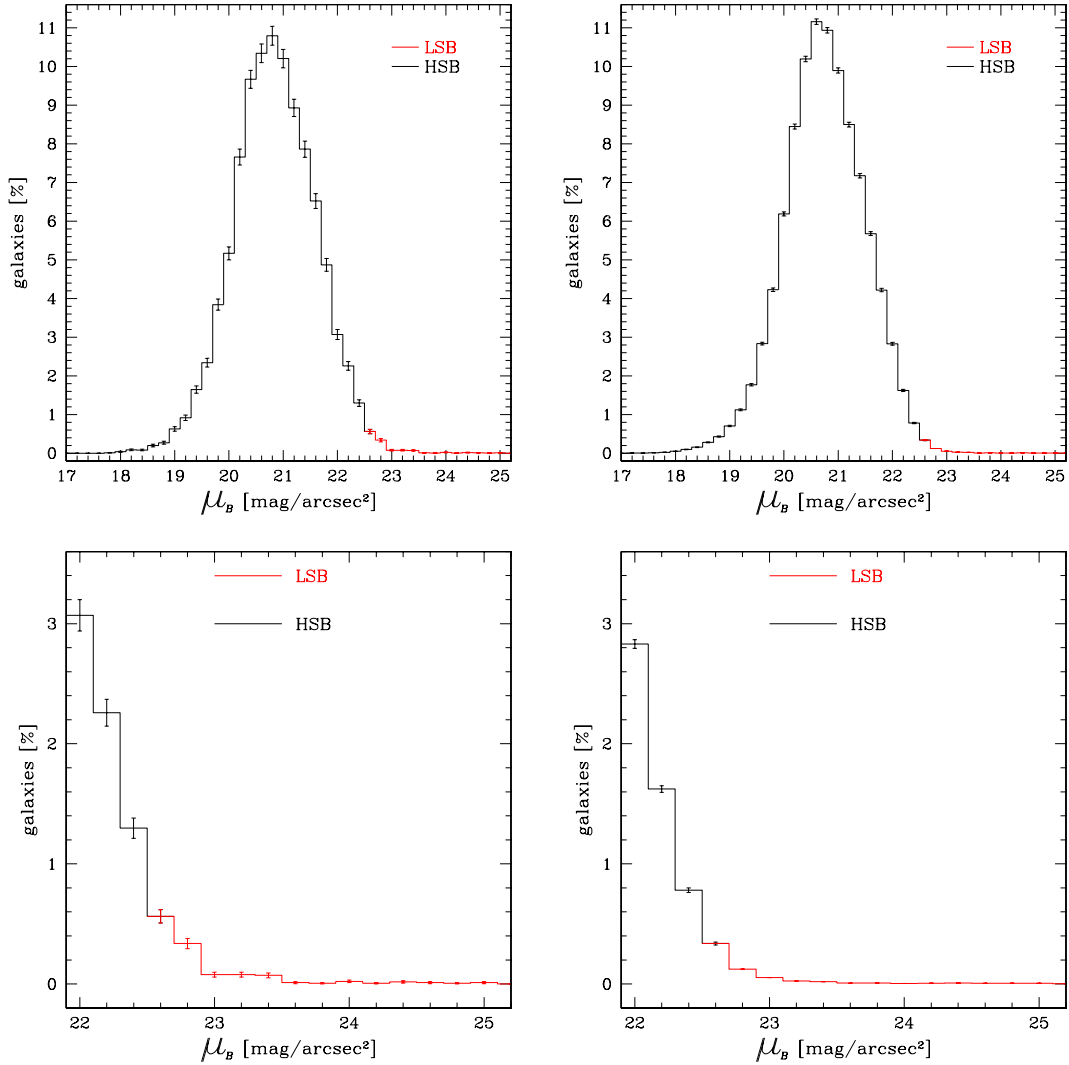
Figure 3.1: The diagrams show the surface brightness distribution of sample HSB (black lines) and LSB galaxies (red lines) from SDSS EDR (left panels) and DR4 (right panels). The central surface brightness in B-band μ_B obtained from exponential fitting of the bands g and r of the SDSS surface brightness profiles and the transformation to Johnson-B following formula 3.8 is plotted versus the relative galaxy number. A total of 18111 galaxies of EDR and 212080 galaxies for DR4 is shown. The lower panels show the zoom into the LSB regions between $22.0 \, \text{mag/arcsec}^2$ and $25 \, \text{mag/arcsec}^2$ of the upper diagrams. In the EDR 232 LSB galaxies and in DR4 1378 LSBs were found.

In order to understand what kind of galaxies were selected by these selection effects, the resulting galaxy population was examined. At the beginning of 2003, when only the EDR of the SDSS was available, the surface brightness distribution of the 18111 sample

galaxies limited to $z \leq 0.11$ from both equatorial stripes of the survey was examined by taking the central bin of the azimuthally averaged surface brightness profile measured by the SDSS pipelines. In that former diagram a bimodal distribution was seen which disappeared by later applying exponential fits to the data. The apparent bimodality was due to the fact that the requirements made for the acquisition of the EDR commissioning data concerning the sky conditions were relaxed, especially for the seeing. This means that several observation runs were integrated into the EDR with a bad seeing of beyond 2.0". Since the central bin of the azimuthally averaged surface brightness profile of the SDSS data consists only of an area of 1 pixel (which corresponds to 0.396" at the sky) it is clear that the flux of this surface brightness bin was reduced significantly by a smear out effect (Blanton 2004, priv. comm.).

Figure 3.1 shows the revised diagram of the EDR surface brightness distribution in B-band (left two panels) obtained from exponential fits to the SDSS surface brightness profiles of each galaxy with a redshift of $z \leq 0.11$. Thereby the lower panel illustrates a zoom into the LSB region of the upper diagram. The right two panels also show the surface brightness distribution, but for the DR4. The surface brightness distribution shown in Figure 3.1 displays a sharply peaked distribution with an extended wing towards the faint end of the distribution. At this wing the LSB galaxies are situated, but the low amount of LSBs found does not really reproduce the real fraction of LSB galaxies which is present in the local universe. This is due to the fact that the SDSS is not generally well suited for LSB search due to the short exposure times of $\sim 54\,\mathrm{s}$ caused by field of view size and TDI observing mode.

One difference which is obvious between the EDR and DR4 is that the the fraction of LSBs within EDR is significantly higher than that in DR4. This can be seen in the lower panels of the Figure 3.1. There the fraction of LSBs is higher in the left diagram which was produced from the EDR than the fractional LSB amount in the right diagram (DR4). In numbers the EDR with the constraints in redshift and redshift confidence (see section 3.2.1) contains 232 LSBs and 17879 HSBs. This means that the EDR contains a fraction of 1.3% LSB galaxies. In the DR4 1378 LSBs and 210702 HSBs are covered, which results in a LSB fraction of 0.65%. Due to the fact that the central surface brightness was obtained by fitting exponential functions to the surface brightness profile, this difference in the LSB fraction between these data releases cannot be caused by seeing effects. Since the EDR is a subset of the DR4 covering 10% of the DR4 area, these differences cannot be caused in local effects. The statistical errors of the LSB fractions are 0.08% for EDR and 0.02% for DR4. This means that the differences in the LSB fraction between the EDR and DR4 are distinct from each other by a factor of $\sim 8\sigma$. Therefore, the differences in the LSB fractions between the two data releases cannot be due to statistical fluctuations. All these facts give strong evidences that the galaxy selection function for spectroscopic targeting had been changed between the data releases. Although the LSB fraction is quite low in the SDSS it is much higher than the fraction of low surface brightness galaxies predicted by the freeman law. With an average surface brightness value of $\mu = 21.65\,\mathrm{mag/arcsec}^2$ and a standard deviation of $\sigma = 0.3\,\mathrm{mag/arcsec}^2$ the Gaussian distribution measured by Freeman (1970) predicts a fraction of 0.23% LSBs to HSBs with a central surface brightness

of $\mu_B \geq 22.5\,\text{mag/arcsec}^2$. The LSB fraction in the DR4 is ~ 3 times higher and in EDR it is actually ~ 6 times higher than predicted by the Freeman Law.

3.2.3 The Luminosity Distribution of the Sample LSBs

After these considerations it is clear that the fraction of LSB galaxies is not very high at all, but the SDSS data set with its large sky coverage, its accurate redshift and the data public available is the only large survey suitable for statistical significant environment studies of LSB galaxies. For these studies it is important to understand, what kind of galaxies the LSB sample consists of concerning for instance morphological type and total luminosity. During the environment studies it turned out that the total luminosity of the selected LSB galaxies depends on redshift. Figure 3.2 shows the histogram of the absolute magnitude distribution of all LSB sample galaxies divided into two symmetrical redshift bins. The left panels show the relative number (in percent) versus the absolute magnitude in the filters g, r and B (from top to bottom) within the redshift interval of $0.01 < z < 0.055$. The right three panels show the absolute magnitude distribution for the same filters, but for the redshift interval of $0.055 < z < 0.1$. For the determination of the absolute magnitudes Petrosian magnitudes were used. The distance modulus was derived from the redshift assuming a Hubble constant of $H_0 = 71\,\text{km} \cdot \text{s}^{-1} \cdot \text{Mpc}^{-1}$ (Spergel et al. 2003). Then the total magnitude was calculated using the equation:

$$M = m - 25 - 5 \cdot log\left(\frac{z \cdot c}{H_0}\right), \tag{3.10}$$

with M the absolute magnitude of a certain filter, m its apparent magnitude, z the redshift (dimensionless), $H_0 = 71\,\text{km} \cdot \text{s}^{-1} \cdot \text{Mpc}^{-1}$ (Spergel et al. 2003) the Hubble constant and c in km/s the speed of light. K corrections (e.g.: Humason et al. 1956, Oke & Sandage 1968), which are corrections of the photometry of galaxies for the fact that sources observed at different redshifts are at different rest-frame wavelenghts in relation to standard stars, were not applied. This was due to the fact that their influence on the absolute magnitude is in the order of magnitude of the photometric error for galaxies in the local universe and therewith negligeble.

It is conspicuous that for the redshift interval of $0.01 < z < 0.055$ all bands show a LSB galaxy population which is dominated by dwarf-like galaxies. The mean values of the absolute magnitude distribution in this redshift intervals are for the different bands $\overline{M}_g = -16.93 \pm 0.08\,\text{mag}$, $\overline{M}_r = -17.50 \pm 0.07\,\text{mag}$ and $\overline{M}_B = -16.58 \pm 0.08\,\text{mag}$. These values place the dominant LSB galaxy population of the redshift interval of $0.01 < z < 0.055$ into a region of dwarf-like, irregular galaxies in the galaxy luminosity distribution. It is similar to the luminosity of the Small Magellanic Cloud ($M_B = -16.5\,\text{mag}$, van den Bergh 2000). Again, the absolute magnitudes in B-band were calculated using equation 3.8 and than averaged. For the higher redshift interval with $0.055 < z < 0.1$ the situation changes. The peak of the distribution migrates towards the brighter region of the absolute magnitude diagram in comparison to the other redshift interval. This means that there the LSB population is dominated by larger galaxies. This is confirmed by the mean values
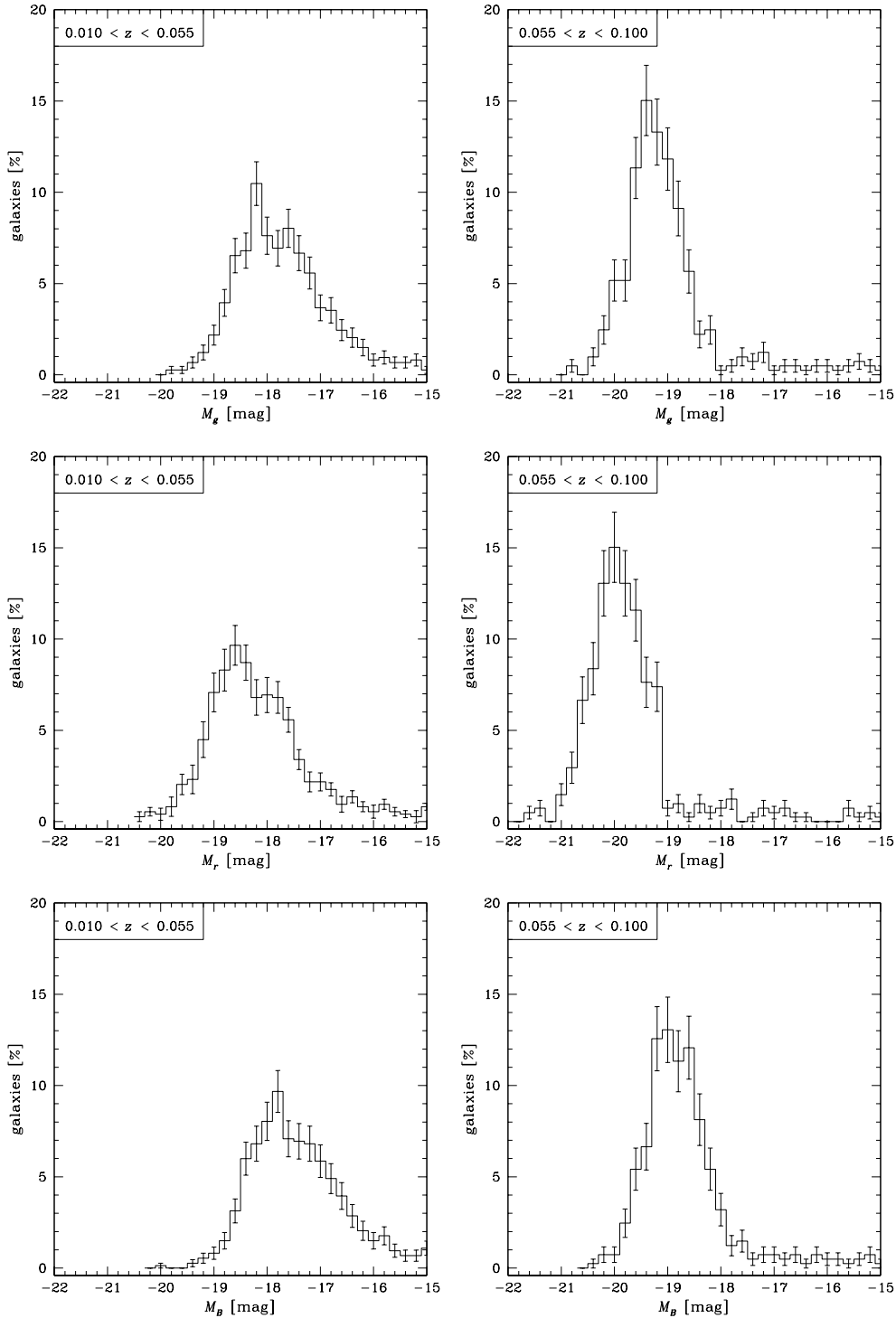
Figure 3.2: The distribution of the absolute magnitude of all sample LSB galaxies with a redshift of $z \leq 0.11$. Left three panels show the absolute magnitude distribution of the LSB galaxies in a redshift interval of $0.01 < z < 0.055$ in the filters g, r, and the resulting B (from top to bottom). Right three panels are the same as left panels, but for the z-range $0.055 < z < 0.1$. Mind that the barycenter of the distribution for the higher redshift interval is shifted towards the in total magnitude brighter (larger) galaxies in comparison to the lower redshift interval.

of the distributions. For the different bands mean values of $\overline{M}_g = -18.67 \pm 0.08\,\text{mag}$, $\overline{M}_r = -19.63 \pm 0.06\,\text{mag}$ and $\overline{M}_B = -18.13 \pm 0.10\,\text{mag}$ were calculated. This value is similar to that of the Large Magellanic Cloud ($M_B = -18.0\,\text{mag}$, van den Bergh 2000). It also places these galaxies in the total magnitude range of spiral HSB galaxies.

The lack of small LSB galaxies at the higher redshift interval is not caused by dimming effects since the Petrosian magnitude is free from cosmological dimming effects (Section 3.2.1). It is obvious that this lack is due to the apparent Petrosian r-magnitude limit of $r < 17.77\,\text{mag}$. It causes smaller galaxies with a low absolute magnitude to be excluded from spectroscopic targetting at the higher redshift interval. For example, a galaxy with a total absolute r-magnitude of $M_r = -17.50\,\text{mag}$ at a redshift of $z = 0.055$ has an apparant magnitude of m_r=19.30\,\text{mag}$ and therefore it would be excluded from spectroscopic targetting by the magnitude limit, unless the field is sparse populated so that there are still fibers left after the application of the strict criterias for spectroscopic targets.

3.2.4   The Size Distribution of the Sample LSBs

More puzzling than the absence of dwarfish galaxies at the higher redshift interval of $0.055 < z < 0.1$ is the apparent lack of large LSBs at lower redshifts of $0.01 < z < 0.055$. Indeed, it is not the case that there are no large galaxies in the lower redshift interval of $0.01 < z < 0.055$, but they are overwhelmed by small galaxies. This effect is not only observed for LSBs but also for HSB galaxies of the SDSS sample. This is seen in Figure 3.3. The upper left panel of the Figure shows the angular Petrosian-r radius in arcsec versus the redshift of the galaxy for all HSBs. At the upper right panel, the same but for LSBs is seen. Red dots are the mean values of the apparant Petrosian-r radius distribution within the corresponding redshift interval, in the upper left panel for HSBs and in the upper right panle for LSB galaxies. The binning of the redshift intervals is $\Delta z = 0.01$.

The distribution of the average angular Petrosian-r radius of both galaxy types (in both upper panels) is quite flat. For HSBs (left upper panel) the average apparant Petrosian-r radius declines by $\sim 60\%$ between the redshift of $z = 0.01$ and $z = 0.1$, whereas the comoving distance (the distance obtained from redshift by assuming Hubble flow) is increased tenfold.

A similar situation is found in the LSB data. The averaged distribution of the angular Petrosian radius (red dots in the right upper panel) shows the same declining trend as for HSBs between a redshift of $z = 0.01$ and $z = 0.1$ but the average apparant radius is only decreased by $\sim 40\%$ within that redshift range. In both diagrams there are three horizontal line-like structures. These lines are artefacts due to a bug of the SDSS pipeline, since it was checked by eye that all objects forming a line in that diagram do definitively not have the same angular size. The problem is known by the SDSS pipline programmers and it is due to the "mismatches between the spectroscopic and imaging data". On the DR4 homepage it is stated that for various reasons, a small fraction of the spectroscopic objects do not have a counterpart in the best object catalogs. In addition, the DR4 does not contain photometric information for some of the special plates, and the retrieval of photometric data from the CAS database requires special care for objects from the special
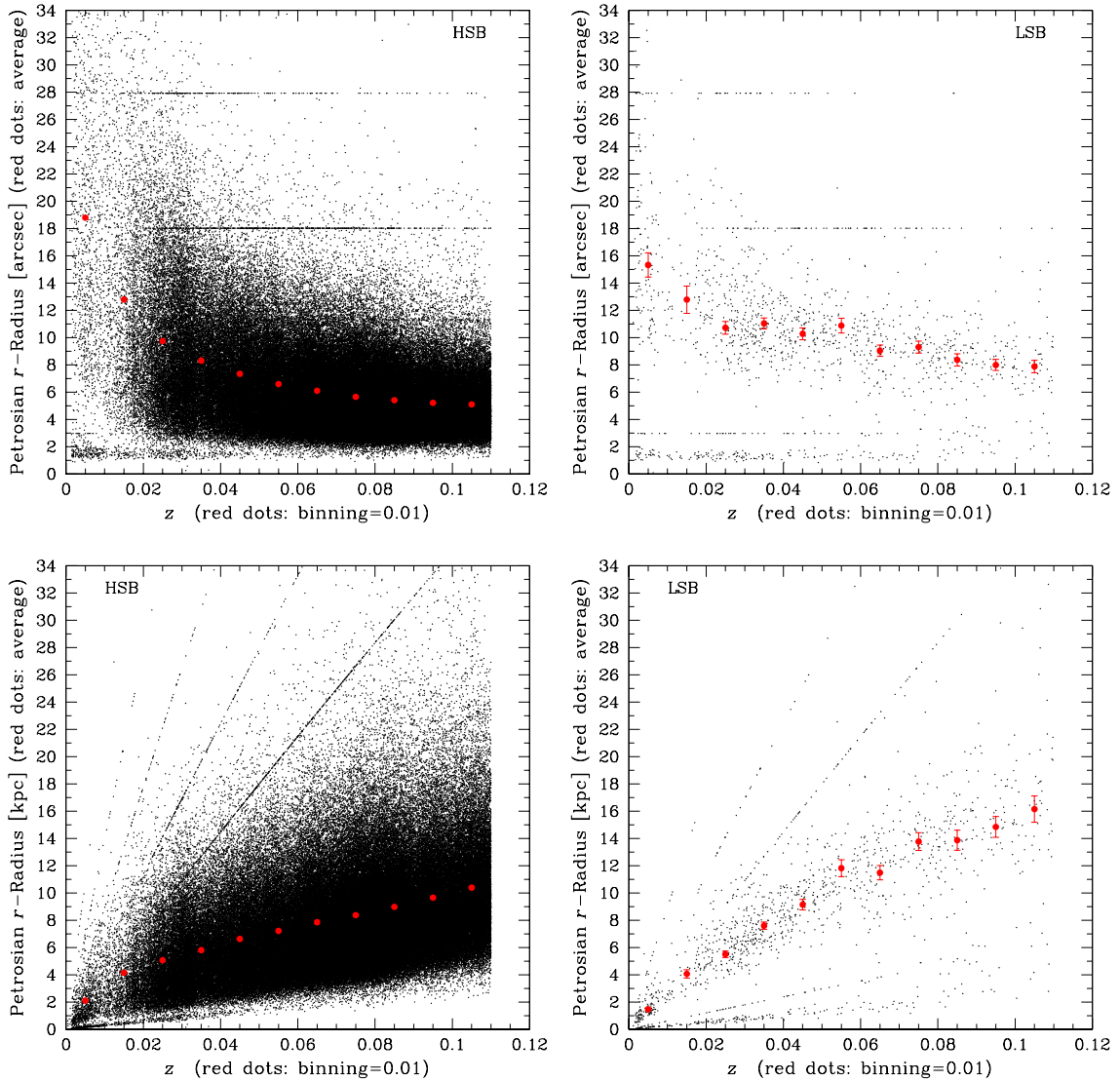
Figure 3.3: Left upper panel shows the distribution of the apparent Petrosian-r radius (in arcsec) against the redshift z of HSB sample galaxies (black dots). Red dots are the average Petrosian radii (in arcsec) within redshift bins with a bin width of 0.01. The statisitcal error has a typical value of 0.07 arcsec and is therewith smaller than the size of the red points. Rightupper panel shows the same as left upper panel, but for the LSB sample galaxies. Here, error bars indicate the statistical error of the indiviual average. Mind, that for a redshift of $z > 0.01$ the LSB galaxies are larger in apparant radius than the HSBs. The statisitcal error is smaller than the size of the red points.

At the lower left panel the distribution of the absolut Petrosian-r radius (in kpc) versus the redshift z is displayed for HSB galaxies. The average of the distribution within redshift bins of 0.01 is shown as red dots. The typical value for the statistical error of these averages is 0.03 kpc. Therewith it is smaller than the size of the points. The lower right panel shows the same diagram as the lower left panel, but for LSB galaxies. Error bars indicate the statistical error of the indiviual average values. Mind, that with increasing z the averaged absolute Petrosian size of the galaxies also grows in both the HSB and LSB case.

plates (see also: www.sdss.org/dr4/start/aboutdr4.html).

The lower panels show the Petrosian radii in kpc calculated from the angular size and the comoving distance obtained from redshift (left panel for HSBs, right panel for LSBs). Since the data are not corrected for Virgocentric infall the comoving distances and therewith the calculated radii are accurate only for redshifts beyond $z = 0.01$. For HSBs the average apparant Petrosian radius decreases by a factor of ~ 2.5 between redshift $z = 0.01$ and $z = 0.1$, but the redshift increases by a factor of ten, the average absolute Petrosian radius also increases. It does not grow linearly with a factor of four but with a factor of 2.5, since the comoving distance is not directly linear with z due to relativistic corrections. The situation for LSBs (lower right panel) is similar, again. The averaged absolute Petrosian radius also rises between a redshift of $z = 0.01$ and $z = 0.1$ with a slope of ~ 4. This is due to a decreasing angular radius with a slope of about 5/3 within a redshift range from $z = 0.01$ to $z = 0.1$ but a comoving distance increased by a factor of ten, minus relativistic corrections. Both the HSB and LSB lower diagram also show artefacts which are the same artefacts as in the upper panels but now producing diagonal lines due to the calculation of the absolute Petrosian radii by calculating the comoving distances from the redshifts.

This effect seen in the diagrams of Figure 3.3, that with increasing distance on average larger galaxies are sampled, is mainly caused by the apparant magnitude limit for spectroscopic follow up of Petrosian $m_r \leq 17.77$ mag. For reaching this magnitude limit galaxies at higher distances must of cause be larger and therewith more luminous in total absolute magnitude in order to reach the $m_r \leq 17.77$ mag limit. This effect is known as the Malmquist (1922) Bias in the literature.

The fact that the sample LSBs must be larger than their HSB equivalents in order to reach this limit due to their low stellar surface densities is obvious. From this it is clear that at lower redshifts, both the LSB and the HSB sample are dominated by dwarfish galaxies, but at higher redshifts these galaxies do not get over the magnitude hurdle. The $m_r \leq 17.77$ mag limit is not a sharp criterion, because in the case that not all fibers are occupied by bright galaxies free fibers are assigned to galaxies which are below that limit, but the frequencies at which this case appears are low. Hence, also a sparse population of dwarfish galaxies is sampled at higher redshifts.

A very important feature resulting of these studies is that now, as one has understood the SDSS selection function, one can perform further statistical analyses on the LSB galaxies contained in the SDSS. Furthermore, the selection function gives the possibility to the researcher to switch the LSB galaxy population between a sample consisting of large LSBs and another sample dominated by samller LSBs just by changing the redshift interval. Moreover, the HSB comparison sample can also be switched between a sample also containing smaller galaxies and a sample without small galaxies. This is important for the next Chapter where the galaxy density in the vicinity of LSBs is investigated and compared to the clustering properties of HSB galaxies.

Chapter 4

Results of the Environment Studies

Knowing what kind of LSB and HSB galaxies were selected for SDSS spectroscopy (Chapter 3) one can now probe further properties of these SDSS galaxies. In this Chapter the investigations in the environment of LSB galaxies in comparison to that of HSBs are described, and the results of these studies are presented.

4.1 What is already known?

In the past, studies of the LSB environment were a problem, because the redshifts were not quite accurate and the statistics were based on low numbers, since the areas covered by the surveys were small. Studies on the environment were done before but only on small scales. Bothun et al. (1993) performed neighbour counting on a sample of 340 LSB disk galaxies embedded in a HSB comparison sample from the CfA redshift survey. They searched for neighbours within cones of a velocity range of ± 250 km/s and a projected radius of 0.5 Mpc centered on each sample LSB galaxy. The authors found a strong statistical deficit of neighbouring galaxies within that cone volume around LSB disks compared to HSB ones. They furthermore investigated the distances to the nearest neighbour and found it to be on average a factor of 1.7 farther away for LSBs than for HSBs. A second study by Mo et al. (1994), who calculated the cross correlation function of LSBs and HSBs, showed that the amplitude of the cross correlation function is for LSBs significantly lower than that of HSBs on scales of $r < 2h^{-1}$ Mpc.

All these facts give hints that the nature of LSBs may be related to their birthplaces within the large scale structure (LSS). A lack of nearby neighbours may have caused the absence of gravitational triggers by nearby galaxies to LSBs, which would disturb the gas potential and initiate star bursts. LSBs can generally be regarded to be as gas rich as HSBs (e.g.: Pickering et al. 1997, O'Neil et al. 2004), but their H I components possess lower surface densities (e.g.: van der Hulst et al. 1993) but higher extensions than that of HSBs. Due to the lack of nearby galaxies it seems that LSBs evolve more quietly than HSBs and therefore produce less stars.

Moreover, Bothun et al. (1997) speculated the initial Gaussian spectrum of density perturbations in the initial universe to be consisting of low- and high-density perturbations, whereas a lot of the low-density perturbations were assimilated or disrupted during the evolutionary process of galaxy formation. However, they believed that a substantial fraction of the low-density fluctuations survived and formed LSB galaxies. In Rosenbaum & Bomans (2004) it is proposed, that the initial density contrast consisted of small scale fluctuations superimposed at large scale peaks and valleys. Small scale peaks led to galaxy formations, whereas large scale peaks resulted in cluster, wall, and filament formation, with large scale minima forming voids. Based on the first results presented in Rosenbaum & Bomans (2004) it is proposed by the authors that LSBs were born in the valleys of the large scale density contrast, whereas HSBs were formed at the large scale peaks. Further on, taking into account the data results, it is concluded that LSB galaxies were formed in the voids of the LSS and have migrated to the outer parts of the filaments and walls due to gravitational infall. The blue colors of LSBs (e.g.: McGaugh & Bothun 1994) and the young ages of their dominant stellar populations (Haberzettl 2005) fit well into that concept, since galaxy formation took place chronologically from higher densities towards lower densities.

4.2   The Environment Studies

For the environment studies the spectroscopic main galaxy samples of the SDSS public data releases (especially DR4) were used. In the following subsections the data download, processing, and analysis for studying the environment of LSBs are described. All programs used for the data query, processing, and analysis presented in this Chapter were developed and written by the author of the present dissertation from scratch (except IRAF STSDAS nfit1d), and the source codes of the programs can be found in Appendix A.

4.2.1   The data obtained from SDSS

The data for the environment studies were obtained from the SDSS public releases by using the SDSS Query Analyzer (SDSS-QA). The SDSS-QA is a tool which provides advanced data downloads with access to about 300 parameters for each object contained in the several public Sloan datasets. For data download, a SQL-query was programmed which transferred the following parameters for all galaxies of the main galaxy sample with a redshift confidence of more than 90%, and a redshift of $z \leq 0.11$ (Chapter 3.2.1) from the SDSS server to the computer of the author of the present work. For each galaxy, an identifier, its position in right ascension and declination, the redshift with error, the azimuthally averaged surface brightness profiles in g- and r-band, the Petrosian magnitudes in the filters u, g, r, i, z, the Petrosian-r radius, and the radii containing 50% and 90% of the Petrosian flux were downloaded.

After data transfer, all Galaxies with a central, Tolman-dimming corrected surface brightness of $\mu_B \geq 22.5\,\mathrm{mag/arcsec^2}$ were flagged as LSB galaxies, otherwise they were

flagged as HSBs. Thereby the central B-surface brightness was obtained by fitting exponential profiles (equation 1.1) to the azimuthally averaged surface brightness profiles measured by the SDSS pipelines and the central surface brightnesses in g and r which were converted into a B-surface brightness using equation 3.8. In order to probe the environment of the LSB galaxies one has to count neighbour galaxies using a certain search volume. It is clear, that as a neighbour both LSB and HSB galaxies count. Additionally, the galaxy density in the vicinity of LSBs was compared to the galaxy density in the vicinity of HSBs. For these two reasons, the LSB and HSB galaxies were stored into one file, but with different flags indicating LSB or HSB property. Hence, and with an corresponding neighbourhood analysis code, it was guaranteed that as neighbour of a scrutinized LSB galaxy (and of course a HSB) both LSB and HSB galaxies count for indicating the surrounding galaxy density.

4.2.2 The Pie Slice

For a first glance at the distribution of the LSB galaxies within the large scale structure (LSS), so called pie slices were plotted from the database obtained as described in the section before. Figure 4.1 shows such pie slice diagrams, where the distribution of right ascension and the redshift of LSB (black dots) and HSB galaxies (green dots) are displayed in polar plots. Left panel contains the right ascension range which was taken from an equatorial scan region of the DR4 with $120° \le \alpha_{2000} \le 240°$ and the declination range of $-1.25° \le \delta \le 1.25°$ is projected onto the plane, whereas the redshift is limited to a value of $z \le 0.11$. This is due to the redshift limit which was implemented into the SQL-query. Right panel shows a pie slice of the same declination range, but with a right ascension of $310° \le \alpha_{2000} \le 360°$ and $0° < \alpha_{2000} \le 60°$. The left panel contains 94 LSBs and 12768 HSBs, the numbers for the right panel are 72 LSBs and 11379 HSBs.

This cut through the distribution of galaxies within the local universe clearly shows the structure of the universe, which is often compared to be sponge-like or to look like suds in soapy water. Indeed, the structure of the universe can be divided –going from highest densities towards low densities– into galaxy clusters, which form the "fingers of god", walls, filaments, and voids, which are comparable to soap bubbles forming suds, except for the cluster structures.

An important clue in order to understand the existence of the class of LSB galaxies is the answer to the question, at which places of the LSS the LSBs were formed. A first impression to this question is given by the pie slices of Figure 4.1. Gazing at the redshift range of $0.05 \le z \le 0.11$, it seems that LSBs are located at the outer rims of the filaments or even in void regions of the LSS. The situation changes, when looking at the LSB distribution within the LSS at lower redshifts with $z < 0.05$. There, the LSB distribution seems to follow the LSS traced by the HSB galaxies, and LSBs are sometimes found in the middle of walls or clusters. If one takes into account the LSB selection function presented in Chapter 3, one knows that at lower redshifts the LSB sample is dominated by dwarfish galaxies, and at higher redshifts the small galaxies are more and more deselected. Only the larger LSBs remain and dominate the LSB sample at higher redshifts of $0.05 \le z \le 0.11$. Then, one
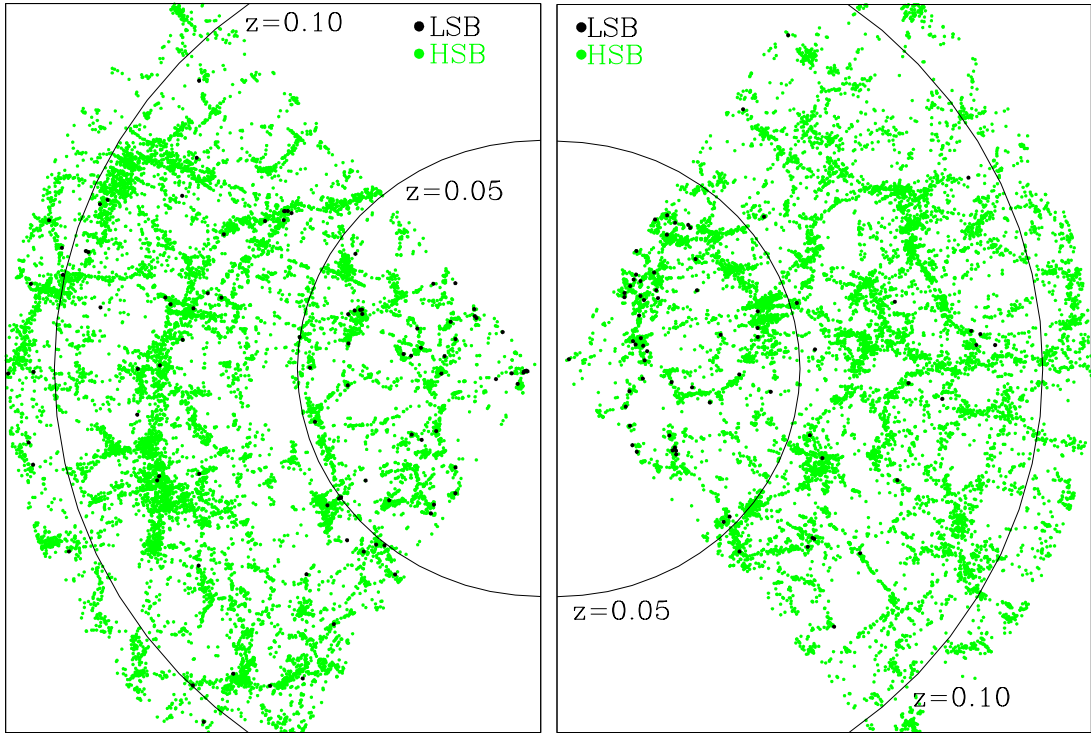
Figure 4.1: Two analyzed pie slices produced from SDSS DR4. Black dots are LSB galaxies and green dots represent HSBs. Left panel shows the distribution of LSBs and HSBs within a right ascension range of $120° \leq \alpha_{2000} \leq 240°$ and a redshift of $z \leq 0.11$ in a polar plot. The declination range of $-1.25° \leq \delta_{2000} \leq 1.25°$ is projected onto the plane. Right panel shows the same, but for a right ascension range of $310° \leq \alpha_{2000} \leq 360°$ and $0° < \alpha_{2000} \leq 60°$. The declination range is again $-1.25° \leq \delta_{2000} \leq 1.25°$. Mind, that within a redshift interval of $0.05 \leq z \leq 0.11$ the LSBs are located at the outer parts of the filaments and walls of the LSS defined by HSBs. However, for a redshift of $z < 0.05$ the situation is not so clear. There one can find LSB galaxies at the outer parts of the filaments as well as in the middle of walls and clusters. Thereby, one has to take into account that at the lower redshift interval the LSB population is dominated by dwarfish galaxies and at higher redshifts the LSB sample mainly consists of larger galaxies.

can draw a first trend that larger LSBs are located at more isolated areas of the universe, whereas this statement is not sure to hold for small, dwarfish LSBs. In order to verify or falsify this first impression, statistical environment studies were performed which are presented in the following subsections.

4.2.3 Neighbour Counting within Spheres

The first impressions from the pie slice that LSB galaxies within a redshift interval of $0.05 \leq z \leq 0.1$ inhabit the outer parts of the filaments and sometimes void regions, had to be probed by doing statistics. Therefore, an algorithm for counting neighbours was developed (Appendix A). The algorithm for neighbour counting works as follows. For each galaxy, a sphere with a certain radius is defined with the scrutinized galaxy in the center. Then the number of neighbour galaxies within this sphere is counted. This step is performed for all galaxies found in the program input file. Since the data of LSB and HSB galaxies are stored in one file which is used as the data input for the program, both galaxy types count as neighbours independent from if the scrutinized galaxy is a LSB or HSB. The radius of the sphere is an input parameter which the user is asked to define at the program start, as well as the names of the input and output files. After the interrogation of the input parameter and files, the program calculates for each galaxy of the input file the comoving distances by applying a Hubble constant of $71 \, \mathrm{kms^{-1}Mpc^{-1}}$ (Spergel et al. 2003) and a light speed of $c = 299792.458 \, \mathrm{km/s}$. Thereby, relativistic corrections for the redshifts were used. Since the environment studies were limited to a reshift range of $0.01 \leq z \leq 0.1$, neither Virgocentric infall was corrected nor more complicated streaming motions than pure Hubble flow was taken into account. After that the right ascension, declination and comoving distances are converted into Carthesian coordinates. Then the code starts neighbour counting within the 3-dimensional distribution of LSB and HSB galaxies by centering a sphere with a radius which was specified at program startup on each galaxy of the input file and then counting the neighbouring galaxies within this sphere.

In order not to distort the statistical results at the borders of the catalogue volume, an edge correction was applied. If not corrected, the number of neighbours would drop down there due to the fact that the sphere would contain a volume without sample galaxies. The borders of the sample were avoided so that galaxies whose spheres were cutting the edges of the sample volume were rejected and not stored in the output file. Since all galaxies in the input file are HSB or LSB type flagged, one has the possibility to divide the result into statistics for the environment of LSBs and HSBs separately. For edge correction the covered volume of the input catalog was sampled with cubes of different sizes which did not cut the borders of the catalog.

Due to the fact that at lower redshifts ($0.01 \leq z \leq 0.055$) the sample LSBs are dominated by dwarfish galaxies and at higher redshifts ($0.055 \leq z \leq 0.1$) mostly large galaxies are contained in the LSB sample (Chapter 3), the environment study had to be separated into these two redshift intervals. For each redshift interval, the environment studies were performed in different runs with several values for the sphere radius. It was varied from $0.8 \, \mathrm{Mpc}$ to $8 \, \mathrm{Mpc}$ in steps of $0.6 \, \mathrm{Mpc}$. The lower border of the scale range ($0.8 \, \mathrm{Mpc}$) was chosen in order to avoid bias effects to the statistics due to fiber placement constraints, since the minimum possible distance between two adjacent fibers is 55" in angular distance. This value corresponds to a minimum distance between two adjacent galaxies of $0.112 \, \mathrm{Mpc}$ at a redshift of $z = 0.1$ for getting spectra of both galaxies. Hence, with a sphere radius of $r = 0.8 \, \mathrm{Mpc}$, effects caused by fiber placement constraints are well sampled. An-

other argument for choosing the lowest sphere radius of the study to be $r = 0.8\,\mathrm{Mpc}$ was the spectral resolution of the SDSS data. The spectral resolution in redshift amounts $\Delta v \simeq 30\,\mathrm{km/s}$ (Stoughton et al. 2002). This corresponds to a uncertainty in comoving distance of $\Delta D \simeq 0.425\,\mathrm{Mpc}$ (assuming Hubble flow). With a starting sphere radius of $R = 0.8\,Mpc$, this uncertainty is oversampled by a factor of two and therefore does not influence the results. By the way, the astrometric resolution in the directions perpendicular to the line of sight amounts $100\,\mathrm{mas}$ (Pier et al. 2003) and can be neglected. The upper border of the scale range ($8\,\mathrm{Mpc}$) of the neighbour counting was chosen, because with higher values the probed volume decreases due to boundary corrections and the statistics drops in significance. However, the chosen scale range is sufficient to probe the spatial distribution of LSBs on group radius scales (1-3 Mpc, Cox 2000, Krusch 2003) and filament sizes ($\sim 5\,\mathrm{Mpc}$, e.g.: White et al. 1987b, Doroshkevich et al. 1997).

The code was fed with the input file containing all LSB and HSB galaxies of the DR4 main galaxy sample from all spectroscopic scan regions with a redshift of $z \leq 0.11$ and a z-confidence larger than 90%.

4.2.4   The Galaxy Cluster Finding Algorithm

After the analysis using the code for neighbour counting, cluster galaxies had to be excluded from the sample in a second statistical analysis for a comparison of the clustering properties of field LSBs and HSBs. This was also done due to the fact that, when calculating comoving distances from redshifts, the velocity dispersion (which can exceed values of $\sigma \geq 1000\,\mathrm{km/s}$) of galaxy clusters mocks an extension of the cluster in the line of sight direction. These structures bias the results in the LSS and had to be removed from the data. Therefore, an algorithm for cluster searching was developed (Appendix A).

Galaxy clusters are conglomerations of galaxies containing at least 50-100 luminous member galaxies with luminosities $L \gtrsim L_* = 2 \cdot 10^{10} L_\odot$ (e.g.: Sparke & Gallagher 2000) and in total several hundreds or thousands of galaxies physically bound together by their mutual gravitation (and additional gravitational components: hot gas, Dark Matter). Moreover, galaxy clusters are characterized by detectable X-ray emission due to their hot ($\sim 10^8\,\mathrm{K}$, e.g.: Sparke & Gallagher 2000) intergalactic gas. Galaxy clusters appear as radial structures called "fingers of god" within the LSS. Due to the velocity dispersion of the galaxies within the cluster potential, the comoving distance of each individual cluster galaxy calculated from the redshift does not represent the exact position in the LSS. Hence, when measuring the distribution of LSBs in the LSS these "fingers of god" caused by clusters disturb the environment studies by producing radial structures which mock radial aligned filaments with a very high galaxy density.

In order to eliminate the "fingers of god" in the LSS, a cluster finding algorithm was developed. This algorithm searches for clusters in the LSS by counting galaxies within a cylinder aligned radially in the line of sight direction with a configurable radius and height. The radius r of the cylinder thereby complies with the radius of the cluster and the height of the cylinder corresponds to its velocity dispersion σ. These two values are
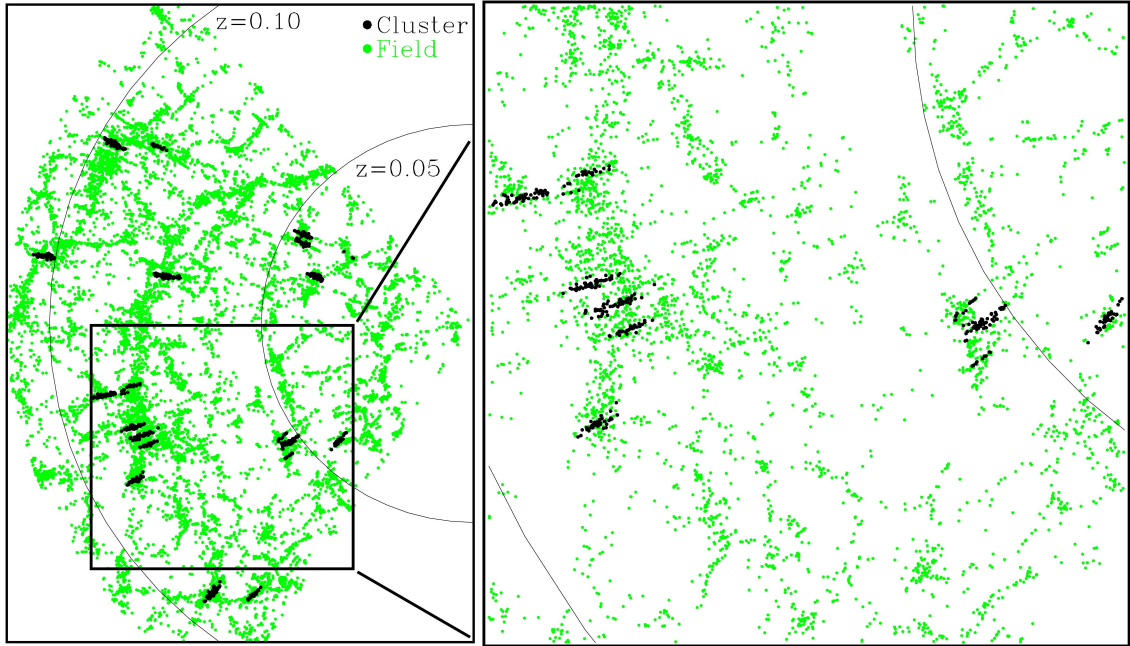
Figure 4.2: Pie slice in order to demonstrate the cluster finding algorithm. The left diagram shows the distribution of all HSB galaxies within a right ascension range of $120° \leq \alpha_{2000} \leq 240°$ and a redshift of $z \leq 0.11$ in a polar plot. The declination range of $-1.25° \leq \delta_{2000} \leq 1.25°$ is projected onto the plane. The galaxies found to be arranged in clusters detected by the cluster finding algorithm are marked with black dots, whereas the field galaxies are displayed as green dots. It can be seen, that the cluster searching code finds the "finger of god"-like structures in the LSS. Additionally, these plots show that all clusters are embedded in wall-like structures of the LSS which indicates that the structure formation has not been completed, yet.

parameters which can be chosen by the user of the program. The minimum number of cluster members ($N_{members}$) can also be set at program startup. The source code of the cluster finding algorithm can be found in appendix A.4. After the development of the cluster finding algorithm the best parameters concerning r, σ, and $N_{members}$ for finding galaxy clusters had to be figured out. Therefore, a parameter study (Appendix B) was performed on a test pie slice region of the LSS with data from DR4. It turned out that, the best results of the hunt for galaxy clusters producing "fingers of god" were achieved with the parameters cylinder radius $r = 2.5\,\mathrm{Mpc}$, velocity dispersion $\sigma = 1000\,\mathrm{km/s}$ and the minimum number of cluster galaxies $N_{members} = 50$. Within the test pie slice, 21 galaxy clusters and in total 583 cluster member galaxies were found with these parameters (Figure 4.2). The results were compared to the galaxy clusters found by the C4 Clustering algorithm (Miller et al. 2005). It turned out that the cluster search algorithm developed for this dissertation found 20 galaxy clusters also found by the C4 code within the test pie

slice. Five clusters were missed by the algorithm, but found by the C4 program, whereas two of the missed clusters lie at the edge of the pie slice (in declination). Therefore, they could not be found by the program (of cause the C4 analyzed the whole data volume, not only the small pie slice, and hence they were not located at the border). One of the found clusters is not found in the C4 catalog and was probably miss-identified. Taking the C4 catalog as reference one can conclude that the code developed for our analysis setup with the parameters $r = 2.5\,\mathrm{Mpc}$, $\sigma = 1000\,\mathrm{km/s}$ and $N_{members} \geq 50$ did not find three of 23 clusters ($\sim 13\%$) and probably miss-identified one ($\sim 4\%$). This comparison shows that the code used here works reasonable for its purpose.

The cluster search code is based on a definition similar to the definition used by Abell (1958) and Abell et al. (1989), but it works in three dimensions. They defined the galaxy clusters mainly by a richness and a compactness criterion. The richness criterion requires that, a cluster must contain at least 50 members that are not more than $2\,\mathrm{mag}$ fainter than the third brightest member. In the compactness criterion it is demanded that a cluster must be sufficiently compact that its 50 or more members are within a given radial distance r of its center. Also the retrieved parameters for optimum cluster search have observational evidences. In general, galaxy clusters possess radii ranging from $r \sim 1\,\mathrm{Mpc}$ up to $r \sim 3\,\mathrm{Mpc}$ and velocity dispersions of $\sigma \sim 400 - 1400\,\mathrm{km/s}$ (e.g.: Cox 2000). For instance, the Coma cluster has a radius of $r = 3.5\,\mathrm{Mpc}$ (Sparke & Gallagher 2000) and an average velocity dispersion of $\sigma \simeq 950\,\mathrm{km/s}$ (Kent & Gunn 1982). Also galaxy groups are bound and show a velocity dispersion. With values for the velocity dispersion of several tens up to a maximum of $\sim 200\,\mathrm{km/s}$ (Cox 2000) the velocity dispersion is in the range of the spectral resolution of the SDSS spectroscopy, which has an accuracy about $30\,\mathrm{km/s}$. Therefore, groups are responsible only for a soft broadening of the LSS in the line of sight direction due to their velocity dispersion, which was neglected in the statistical environment investigations.

The cluster finding algorithm was not developed in order to perform membership determinations on galaxies within galaxy cluster regions (like the C4 code does), but to identify "finger of god" structures due to galaxy clusters within the LSS, whose areas then can be excluded from environment studies. However, the implementation of a color analysis in order to determine cluster membership probabilities for galaxies in the cluster region is possible. This would provide several possible applications for the program in addition to the use in the present dissertation.

The cluster finding algorithm was applied to the file containing the DR4 LSB and HSB sample after the neighbour counting within spheres. The program produced a file containing all (LSB and HSB) galaxies of the input files except the cluster galaxies of the clusters found by the program. This means that the cluster galaxies were removed from the galaxy sample file (containing neighbourhood informations) retroactively, which means that only the distribution of field galaxies flows into the statistic. Otherwise, if one performs the cluster removal before environment analysis, one would produce holes into the large scale structure which had to be masked out before the environment analysis. If not masked out, they would distort the statistics like boundary effects (which were also excluded). Therefore, it is the more elegant method to first perform the environment

studies and then to remove cluster galaxies from the sample subsequently.

The properties of the cluster LSBs were not examined in the framework of the present dissertation. However, it is important, that the number of cluster LSBs is, with a value of 21, very low (20 were found in the lower redshift interval and one at higher redshift). Since the LSB population of clusters is known to mainly consist of dwarfs (e.g.: Davies et al. 1988, Bothun et al. 1991, Ulmer et al. 1996), this low amount of LSBs found in clusters is due to the selection function (Chapter 3).

4.2.5 Introduction to the Galaxy Bias

The galaxy bias is a term from cosmology and is normally used to describe the difference in the clustering properties between galaxies and Dark Matter on large scales. Since galaxies contain only a small fraction of the total mass of the universe, they are not expected to be very good tracers of the total mass distribution. Furthermore, the initial conditions of the primordial gas, which galaxy formation requires for cooling and fragmentation, were not given at all places in the initial universe (e.g.: White & Frenk 1991). Moreover, galaxy interaction and merging takes place for individual galaxies (forming more massive galaxies, e.g.: Cole et al. 2000), as well as for groups and galaxy clusters, which also accrete substructures and merge (e.g.: Zabludoff & Mulchaey 1998 for groups; Zabludoff & Zaritsky 1995 and White et al. 1993 for clusters) . Of cause, these facts influence the distribution of galaxies in the universe.

A simple explanation for the galaxy bias is the so called natural bias first mentioned by White et al. (1987a). In this scheme galaxies form inside Dark Matter halos, whereat in regions of large scale overdensities, the halos form first (and therewith the galaxies) with respect to halos in underdensities. This model would only produce a galaxy bias which would exist briefly. However, even the Dark Matter halos in the low density regions will have collapsed sooner or later, and therewith the galaxy bias would have vanished. Another model is the high peak bias, in which it is assumed that galaxies form only in Dark Matter regions which possess a density above a certain threshold (e.g.: Coles 1993).

In order to define the galaxy bias, some more cosmological quantities have to be introduced. The density contrast

$$\delta(\overrightarrow{X}) = \frac{\rho(\overrightarrow{X}) - \overline{\rho}}{\overline{\rho}} \qquad (4.1)$$

describes the deviation of the local density from the averaged density, whereas $\rho(\overrightarrow{X})$ is the local density at the position vector $\overrightarrow{X}$ and $\overline{\rho}$ the mean density of the whole density field. For galaxies the density contrast can also be expressed in terms of number densities:

$$\delta(\overrightarrow{X}) = \frac{N(\overrightarrow{X}) - \overline{N}}{\overline{N}}, \qquad (4.2)$$

with $N(\overrightarrow{X})$ as the number density of galaxies within a certain volume at the location

described by the position vector $\overrightarrow{X}$ and $\overline{N}$ as the averaged number density of the density field.

As said before, the galaxy bias usually describes the bias between the distribution of galaxies and the total matter. If the density contrast refers to the galaxy contrast, it is usually indicated as δ_{g}, when related to the total matter content it is noted as δ_{m}. The density contrast δ is normally measured within volumes formed by spheres of a certain radius R. In that case it is called δ_R. For galaxies the density contrast within a sphere with a certain radius R can be also expressed in terms of number densities (corresponding to equation 4.2):

$$\delta_R(\overrightarrow{X}) = \frac{N_R(\overrightarrow{X}) - \overline{N}_R}{\overline{N}_R}, \tag{4.3}$$

with N_R the number of galaxies within the sphere of a certain radius and $\overline{N}_R$ the number density within that sphere averaged over the whole space. Averaging the local density contrasts within a sphere of a certain radius over the whole space delivers $< \delta_R > = 0$, but a measure for the lumpiness of the galaxies or matter on the scales of R is the second moment $< \delta_R^2 >$, which is also called variance. The more clustered a galaxy or matter distribution is the more inhomogeneous it is, which increases the variance. Therefore, it is obvious that higher values of $< \delta_R^2 >$ correspond of a higher degree of clustering in the scrutinized galaxy or matter distribution. On the scale of $R = 8.0\,\mathrm{Mpc}$ the square root of the second moment of the density fluctuations is often called σ_8, which is an important quantity in cosmology.

The linear stochastic galaxy bias between the distribution of galaxies and the total matter content is defined as:

$$b(R) = \sqrt{\frac{< \delta_{R,\mathrm{g}}^2 >}{< \delta_{R,\mathrm{m}}^2 >}} \tag{4.4}$$

4.2.6   The LSB-HSB Galaxy Bias

In the present dissertation, for the first time the stochastic bias is now used in order to quantify the bias in the large scale distribution between LSBs and HSBs. Therefore, it is christened as the "LSB-HSB galaxy bias" by the author of the present dissertation. From the neighbour counting within spheres of the radius R for LSBs and HSBs the galaxy number density N at the location of each galaxy was directly obtained. The second moment of the density contrast was then calculated for the density field at the location of all sample LSBs using the equation

$$< \delta_{R,\mathrm{LSB}}^2 > = \frac{1}{n} \sum_{i=1}^{n} \left(\frac{N_{i,R,\mathrm{LSB}}}{\overline{N}_{R,\mathrm{LSB}}} - 1 \right)^2, \tag{4.5}$$

which corresponds to equation 4.3. However,in this case it is not calculated for all galaxies but only for spheres which are centered at the sample LSBs. Thereby, $N_{i,R,\mathrm{LSB}}$ is the number of (LSB and HSB) galaxies within a sphere of the radius R centered on the LSB galaxy i or expressed in a different way the galaxy number density within a radius R at the location of the ith LSB galaxy. The quantity n is the total number of LSBs and $\overline{N}$ is the number of (LSB and HSB) galaxies within that radius R averaged over all LSB galaxies.

For HSBs the same equation holds, but at this time indicated with the label "HSB" at certain places:

$$< \delta_{R,\mathrm{HSB}}^2 > = \frac{1}{n} \sum_{i=1}^n \left(\frac{N_{i,R,\mathrm{HSB}}}{\overline{N}_{i,R,\mathrm{HSB}}} - 1 \right)^2 . \tag{4.6}$$

This means that the second moment of the number densities within spheres of the radius R but only at the locations centered on HSB galaxies is calculated.

Using these equations (4.5, 4.6) in combination with the results of the environment studies within spheres of the radius R, the average density contrast at the locations of LSBs and the same quantity at the locations of HSBs were calculated. From these results, the stochastic bias parameter $b(R)$ was obtained using the following equation (which is a redefinition of equation 4.4) to show the different clustering properties of LSBs and HSBs:

$$b(R) = \sqrt{\frac{< \delta_{R,\mathrm{LSB}}^2 >}{< \delta_{R,\mathrm{HSB}}^2 >}}, \tag{4.7}$$

with R the sphere radius, $< \delta_{R,\mathrm{LSB}}^2 >$ the second moment of the LSB density contrast in dependence of the radius of the probing sphere and $< \delta_{R,\mathrm{HSB}}^2 >$ the same but for the sample HSB galaxies.

With the definition of this parameter it is now possible to express the differences in the LSB and HSB environment in terms of the density contrast and galaxy bias. This is usually used to show the differences between the galaxy density and Dark Matter distribution in cosmology, but in this case it is also well suited to display the different clustering properties of LSB and HSB galaxies.

4.3   Results of statistical Investigations

The statistical investigations were done in order to either proof or falsify the impression obtained from the pie slice that LSB galaxies are located at the outer parts of the filaments and walls and partially in void regions. Therefore the analysis counting neighbours as described in section 4.2.3 was performed on different sphere radii.

4.3.1   Results of averaged Neighbour Counting within Spheres

The number of neighbours were averaged for LSB and HSB galaxies. Due to the the SDSS selection function the sample contains LSB galaxies of different size and total luminosity
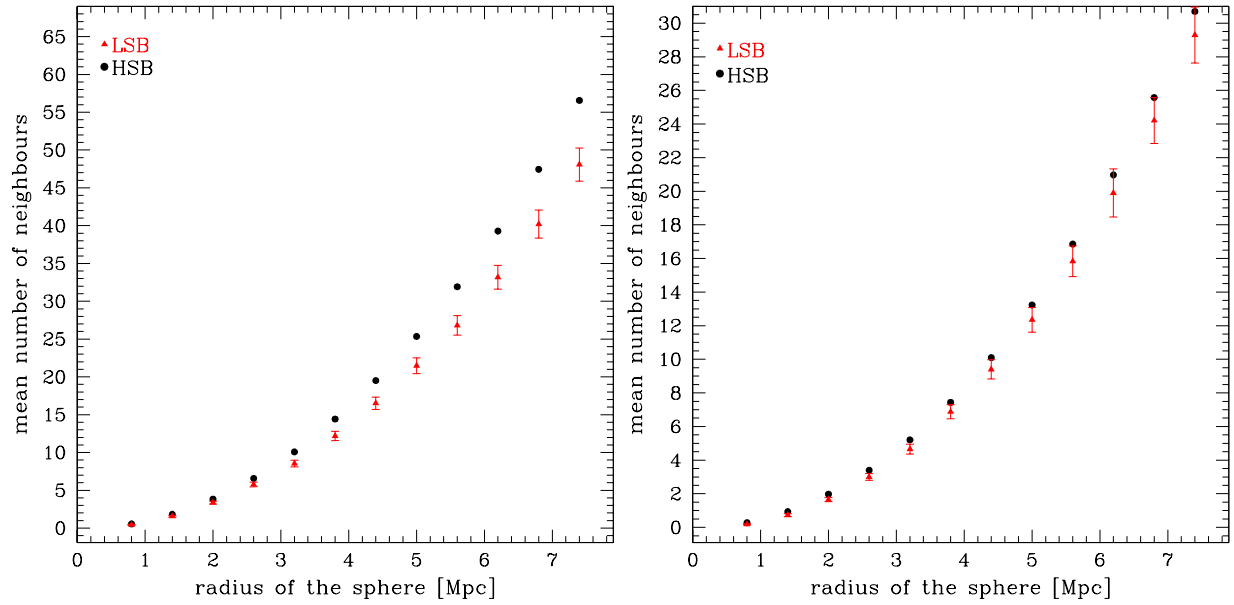
Figure 4.3: The diagrams show the average number of neighbours for LSBs (red triangles) and HSBs (black dots) versus the radius of the sphere within which the neighbours were counted. Both plots are not corrected for cluster galaxies. Left diagram displays the results of the redshift interval of $0.01 \leq z \leq 0.055$, right panel shows the same but for the redshift range of $0.055 \leq z \leq 0.1$. The average number of neighbours stays for LSBs systematically below the values of the HSB statistics both for the lower redshift interval (left) and the higher redshift interval (right).

at different redshifts, namely the low redshift interval of $0.01 \leq z \leq 0.055$ is dominated by dwarfish LSBs. The higher redshift range of $0.055 \leq z \leq 0.1$ contains mainly large LSBs (Chapter 3). Therefore the examinations on the environment were divided into two symmetric redshift bins corresponding to these redshift intervals.

Figure 4.3 shows the average number of neighbours for LSBs (red) and HSBs (black) versus the sphere radii within the redshift intervals $0.01 \leq z \leq 0.055$ (left panel) and $0.055 \leq z \leq 0.1$ (right panel). In order to produce this diagram neighbour counting was performed in several runs within spheres with radii between $0.8\,\mathrm{Mpc}$ and $8\,\mathrm{Mpc}$ in steps of $0.6\,\mathrm{Mpc}$. For each sphere radius the number of neighbours was averaged for the LSB galaxies and for the HSB galaxies (as neighbour both galaxy types counted). In the lower redshift interval ~ 400 LSBs were probed in comparison to ~ 31000 HSBs. For the higher redshift interval the sample contains ~ 200 LSB and ~ 69000 HSB galaxies. In this case, cluster correction was not applied to the data. The data show that LSB galaxies have on average less neighbours than HSB galaxies on scales between $0.8\,\mathrm{Mpc}$ and $8.0\,\mathrm{Mpc}$. This is the case for both redshift intervals. This means that dwarfish LSBs as well as large LSBs are preferably found in regions with lower galaxy density than in the vicinity of HSBs. Since the cluster regions were not yet eliminated from the data set, one can draw a first
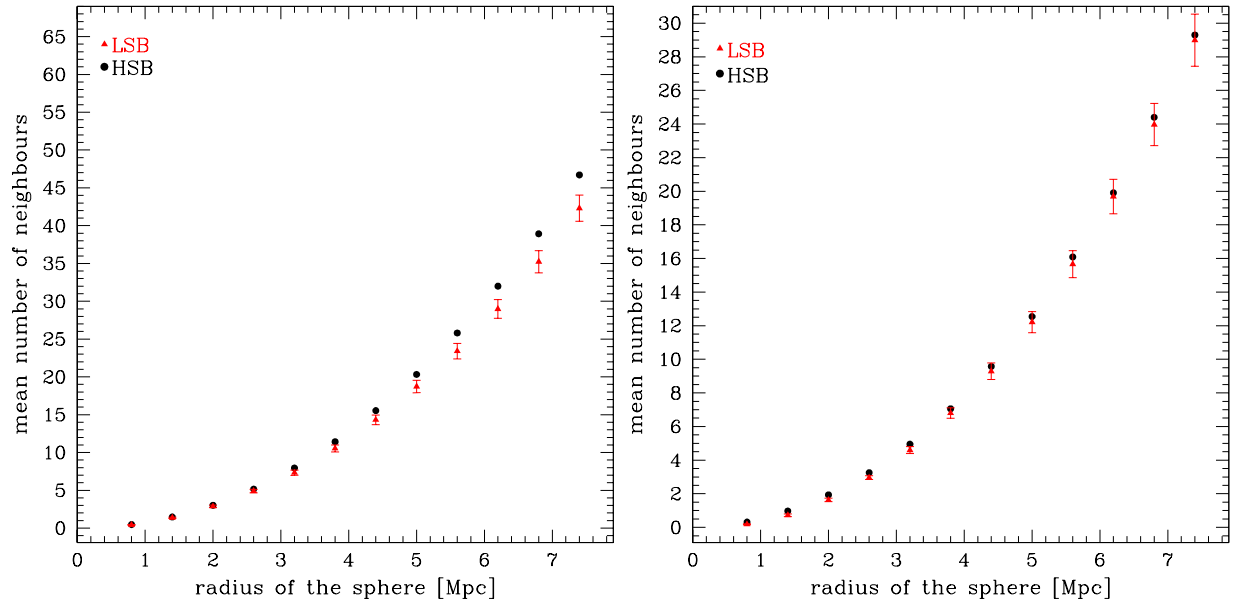
Figure 4.4: The panels show again the average number of neighbours for LSBs (red tri-angles) and HSBs (black dots) versus the sphere radius within the two redshift intervals (left: $0.01 \leq z \leq 0.055$, right: $0.055 \leq z \leq 0.1$), but at this time the cluster galaxies were removed from the statistics (as described in section 4.2.4). This means that the distribu-tion of LSBs in comparison to HSBs was probed in the field. On average the LSB galaxies still have less neighbours than HSBs but the signal is not so strong (but still significant) as if we average over cluster and field galaxies (Figure 4.3).

preliminary conclusion that LSBs are at least less often located in clusters than HSBs.

The next step was to probe the location of LSBs in the LSS without clusters. For that, the cluster galaxies were removed from the statistics using the cluster finding algorithm (section 4.2.4). This means, that all galaxies, which are located in a LSS volume occupied by a cluster, were removed from the statistics that it was averaged over pure field galaxies. Figure 4.4 shows the results of that study. Again, two redshift bins (left panel: $0.01 \leq z \leq 0.055$, right: $0.055 \leq z \leq 0.1$) were examined. This means that galaxies which have more than 50 neighbours within a cylinder with a radius of $3\,\mathrm{Mpc}$ and a height of $1000\,\mathrm{km/s}$ aligned with its axis towards the line of sight were rejected. Again, the number of neighbours were averaged for LSBs and HSBs at different sphere radii. The diagrams show that on average LSB galaxies have less neighbours than HSB galaxies on all probed scales for both dwarfish and large LSB galaxies, since all triangles representing the average LSB number of neighbours are located systematically below the corresponding averaged values for HSBs. For the redshift bin with $0.01 \leq z \leq 0.055$ (left panel) it becomes statistically significant at a sphere radius of $3.2\,\mathrm{Mpc}$. For the higher redshift bin (with $0.055 \leq z \leq 0.1$, right panel) it is statistically significant between $2\,\mathrm{Mpc}$ and $3.8\,\mathrm{Mpc}$. As all LSB values are located below the HSB values, one can argue that the effect is also seen

on that scales with low statistical significance, where the error bars of LSB points and HSB points in the diagram overlap. One can argue this way, since the probability is small that this effect, namely that all LSB points are located below the HSB values is caused by statistical noise.

The statistical significance of the statement that LSB galaxies have on average less neighbours than HSBs had to be probed. For that, Kolmogorov-Smirnov (KS, Chakravarti et al. 1967) two sample tests were performed on the LSB and HSB distribution of neighbours from which the average values were calculated. The KS test is intended to probe the null hypothesis that two data samples come from the same distribution. Therefore, it is suitable by inverting the results to test if the LSB and HSB neighbouring distribution are different. Or said concretely, we use the (inverted) KS test results in order to probe the inverted null hypothesis that LSB galaxies have less neighbours than HSBs on different scales. Since the KS statistic is used for unbinned data sets, it was applied to the unbinned number of neighbour distribution of LSBs forming the first data sample and the same distribution for HSBs producing the second test data sample.

The results are presented in table 4.1 and 4.2. Thereby, table 4.1 refers to the significance of the null hypothesis in Figure 4.3 with respect to the corresponding scale radii. This Figure contains statistics including both cluster and field galaxies. For the lower redshift range with $0.01 \leq z < 0.055$ (Figure 4.3, left diagram), our hypothesis that LSB galaxies have on average less neighbours than HSBs holds with more than $1\,\sigma$ probability for the scale range of $0.1\,\mathrm{Mpc}$ to $2.6\,\mathrm{Mpc}$ and with around $2\,\sigma$ probability for scales between $3.2\,\mathrm{Mpc}$ and $5.0\,\mathrm{Mpc}$. For the scale interval of $5.6\,\mathrm{Mpc}$ to $8.0\,\mathrm{Mpc}$, a significance of around $3\,\sigma$ is reached for this hypothesis. Since these statistics are not adjusted from cluster galaxies, one can draw the conclusion that within that redshift range, there is a deficit of LSB galaxies in clusters or field regions. Now, one should take into account the selection function for LSBs from Chapter 3, which shows that this scrutinized redshift range is dominated by dwarfish LSB galaxies. Then, this result shows that there exists a density contrast for small LSBs, which are on average located in a less dense environment than field and cluster HSBs. In diagram 4.3/right panel this hypothesis holds with explicitly more than $1\,\sigma$ significance for values of the sphere radii between $0.8\,\mathrm{Mpc}$ and $2.0\,\mathrm{Mpc}$. For the scale values of $2.6\,\mathrm{Mpc}$ and $3.2\,\mathrm{Mpc}$ the probability of the hypothesis is still around $1\,\sigma$, but it drops below that value for higher scale radii. However, all LSB neighbouring values in Figure 4.3/right at that scales are located systematically below the average number of neighbours for HSBs. This indicates that this effect is real with a higher probability and over a larger range of radii than the KS test indicates.

Table 4.2 refers to the Figure 4.4 and gives probabilities that the (inverted) null hypothesis that LSB galaxies have less neighbours than field HSBs is true on different scales for two redshift intervals. Figure 4.4 contains the comparison between field LSB galaxies and field HSBs, since all cluster galaxies were removed from statistics.

For the redshift range of $0.01 \leq z < 0.055$ the following situation turns out to be as follows. For the scale values of $0.8\,\mathrm{Mpc}$ and $1.4\,\mathrm{Mpc}$ this hypothesis holds with more than $1\,\sigma$ significance. The sphere radii of $2.0\,\mathrm{Mpc}$ and $2.6\,\mathrm{Mpc}$ have a probability of around 50% for the trueness of the hypothesis. On scales between $3.2\,\mathrm{Mpc}$ and $4.4\,\mathrm{Mpc}$ the statement

Table 4.1: Significance of neighbour counting statistics. Two sample KS tests were performed to probe the probabilities of the hypothesis that LSB galaxies have less neighbours than HSBs on different scales (sphere radii). Thereby, the probabilities in the table refer to each pair of data points of the diagrams in Figure 4.3.

Significance of Statistics		
z-range / refers to Figure	radius [Mpc]	significance [%]
$0.01 \leq z < 0.055$	0.8	91.38
Figure 4.3 (left)	1.4	90.71
not cluster corrected	2.0	74.23
	2.6	69.11
	3.2	94.25
	3.8	91.16
	4.4	94.37
	5.0	97.88
	5.6	99.26
	6.2	99.01
	6.8	98.55
	7.4	99.93
	8.0	99.48
$0.055 \leq z < 0.1$	0.8	79.26
Figure 4.3 (right)	1.4	91.51
not cluster corrected	2.0	79.77
	2.6	64.48
	3.2	64.66
	3.8	52.17
	4.4	47.61
	5.0	55.95
	5.6	57.57
	6.2	34.50
	6.8	40.86
	7.4	44.38
	8.0	33.27

possess clearly more than $1\,\sigma$ probability. And for the sphere range of $5.0\,\mathrm{Mpc}$ to $8.0\,\mathrm{Mpc}$ the significance is with values of $2\,\sigma$ up to $3\,\sigma$ quite high.

For the higher redshift interval with $0.055 \leq z < 0.1$ the situation is not so clear. The first three scale values with $0.8\,\mathrm{Mpc}$, $1.4\,\mathrm{Mpc}$ and $2.0\,\mathrm{Mpc}$ have a significance for the hypothesis of around and about $1\,\sigma$. However, the probability that the hypothesis holds at higher sphere radii is low, below 50%. Nevertheless, this does not mean that on that scales LSB and HSB field galaxies share the same clustering properties, since the number of

Table 4.2: Significance of neighbour counting statistics continued. Again, two sample KS tests were performed to probe the probabilities of the hypothesis that LSB galaxies have less neighbours than HSBs on different scales (sphere radii), but this time the table entries refer to the diagrams of Figure 4.4.

Significance of Statistics		
z-range / refers to Figure	radius [Mpc]	significance [%]
$0.01 \leq z < 0.055$ Figure 4.4 (left) cluster corrected	0.8	70.22
	1.4	69.24
	2.0	49.12
	2.6	56.81
	3.2	84.08
	3.8	77.84
	4.4	87.88
	5.0	95.06
	5.6	98.18
	6.2	97.63
	6.8	96.73
	7.4	97.39
	8.0	98.67
$0.055 \leq z < 0.1$ Figure 4.4 (right) cluster corrected	0.8	68.80
	1.4	86.59
	2.0	64.36
	2.6	41.88
	3.2	41.57
	3.8	27.71
	4.4	37.05
	5.0	35.56
	5.6	38.55
	6.2	16.07
	6.8	21.55
	7.4	23.97
	8.0	16.41

neighbours is on average still lower for LSBs than for HSBs, but for each value in diagram 4.4/right considered individually, the density contrast is not significant on scales of 2.6 Mpc and above. However, taking into account that the average number of neighbours for LSBs always stays below the values for the field HSBs, shows that altogether the effect is present, although the environment study on a single scale value is not significant for values above 2.6 Mpc. This is still an effect of small numbers, which will be improved with further data sets covering larger sky areas (e.g.: SDSS-II).

4.3.2 Results of the LSB-HSB Galaxy Bias

The LSB-HSB galaxy bias is a helpful redefinition of the bias in the density contrast normally used to display the stronger clustering of galaxies in comparison to Dark Matter in cosmology. In the present dissertation it was used in order to probe if LSBs reside in a less dense environment than HSBs.

The results obtained from probing the LSB-HSB galaxy bias are presented in Table 4.3. In that Table, the values for the second moment of the density contrast for LSBs calculated using 4.5, for HSBs (equation 4.6), and the resulting values for the LSB-HSB bias parameter calculated from equation 4.7 are given. These values are displayed in dependence on the sphere radius. The results are again divided into the two redshift bins as used several times before. Furthermore, a division of the results into the cases "not cluster corrected" and "cluster corrected" is done. The first case probes the LSB galaxy bias with respect to all (field and cluster) HSBs. The second case tests if the distribution of LSB galaxies is biased against field LSBs.

For these particular cases the variance of the density contrast and the LSB-HSB bias parameter were calculated from environment studies with spheres of the radius 8.0 Mpc, 5.6 Mpc and 3.2 Mpc. The first value of $R = 8.0$ Mpc was chosen in order to compare the averaged squared density contrast directly with σ_8 from results obtained by other redshift surveys in the literature. $R = 5.6$ Mpc probes the LSB-HSB bias on scales of the size of large scale structure filaments (~ 5 Mpc, e.g.: White et al. 1987b, Doroshkevich et al. 1997). The value of $R = 3.2$ Mpc was selected for testing the LSB-HSB clustering on scales of the diameter of clusters. Furthermore, this radius undersamples the averaged size of filaments only marginally. Therefore, it can be used to support the results obtained from the bias study of $R = 5.6$ Mpc concerning the filaments, which of course also shows structure on scales of $R = 3.2$ Mpc. It is not reasonable to calculate the bias using studies based on spheres with smaller radii, because using spheres of a radius R means that the local galaxy density is averaged over a sphere of the radius R. If the radius is chosen too small, the fluctuations of the density from galaxy to galaxy get too high. Since the bias is a measure of fluctuations, the study is less meaningful when choosing lower values for R. This can also be explained in another way. The radius R of the sphere is a kind of smoothing parameter for the density field. If one chooses this parameter to be low, the smoothing effect is too low, and the noise overwhelms the signal. This effect can directly be seen in Table 4.3. For all cases and redshift ranges as well as for both galaxy types the variance of the density contrast increases with decreasing sphere radii.

With extracting the square-root of the values $< \delta^2_{8,\mathrm{HSB}} >$ of the different redshift ranges one gets results which correspond to σ_8 and can be compared to the results of other redshift surveys (the small fraction of the LSB contribution to the value is in that case neglected). For this comparison, the not cluster corrected case containing both field and cluster galaxies was consulted, which corresponds to the same case probed in other surveys. For the redshift interval of $0.01 \leq z < 0.055$ the result

$$\sqrt{< \delta^2_{8,\mathrm{HSB}} >} = 1.02 \pm 0.10$$

Table 4.3: LSB-HSB galaxy bias parameter. The Table shows the second moment of the density contrast for LSBs and HSBs as well as the bias parameter b in dependence of the sphere radius R. Note that the values of b are significantly below 1 except for the cluster corrected redshift interval of $0.01 \leq z < 0.055$ where $b \sim 1$ holds.

LSB-HSB Galaxy Bias			
redshift: $0.01 \leq z < 0.055$ / not cluster corrected			
$R\,[\mathrm{Mpc}]$	$< \delta^2_{R,\mathrm{LSB}} >$	$< \delta^2_{R,\mathrm{HSB}} >$	$b(R)$
8.0	0.798	1.039	0.876
5.6	0.912	1.256	0.852
3.2	1.081	1.460	0.861
redshift: $0.055 \leq z < 0.1$ / not cluster corrected			
$R\,[\mathrm{Mpc}]$	$< \delta^2_{R,\mathrm{LSB}} >$	$< \delta^2_{R,\mathrm{HSB}} >$	$b(R)$
8.0	0.612	0.745	0.906
5.6	0.643	0.835	0.877
3.2	0.769	1.026	0.866
redshift: $0.01 \leq z < 0.055$ / cluster corrected			
$R\,[\mathrm{Mpc}]$	$< \delta^2_{R,\mathrm{LSB}} >$	$< \delta^2_{R,\mathrm{HSB}} >$	$b(R)$
8.0	0.600	0.596	1.002
5.6	0.649	0.655	0.994
3.2	0.799	0.782	1.009
redshift: $0.055 \leq z < 0.1$ / cluster corrected			
$R\,[\mathrm{Mpc}]$	$< \delta^2_{R,\mathrm{LSB}} >$	$< \delta^2_{R,\mathrm{HSB}} >$	$b(R)$
8.0	0.607	0.705	0.927
5.6	0.637	0.775	0.906
3.2	0.756	0.931	0.902

was obtained. For the range $0.055 \leq z < 0.1$ the value

$$\sqrt{< \delta^2_{8,\mathrm{HSB}} >} = 0.86 \pm 0.10$$

holds. The errors are a first guess obtained from the scatter of the values in Table 4.3. For a more accurate determination of the uncertainties, Monte Carlo simulations are necessary, but this would go beyond the framework of the present dissertation. Both values agree with the results obtained for the Las Campanas Redshift Survey (LCRS, Shectman et al. 1996) in the literature. Matsubara et al. (2000) obatined a value of $\sigma_8 = 0.79 \pm 0.08$ by performing a Karhunen-Loeve transformation eigenmode analysis on the LCRS data. Astronomical textbooks give a value of $\sigma_8 \sim 1$ for the clustering properties of the galaxies measured in the LCRS (e.g.: Sparke & Gallagher 2000).

For the study containing field and cluster galaxies within the redshift range of $0.055 \leq z < 0.1$ the density contrast for LSBs (equation 4.5) stays clearly below the value obtained

for HSBs (obtained from equation 4.5) for both the cluster corrected case containing only field galaxies as well as the case containing cluster and field galaxies. This holds for all tested scales ($r = 8.0, 5.6, 3.2 \, \mathrm{Mpc}$). Thereby the density contrast for LSBs is below that value of HSBs indicating that LSBs are less strongly clustered than HSBs. This is also seen in the bias parameter b. For this redshift range it contains values between $b = 0.906$ and $b = 0.866$ for the cluster and field galaxy case and values in the interval of $b = 0.927$ and $b = 0.902$ for the case containing only field galaxies. These two cases do not differ a lot. This shows that the galaxy environment of LSBs within the redshift interval of $0.055 \leq z < 0.1$ is clearly less dense than that of HSBs for both the cluster corrected and not corrected case.

The first case shows a little bit lower bias parameter than the case containing pure field galaxies. This is due to the fact that clusters of course rise the variance of the density contrast. The sample LSBs are not often located in clusters (only one LSB of that redshift range was found in a cluster). This would explain the increased bias parameter in the case of pure field galaxies with respect to the case containing field and cluster galaxies. Nevertheless, the bias parameter holds below one for the comparison of the density contrast between field LSBs and field HSBs within that higher redshift interval. Taking into account the fact that the LSB population of that redshift range is dominated by larger LSBs (Chapter 3), this gives strong evidence for a scenario in which the larger type LSBs formed and evolved in a lower density region than HSBs. Since there is still a lower density contrast for LSBs against that of HSBs in the cluster corrected case containing pure field galaxies, this gives strong support for the initial impression from the pie slice (Section 4.2.2). This impression was, that for the higher redshift interval $0.05 < z < 0.1$ the (larger) LSB galaxies are located at the outer rims of the LSS, and some of them are even found in void regions.

The examinations on the density contrast and bias parameter of LSB and HSB galaxies within the redshift range of $0.01 \leq z < 0.055$ delivered similar results except for the cluster corrected case. There, a difference in the density contrast between these two galaxy populations is not found. This results in a bias parameter of $b \sim 1$. Taking into account that the LSB population in this redshift range is dominated by small, dwarfish LSB galaxies, one can conclude that these galaxies are found in an environment which is more similar to that of HSBs. However, the average neighbour diagram of that case shows the presence of a density contrast (Figure 4.4, left).

In the case of cluster and field galaxies (and the same redshift interval of $0.01 \leq z < 0.055$), a significant difference in the density contrast with differences of ~ 0.2 up to ~ 0.4 are found. This results in a bias parameter of $b \sim 0.86$ indicating that these mainly smaller LSB galaxies do not have the same clustering properties like cluster and field HSBs combined. Taking into account the result above from the cluster corrected case, that there is no difference between the clustering properties of field HSBs and LSBs, it follows that they must be rare in clusters. This is also shown in the numbers of LSBs from the neighbour counting study, whereas the number of LSBs is decreased only by $\sim 5\%$ when applying the cluster correction. The number of HSBs is decreased by more than 7% in case of cluster correction. All in all the galaxy bias study confirms the impression from

the pie slice as well as the results of the mean number of neighbour diagrams (Figures 4.3, 4.4). The vicinity of LSB galaxies indeed shows a less galaxy number density than that of HSBs. This holds for the sample containing preferably larger LSBs as well as the small LSBs. Only in the comparison between the environment of small LSBs and field HSBs, no significant bias is found.

In all cases of the determined density contrast, the values are increased with decreasing sphere radius. This shows the smoothing effect of the sphere radius discussed before. Therefore, it is not reasonable to use too small sphere radii (smaller than 3.2 Mpc) since the noise would get to high, and the difference in the density contrast between LSBs and HSBs would disappear in the noise. Furthermore, the used sphere radii correspond to suitable values in order to probe differences on scales of the structures which form the LSS.

4.4 Conclusions

It was shown using several ways that the environment of LSB galaxies consists of a less high galaxy number density than the environment of HSB galaxies. The average number of neighbour galaxies is lower for LSB galaxies than for HSB galaxies. This holds for all cases (containing clusters and field galaxies and the pure field galaxy case) and the two examined redshift intervals. Furthermore, this was fact for all examined scales in the range between 0.8 and 8.0 Mpc. Actually, it could be proven that LSB galaxies have less neighbours on those scales than field HSB galaxies. This is important, since LSBs are blue galaxies and therefore they are not expected to appear in clusters frequently. Therefore, they are preferably field galaxies. Since they are even less clustered than field HSB galaxies, the environment could play a major role in the fact that these galaxies evolved to LSBs and did not become HSBs, although they have enough gas masses to form as many stars as HSBs.

The statistical significance of the result would be relatively low, if all the cases and scale lengths would be considered separately. However, the fact that all averaged LSB neighbour counts lie systematically below that value of the HSB counts, gives strong evidence that the effect is true and not due to statistical noise. Furthermore, the investigations on the LSB-HSB galaxy bias show that there is an offset in the density contrast between LSB and HSB galaxies, in that direction that LSBs have a less dense environment than HSBs. This holds for both redshift ranges in the case probing field and cluster galaxies, and in the case containing pure field galaxies in the higher redshift interval. Merely, the case of field galaxies in the lower redshift interval does not show a significant LSB-HSB bias, implying a possible change in the evolution of dwarf LSBs.

All the presented results fit well into the following formation scenario, which was proposed by Bothun et al. (1997). Galaxy formation takes place due to an initial Gaussian spectrum of density perturbations with much more low-density fluctuations than high density ones. Many of these low-density perturbations are lost due to the assimilation or disruption during the evolutionary process of galaxy formation but a substantial percent-

age of the fluctuations survives and is expected to form LSB galaxies. Further on, one can assume that the spatial distribution of the initial density contrast consists of small scale fluctuations superimposed on large-scale peaks and valleys. Small-scale peaks lead to galaxy formation, whereas the large-scale maxima induce cluster and wall formation of the LSS. Based on the results presented in this dissertation, it is proposed that the galaxies formed in the large-scale valleys may develop into LSB galaxies due to their isolated environments whereas HSB galaxies formed mainly on the large-scale peaks. The isolation of LSB galaxies on intermediate and small scales must have effected their evolution since tidal encounters acting as triggers for star formation would had been rare. Also the infall of massive gas clouds would had been improbable or seldom in that regions of the initial universe. Hence, no effective star formation was induced in LSBs. The results give strong evidence for this scenario, since the observed isolation of LSB galaxies takes place on scales between 0.8 and 8 Mpc. This also includes scales in the range of 5 Mpc, which is exactly the typical size of LSS filaments (e.g., White et al. 1987b, Doroshkevich et al. 1997). This means that the isolation of LSBs takes place on scales beyond the size of all structures (containing matter in form of galaxies) in the LSS, namely clusters, walls and filaments.

Hence, we conclude that LSB galaxies were formed in the regions of lower density in the initial universe. These regions then later became the voids of the LSS due to the fact that the higher density regions started to clump into clusters, walls and filaments of the LSS caused by gravitation. Until today, the LSB galaxies which were formed in underdense regions have migrated to the edges of the filaments due to gravitational infall, but some of them still remain in the voids where they were born. Due to the surrounding low density environments of LSBs, gravitational triggers by encounters with neighbouring galaxies were rare and the infall of massive gas clouds were improbable. Hence, a sufficient trigger for star formation lacked for LSB galaxies. They evolved more quietly and slowly with a gas surface density permanently below the Kennicutt (1998a) criterion resulting in a very low star formation efficiency. This scenario also corresponds to the results, that LSB galaxies are on average bluer than HSBs (e.g.: McGaugh & Bothun 1994, de Blok et al. 1995, van den Hoek et al. 2000) with low metallicities (McGaugh 1994). Since galaxy formation takes place at first in higher density regions and later in lower densities (e.g.: Springel et al. 2005), the LSB galaxies are expected to be on average younger than their HSB colleagues. This would result in blue colors and lower metallicities, due to a lower age of the dominant stellar population. An examination of the age of the dominant stellar population in seven LSB galaxies showed that this age ranges from 1.4 Gyr up to 7 Gyr (Haberzettl 2005). This means that the seven sample LSBs had their major star formation event at a redshift of $0.2 \lesssim z \lesssim 0.5$. These are all hints to the scenario that LSBs did not form stars sufficiently due to their location in low density environments. For a further discussion see Chapter 7.

Chapter 5

Current Star Formation Rate of LSBs

In addition to studies of the SDSS public available data, a project with follow up observations was defined and is currently running. For this project, observing time at the 2.2 m telescope of the Calar Alto Observatory / Spain was granted, and observations were performed. The goal is to measure the current Star Formation Rate (SFR) of LSB galaxies using Hα narrowband exposures and to put it into a context with their environments.

Why is it not possible to use the SDSS data in order to obtain the current SFR from the Hα line of the SDSS spectroscopy? This is due to the small aperture covered by the fibers centered at each spectroscopy target galaxy. The aperture of the fiber is 3" which corresponds to a diameter of 3 kpc for a galaxy with a redshift of $z = 0.05$. This aperture of the fiber is placed on the center of the galaxy. However, current star formation mainly takes place in the disk and in the spiral arms of the galaxies, but not in the center. Hence, the flux of the Hα line measured in a spectrum, which was obtained from the central 3 kpc of the galaxy, is not a good indicator of the current SFR. Figure 5.1 shows an Hα image (left) of the galaxy "SDSS 986_538" (Plate_Fiber numbers as identifier) obtained at the 2.2 m telescope of the Calar Alto Observatory. The composite image obtained from the SDSS imaging data is shown, too (right). Both images are scaled equally. The Hα image shows that the main flux in Hα is produced in the front spiral arm, which is not covered by the fiber centered on the galaxy. In that case, as well as in many other cases, the Hα flux from the center, as obtained from the SDSS spectra, is not useable for measuring the current SFR of the galaxies.

5.1 Project Description

As described in Chapter 1, LSB galaxies generally possess a gas surface density which is below the Kennicutt (1989) criterion for the formation of giant star forming molecular clouds (Pickering et al. 1997). However, their total content in gas mass should be sufficient to form stars frequently and to brighten the stellar disk like HSB galaxies do. The possible cause for that star forming behaviour is found in the environment (Chapter 4, see also Bothun et al. 1993, Mo et al. 1994, Rosenbaum & Bomans 2004). LSB galaxies are
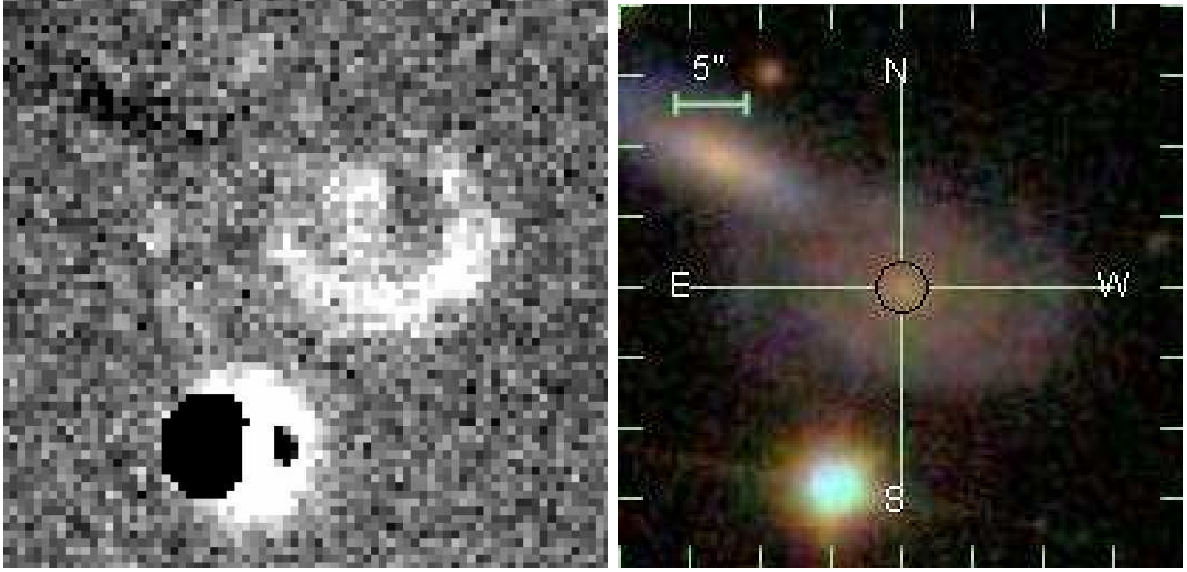
Figure 5.1: Continuum subtracted Hα image of the LSB galaxy SDSS 986_538 (left panel). It consists of 2×1800 s exposures obtained at the 2.2 m telescope of the Calar Alto Observatory, Spain (left panel). The colored image (right panel) is a composite image of the same galaxy obtained from the SDSS data and produced by the SDSS pipelines. The size and location of the fiber for the SDSS spectroscopy are indicated by the black circle. The main flux in Hα comes from the front spiral arm and not from the center, where the fiber obtains the flux from. Therefore, the SDSS spectroscopic data is not suited for measuring the current SFR. Note that the superimposed galaxy at the upper left of the colored image vanishes in the Hα image, since it has a different redshift. Hence, it is not a real neighbour, but only a projected one.

more isolated than HSBs on scales ranging from 0.8 Mpc up to 8.0 Mpc and below 0.5 Mpc (Zaritsky & Lorrimer 1993). HSBs, which favour a dense environment, form stars sufficiently, but LSBs form stars less frequently. Therefore, a difference in the current SFR is expected between LSBs which are located in an extreme isolation like in voids, and LSBs which are found in more dense environments like at the edges of the filaments. Extremely isolated LSBs are expected to show less current star formation than LSBs in environments with higher galaxy densities.

In order to probe this hypothesis, whose verification would deliver a further hint for the verification of the formation scenario of LSBs (Chapter 7), Hα observations (as current SFR indicator) of LSBs at the 2.2 m telescope of the Calar Alto observatory have been done and are still running. Since the environment of each of the LSBs found in the SDSS was known from the studies (Chapter 4), the follow up observations were performed for a subsample containing 60 LSBs with a number of neighbours varying between 0 and 10 (and sporadic beyond 10) on a scale of 2.6 Mpc. The observations were divided into several blocks. The first one was performed in September 2003, another one in November 2004,

the third one in April 2005 and the last one in December 2005. A further observation run is planned for March 2006.

Since taking spectra of individual LSB galaxies is a very telescope time consuming activity, it is possible to observe only few objects during one observation run. To perform those observations on a sample of 30 objects or more would consume more than 15 nights at a telescope like the Calar Alto 2.2 m. Therefore, for the project another way was used to probe the star formation of LSBs in dependence of environment. The project planned to measure the current SFR by Hα narrowband images of a sample of 60 LSBs taken from the SDSS DR 3. The goal was to search for a link to the surrounding galaxy density which comes from the environment studies of Chapter 4. The sample contains two random samples of 30 LSBs each. One part is from the equatorial area of the SDSS observable in autumn, the other 30 LSBs are located in the northern cap area which can be best observed in spring. The sample size was chosen in order to give a good compromise between telescope time consumption and statistical significance.

The correlation of the SFR of LSBs with their spatial distribution requires precise redshift data, as delivered by the SDSS. Therefore, it is not possible to use present Hα surveys for our studies, since they do neither overlap with the equatorial strips of the SDSS public releases nor provide their own spectroscopic redshift information. However, a comparison of the current SFR of those galaxies to that of HSB galaxies using the forthcoming results of present day Hα surveys like the SINGS (Kennicutt et al. 2003) and SINGG (Meurer et al. 2001) survey was planned, too. By comparing the SFRs of LSBs to that of HSBs, the results will not only provide progress in the understanding of the formation and evolution of LSB galaxies but also contribute to the galaxy formation and evolution scenarios in general.

5.1.1 The Setup of the 2.2 m Telescope

Since only sky regions from the northern hemisphere are contained in the SDSS, it is reasonable to perform follow-up observations using telescopes at sites located at northern latitudes. Therefore, the Centro Astronómico Hispano Alemán (CAHA) at Calar Alto was used. The CAHA 2.2 m telescope in connection to the focal reducer and spectrograph unit "CAFOS" is a very suitable instrument for the intended SDSS follow-up project.

The 2.2 m telescope of the CAHA is an f/8 telescope of the Ritchey-Chrétien design with an aperture of 2200 mm diameter and an effective collecting area of $2.942 \, \mathrm{m}^2$. It is located at a latitude of ϕ=37°13' 24" N, a longitude of λ=2°32' 45.66" E and at an altitude of 2168 m. It is pivoted traditionally with an equatorial fork mounting.

For the SDSS follow up program, the Calar Alto Faint Object Spectrograph (CAFOS) was used consisting of a focal reducer and a spectrograph unit. The focal reducer sets down the aperture ratio of the 2.2 m telescope from f/8.0 to f/4.2. This instrument provides direct imaging, spectroscopy with grisms and a longslit or multi-object masks. Polarimetry can be performed directly and with grisms. Additionally, the polarimetry device can be replaced by a unit containing a Fabry-Pérot-Etalon which provides the possibility of imaging spectroscopy. The Etalon has a rather moderate resolution of between 15 Å and

23 Å and a separation between adjacent orders of about $20\times$ this value (between 300 Å and 450 Å). In order to avoid contamination with other orders, an order separation filter with a Full-Width of Half Maximum (FWHM) of ≤ 300 Å can be used in the filter wheel.

For pure spectroscopy, a longslit of tuneable width between $30\,\mu$m and $1000\,\mu$m, which corresponds to an apparent size of 0.35" up to 12" and a length of $50\,$mm (=9') is available. In order to take multi-object spectra, two focal plane masks can be inserted by the user, but those masks must be produced by the users themselves. As dispersive elements, up to eight grisms of several wavelength ranges and resolutions varying from $1.8\,$nm/arcsec up to $0.4\,$nm/arcsec ($0.98\,$nm/pixel to $0.20\,$nm/pixel for the SITe-1d chip) are available. For pure imaging, a filter wheel with twelve filter positions is present, which can be equipped with filters from the CAHA filter set (Johnson, Cousins, Gunn, Narrowband etc.).

The standard CCD for CAFOS is a SITe-1d 2k×2k chip with a pixel size of $24\,\mu$m (i.e. 0.53"/pixel). This provides the widest field of 16' diameter and the best performance regarding read-out noise and image quality with respect to the other possible solutions (Loral-80 or Tektronics-13c chip).

5.1.2   Data Acquisition for the Project

The data acquisition was planned to be performed during several observation runs. The first one was done in September 2003. During this run, not only Hα images but also longslit spectra of 4 void galaxies using the grisms g100 and b100 as dispersive elements were taken. The following runs were scheduled for November 2004 and the other one for April 2005. Due to bad weather only seven galaxies in the first run and only six objects in the second run were observed. However, during the observations the weather conditions were unstable. One more object was obtained in service mode under good conditions, since two hours of observation time of the second run had to be ceded for a target of opportunity and were given back in service mode. When it became clear that the weather would be unstable during the observation runs, it was decided to limit the observations only to objects with a very low and very high surrounding galaxy density. Therefore, it should be possible to draw first qualitative conclusions from this project without a quantitative statistical study. The proposals were signed with a flag that observation time was lost due to bad weather during previous runs and resubmitted. Hence, observation time for two more runs, one in November 2005 and the second one in April 2006 was granted.

The Hα line intensity was measured using the Fabry-Perot Etalon of CAFOS in the imaging spectroscopy mode, except for the very first observation run. There, narrow band filters of different wavelengths were used. However, the Etalon proved to be the optimal way in order to select for each galaxy individually redshifted Hα lines. In the case of the Fabry-Perot Etalon, narrow band passes were used as order separation filters ($\lambda\,$[nm]/FWHM [nm]: 674/18, 690/20, 703/34, and 716/14). They were placed into the optical path behind the Etalon for the suppression of adjacent orders. Two Hα images were taken for each galaxy with an exposure time of $1800\,$s each under good conditions and of $2700\,$s each, if the transparency of the atmosphere was bad. For the subtraction of the continuum, a broad band image was taken in the Gunn-r bandpass ($\lambda\,$[nm]/FWHM [nm]:

656/84 or 663/105) which overlaps in wavelength with the redshifted Hα lines of the sample galaxies. It was decided to use the Gunn-r filters instead of Johnson-R bandpasses, since they provide a better link to the SDSS photometry, which is based on modified Gunn filters. The exposure time for the r-band images was 300 s for all galaxies. During the night also observations of spectrophotometric standard stars were done. For each galaxy a standard star frame was taken with the same Etalon setup in wavelength and order separation filter as for the galaxy before the changeover to the next sample object. The stars GD 50, G 158-100, BD +25-4655, and Feige 34 were used as spectrophotometric standards in the run of November 2004. During the nights in April 2005, the spectrophotometric standard stars HZ 21 and HZ 44 were observed due to best visibility. The Etalon was calibrated before dusk and recalibrated several times during the night as it is very sensitive to temperature changes.

For data reduction purposes at least 10 bias frames for each night were taken before starting the observations. Domeflats were also made at that time for the Gunn r filters (at least three per filter per night) and for the narrowband filters used for order separation. For each galaxy two domeflats were made in imaging spectroscopy mode with the Etalon tuned to the wavelength of the redshifted Hα line of the scrutinized galaxy. When the sky was clear at dusk or dawn skyflats for the Gunn-r filters were taken, too.

5.1.3 Data Reduction for the Project

The software package 'Image Reduction and Analysis Facility' (IRAF, Tody 1986) was used to perform the reduction on the data of the project. Each calibration and science frame was overscan corrected as a first reduction step. The bias frames of each night were combined to a masterbias which was subtracted from all flatfield and science exposures of the corresponding night. The Gunn-r flats of each night were combined to a masterflat and normalized to an average count rate of 1. If skyflats were available for the corresponding night, they were used, otherwise domeflats were taken.

Each science frame was cosmic ray corrected using the LACOS algorithm by van Dokkum (2001). Then, the r-science frames were divided by the normalized masterflat. The reduction of the Hα science frames was more complicated. Since the Hα line of each galaxy had a different redshift, one had to produce a masterflat for the Hα science frame of each galaxy. All domeflats of one night with one Etalon frequency setup were combined to a masterflat for the Hα frames of a certain galaxy and normalized to a count rate of 1. Additionally, all domeflats of each night of a certain narrow band filter were combined to a normalized masterflat.

For the production of the special masterflat for the Hα images of each galaxy, the normalized masterflat of the corresponding narrowband order separation filter was multiplied with the normalized Etalon masterflat of the certain galaxy. The Hα images of each galaxy were then divided by the corresponding factor flat produced as described before. After that, the Hα science frames of each object were combined. Since both the science images and the factor flats showed diffraction annuli in the outer part of the image due to interference patterns in the Etalon, it was necessary to flatten the Hα science frames ad-

ditionally. Therefore, the image background consisting of sky background and interference pattern was fitted using the software tool SExtractor (Bertin & Arnouts 1996).

For each galaxy, the continuum was subtracted in the combined Hα image using the r-band exposures. For the calibration to the same flux level, at least six stars near the center were photometricly measured in both frames. Therefore, a simple PSF-fit was done to the stars using IRAF and the flux was measured. The flux relationship between the two frames was measured by fitting a linear function to the flux values of the stars in both frames. Then the r-band image was divided by the slope obtained by the fit and this image was subtracted from the combined Hα image. Data acquisition and reduction is ongoing for this project but preliminary results are presented in the following Section.

5.2   Status Report for the Project

Due to bad weather, up to now only 27 galaxies of the sample were observed. The objects selected for observations were chosen to either have a very low number of neighbours (0-1) on a scale of 2.6 Mpc or to possess a high number of neighbours (≥ 5) on that scale. During the run in November 2004 also objects with 2 or 3 galaxies in their vicinity were observed, but for the further runs it was decided to choose objects with more extreme values for the number of neighbours. Therefore, the expected effect should be observable, although the data acquisition is not yet finished. However, is should not yet be possible to resolve a detailed gradient in the current SFR when going from dense environment to lower density regions.

5.2.1   Preliminary Results

Due to the fact that the data obtained from the Calar Alto runs is not completely reduced, since the last observation run was in December 2005, only preliminary results can be shown. As a measure for the current star formation activity, the number of H II regions was counted in these data. This method has the advantage that it also works for galaxies whose raw images have not yet been reduced. For all sample LSBs which were observed up to now during several runs at Calar Alto, the Hα images and for comparison reasons the r-band images were checked by eye. It was searched for plain H II regions and their numbers were counted. Then, the database obtained from the environment studies (Chapter 4) was used to look up the number of neighbours of the observed LSB galaxies on a scale of 2.6 Mpc.

Figure 5.2 shows the number of H II regions versus the number of neighbours for the sample galaxies which have been observed. Since the values are discrete ones, some points in the diagram are multiple covered by different galaxies. A trendline obtained from a linear regression with a likelihood of the fit of $\chi^2 = 0.38$ was added to the plot. In this diagram a trend, that the galaxies with a large number of neighbours (≥ 6) possess H II regions more frequently than LSBs which inhabit regions of lower galaxy density is seen. However, this results are preliminary, since the search by eye is subjective and the number of objects is low, but a first trend for the hypothesis, that environment influences the
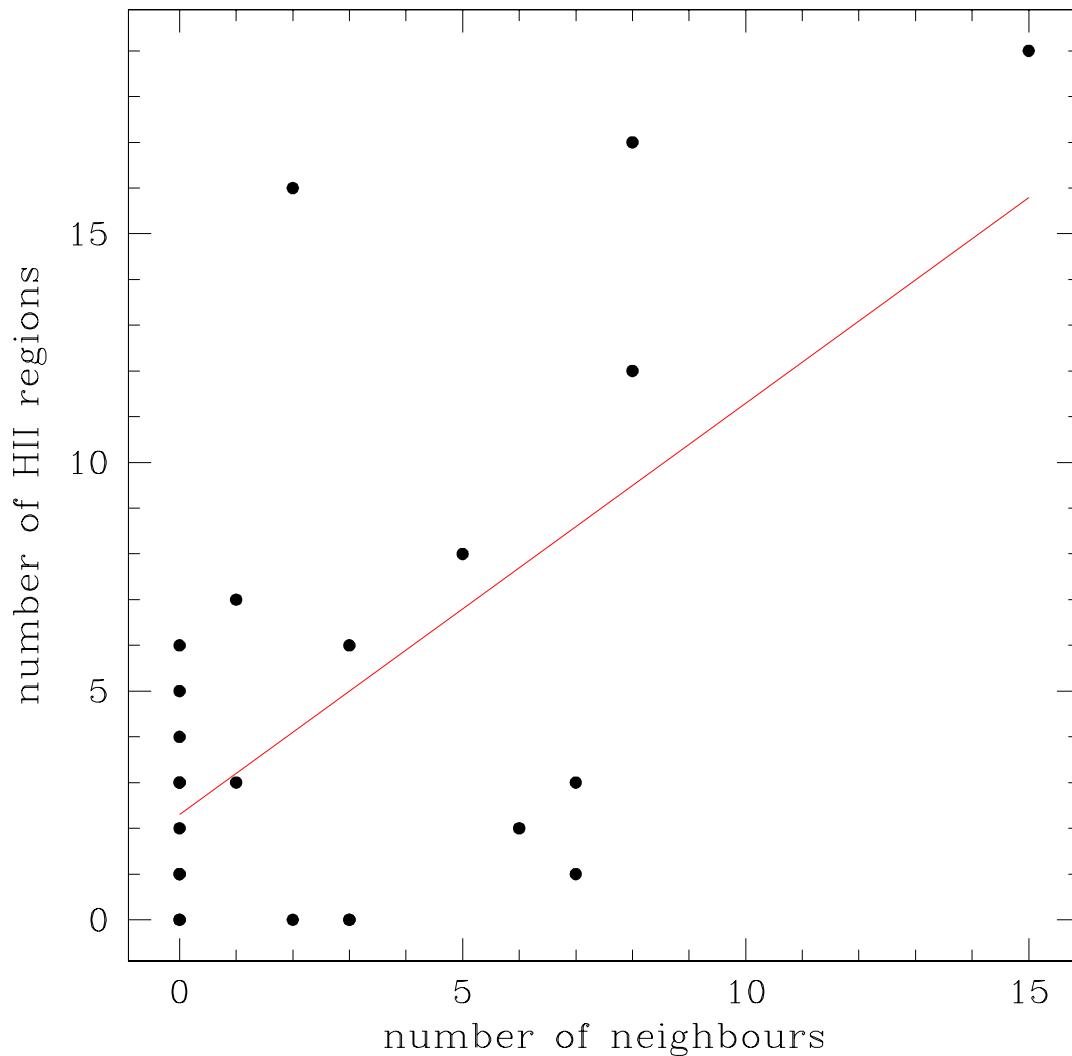
Figure 5.2: The diagram shows the number of H II regions vs. number of neighbours of the galaxies, which are observed up to now for the current SFR of LSBs project. A first trend can be seen, that a higher number of neighbours results in a larger amount of H II regions. This indicates an increased current SFR.

current star formation for LSBs is found.

The Hα image of Figure 5.1 shows that publications, which use the spectroscopy of the SDSS in order to derive the current SFR (e.g.: Gomez et al. 2003, Hopkins et al. 2003, Goto 2005), are rather questionable. Gomez et al. (2003) used the Hα emission line of the Sloan fiber spectroscopy in order to determine the current SFR of each galaxy within a volume limited sample of 8598 galaxies with a redshift range of $0.05 \leq z \leq 0.095$. They

found, that the overall distribution is shifted to lower values in environments, which possess a high local projected galaxy density. The galaxy population of the field regions showed a higher average SFR than that in clusters. Furthermore, they examined the star forming behaviour as a function of clustercentric radius in 17 galaxy clusters. This resulted in a change in the SFR distribution in comparison to the SFR distribution in the field at cluster radii of 3-4 virial radii, when going from outer to inner radii. However, this is the opposite behaviour than observed in the LSB current SFR presented here. This might be caused by the fiber effect, since Gomez et al. (2003) concluded on the total SFR of the galaxies from its central value.

Even if the smear images of SDSS spectroscopy are used (see Chapter 2), as it is the case in the work of Hopkins et al. (2003), the effective aperture covered is still small (5"×8"). In that case, also aperture corrections are wrong, which were done by assuming the Hα emission directly to scale with the stellar continuum. This is due to the fact, that the main Hα flux comes from specific H II regions of the galaxy and not from the stellar continuum. Hence, in order to measure the current SFR of local galaxies with extensions much larger than the apparent fiber size, data obtained from the SDSS fiber spectroscopy is useless.

Chapter 6

The Search for AGN Activity in LSB Galaxies

In this Chapter the search for AGN activity in the LSB galaxies is described. For this search, the LSB SDSS DR4 sample obtained from the environment studies of Chapter 4 was used. Therefore, it was evident to study the environment of the AGN LSBs, too.

6.1 A brief History of Active Galactic Nuclei

The discovery of AGN galaxies started with an observation done by Fath (1908). He found strong emission lines in the spectra of the spiral galaxy NGC 1068. In 1943, Carl Seyfert found in the spectra of 12 galaxy cores strong broad emission lines of ions, which could only be ionized by a powerful energy source with higher energies than photons of young stars – which ionize H II regions – deliver (Seyfert 1943). Moreover, these galaxies showed cores with an extremely high surface brightness. Some of the galaxies possess broad lines with a full width at half maximum (FWHM) of about $\sim 8500\,\mathrm{km/s}$.

The so called Active Galactic Nuclei were found to emit radiation over the whole electromagnetic spectrum from γ- and X-ray, ultraviolet, over optical, down to the radio waves. They achieve luminosities of around $10^{12}L_\odot$. They possess very compact emitting regions of not more than $100\,\mathrm{pc}$, which is known from variability measurements taking into account the speed of light. In the 1950s many of the strong radio sources were identified with optical counterparts consisting of luminous elliptical galaxies. These galaxies were called radio galaxies. Resulting of the 3C and 3CR catalogues which are surveys of the northern hemisphere at radio frequencies of $\nu = 158\,\mathrm{MHz}$ and $\nu = 178\,\mathrm{MHz}$, Matthews & Sandage (1963) found a point like (and stellar like) source named 3C48 with a complex spectrum consisting of a blue continuum and strong broad emission lines. A second, similar object (3C273) was identified with its optical, point- and stellar-like counterpart (Schmidt 1963). This type of object was called Quasar for quasi-stellar radio source. Later, radio quiet quasars were discovered by searching photo plates for objects which looked apparently stellar on images, but possessed too strong infrared or ultraviolet emissions to be stars.
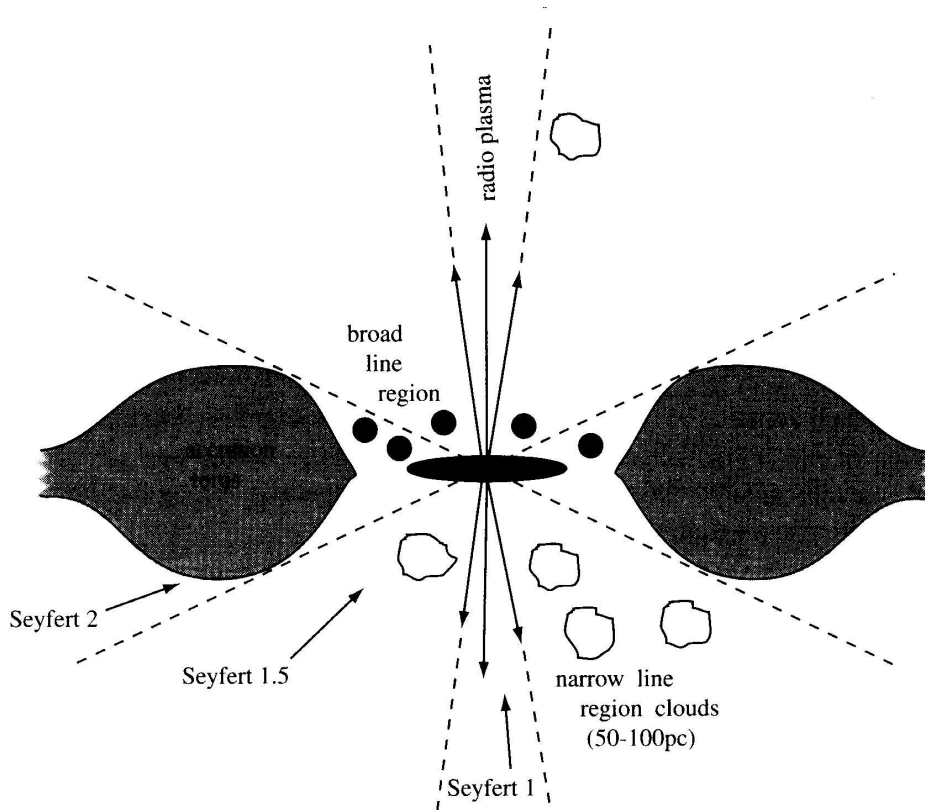
Figure 6.1: From Sparke & Gallagher (2000): A simple model for AGNs including relativistic twin jets aligned perpendicular to the plane of the accretion disk. The fast moving gas clouds of the broad line region are ionized by radiation produced in the jets and the accretion disk. The more diffuse and slow moving gas clouds of the narrow line region are located at larger radii. If the galaxy is observed face-on, the light of both regions reach the observer who gets spectra dominated by broad lines. This case forms then a Seyfert 1 galaxy. If the galaxy is aligned near to edge-on, the broad line region is obscured by the accretion torus and the spectra contain only narrow lines. This is the Seyfert 2 case. A mixed type appears, if the galaxy is seen under an angle between edge- and face on. The emission line in its spectra then show narrow peaks with broad wings (Seyfert 1.5).

These objects were called Quasi Stellar Objects (QSOs).

These phenomenons and its different appearances described above are today ascribed to one simple AGN model representation called unified model (Figure 6.1), which looks different, if one observes it at different distances and angles. Thereby, the presence of a supermassive black hole ($M_{BH} \sim 10^6$-$10^{10} M_\odot$, Sparke & Gallagher 2000) in the center of an AGN galaxy is assumed, which accretes matter from its vicinity due to its deep gravitational potential well. Thereby, the infalling gas and stars loose potential energy when falling into the black hole and the potential energy is transformed into kinetic energy. The infalling

matter normally possesses angular momentum. Therefore, it cannot fall directly onto the black hole, since the angular momentum would produce a barrier potential. Hence, due to angular momentum conservation and impulse transfer with other infalling particles (friction), the accretion has to take place in an accretion disk. If the forces caused by friction are much smaller than the gravitational force, the accretion disk starts to rotate following the Kepler-laws. In that case the differential rotation of the Keplerian accretion disk in connection with the friction causes the gas to heat and to loose kinetic energy. Hence, it spirals down to the black hole. Due to viscosity and friction, the kinetic energy of the accreted matter is transformed into heat, which causes radiation. Often the AGN phenomenon is ascribed to a relativistic jet, located in the center and aligned perpendicular to the plane of the accretion torus. In a nutshell, this is due to the inward flow of the hot ionized gas. Thereby, the magnetic field lines are pulled inward. Close to the black hole, the field density is high enough to produce a relativistic jet. One has to point out, that this is a brief summarization of complicated magnetohydrodynamic processes. The jet is responsible for a part of the infrared flux and all of the radio flux caused by relativistic electrons emitting synchrotron radiation. These electrons also scatter some radio or infrared photons up to higher energies. Hence, γ-rays are produced. The X-rays and ultraviolet radiation comes from the hottest innermost part of the accretion disk and partially from the jet, whereas visible light is also produced in the disk and partially in the jet. The infrared photons come from dust grains surrounding the disk, heated up by the radiation of the nucleus.

Seyfert galaxies are preferably spiral galaxies. They are divided into 2 subtypes, the Seyfert 2 with narrow (FWHM$\leq$1000 km/s) emission lines, and the Seyfert 1 which show broad (1000 km/s$<$FWHM$\leq$10000 km/s) lines. Their nuclei are point sources in X-ray and radio observations, whereas they appear weak in the latter ones. Due to obscuration of the central region, Seyfert 2 are normally less luminous than the Seyfert 1 types. A mixed type exists, which shows spectra with sharp peaked emission lines settling on broad wings. These galaxies are called Seyfert 1.5. Around 25% of Sa and SB spirals have even less luminous nuclei than the the Seyfert 2 classified galaxies and spectra with emission lines, which do not require high energies for ionization (like [OI]λ6300 and the [SII] duplet λ6716, λ6731). These objects are called Low Ionization Nuclear Emission Regions (LINERs) and they do not necessarily require an AGN as the powerful engine for ionization. These spectra could be also produced by a starburst in the nuclear region of the galaxy.

6.2 AGN Activity in LSBs, not likely?

The phenomenon of AGN activity in connection to LSB property of those galaxies is not well examined, so far. This may be caused by the fact that one expects LSB galaxies not to be common hosts of AGNs, since they possess low stellar and gas surface densities which are thought to make AGN feeding improbable or even impossible. However, is known, that giant LSB galaxies often show (mainly weak) AGN activity, like the famous Malin 1 LSB (Bothun et al. 1987, Impey & Bothun 1989). It turned out that this galaxy and other

giant LSBs are preferential Seyfert galaxies of type 1, like Malin 2 (Bothun et al. 1990) and $1226 + 0105$ (Sprayberry et al. 1993, 1995). A more systematic study by Schombert (1998) showed that the fraction of AGN activity in LSB galaxies is with around 50% much higher than that in HSBs (10%-20%, Hao et al. 2005a,b and Sparke & Gallagher 2000). These studies show that the AGN phenomenon in LSBs is more common than expected, due to the lower HSB fraction as well as the imagination that the AGN feeding is harder to maintain in LSBs since the stellar and gas surface densities are lower in LSBs than that in HSBs. Expecting giant LSBs to be no common AGN hosts but finding them to be more frequently active then HSBs, implies that the processes for AGN feeding are not well understood. This results exclusively concern giant LSBs, but what is known about AGN activity in smaller LSBs? Much less than about giant LSBs. A first step in the right direction was done by Hao et al. (2005b) and Hao et al. (2005a). They did not search for AGNs in LSBs but they studied the AGN activity also on low luminosity galaxies in the SDSS.

6.3 The Search for AGNs in LSB Galaxies

In order to perform the search for AGN activity, the equatorial region of the SDSS DR4 with the right ascension range of $120° \leq ra \leq 260°$ was used. The limit on this region was due to the fact that the emission line data stored on the SDSS server is not sorted for the inclusivity to its source galaxy. Therefore, self-made sort algorithms had to be produced in order to assign the right lines to each galaxy. Hence, the limiting factor was computing power, which achieved moderate program run times when limiting to this area.

At the beginning the SDSS-QA tool was used for downloading the data. It was queried for the emission lines [OIII] $\lambda 5007$, [NII] $\lambda 6584$, Hα $\lambda 6562$ and Hβ $\lambda 4863$ of each LSB and HSB galaxy in the region described above with a redshift of $z \leq 0.1$. The LSB galaxies were obtained by fitting exponential functions (equation 1.1) to the azimuthally averaged surface brightness profiles (provided by the SDSS DR4) in the bands g and r of all the sample galaxies and then transforming the values to a central surface brightness in Johnson B using the transformation found by Smith et al. (2002). All galaxies fulfilling the LSB criterion $\mu_B(0) \geq 22.5 \, \text{mag/arcsec}^2$ were selected. Thereby, no correction for Tolman-dimming was applied. At the time the analysis was performed, the correction for Tolman-dimming was not yet implemented into the code. However, this is justified in the case of AGN LSBs due to the following reasons. AGN LSB galaxies are expected to possess a bulge. This was verified during the analysis (Section 6.4.3). Anyway, the selection criterion refers to the central disk luminosity. Bulge-disk decomposition was not performed due to the fact that it is impossible to do it for several 100000 galaxies by hand, and no fully automatic routines for bulge-disk decomposition are available. However, a bulge leads to a overestimation of the central disk surface brightness of the fit. Hence, also if not Tolman-dimming corrected, the selected galaxies are definitely LSBs. For the distinguishing between LSBs with AGN properties and starburst galaxies in the diagnostic diagram (following Osterbrock 1989, see Figure 6.2), a model for extreme starburst galaxies from Kewley et al. (2001) was plotted
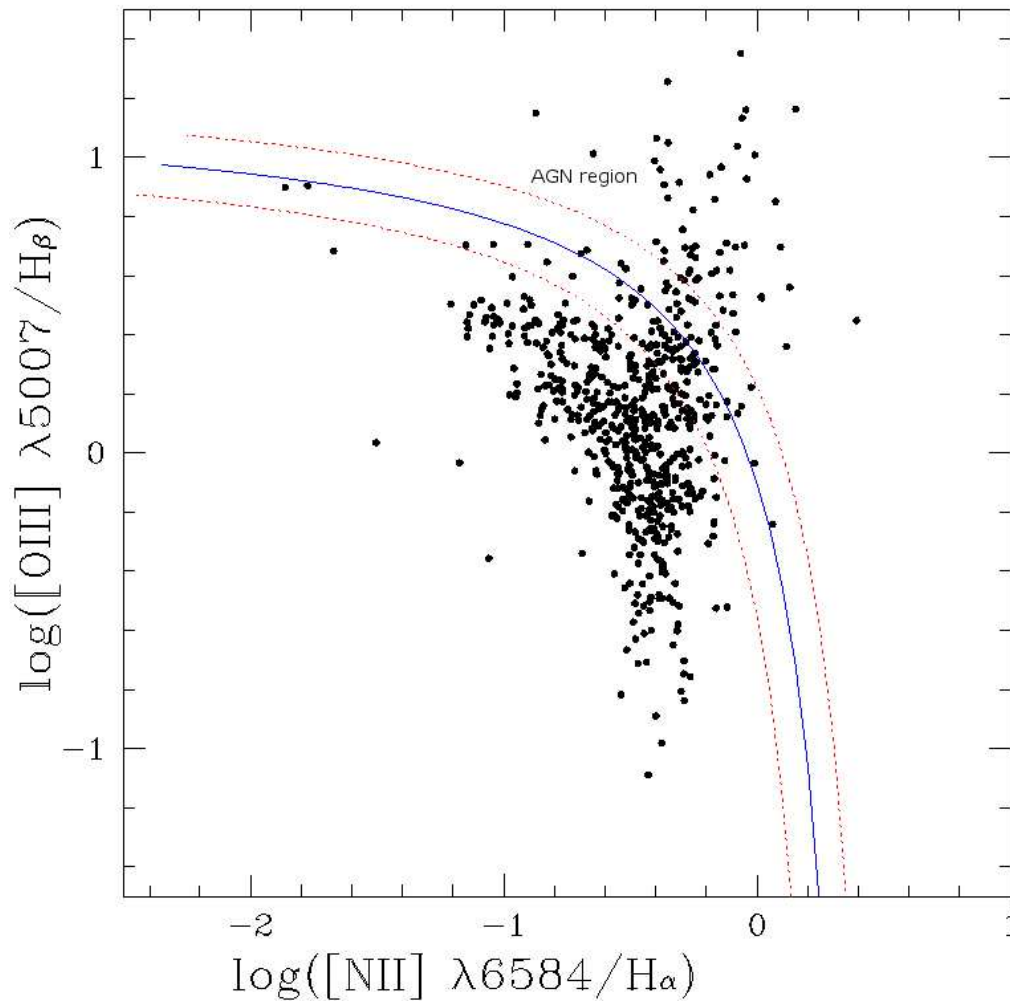
Figure 6.2: Diagnostic diagram for the selection of AGN LSBs (following Osterbrock 1989). It shows the logarithmic line ratios [OIII]λ5007/Hβ versus the line ratios [NII]λ6584/Hα which is the best suited diagnostic diagram for distinguishing between AGN and galaxies without AGN activity. The blue line is the division line between starburst galaxies and AGNs from Kewley et al. (2001). The red dashed lines are the error margins of the model. In the present dissertation, only LSB galaxies beyond the right dashed red line were assumed to be AGNs. In number 61 AGN LSBs were found.

(the blue, solid line) with its error margins (red, dashed lines). For the selection of AGN LSBs, all galaxies populating the area above the upper right (red, dashed) error line of the Kewley et al. (2001) model were chosen. This keeps the probability high that the AGN LSB sample is not contaminated by starburst galaxies. Hence, 61 AGN LSBs were found. It is conspicuous, that the region in the lower right of the diagnostic diagram, where LINERs

would be located, is not populated.

6.4   Results of the Search for AGN LSBs

The found AGN LSBs were examined for bulge-luminosities and environment. In the following, the results of these studies are presented.

6.4.1   The Frequency of AGN Activity in LSB Galaxies

In the diagnostic diagram 61 LSB galaxies are placed in the region where the emission line ratios can only be achieved by AGN activity and not by starbursts (Figure 6.2). The SDSS spectra of these galaxies were revised by eye and it was found that the majority of these galaxies shows typical signs of AGN activity. In that cases, well pronounced emission lines in [OIII] $\lambda5007/$ $\lambda4959$, [NII]$\lambda6584$, [SII]$\lambda6716/$ $\lambda6731$ and others were seen. Only four LSBs classified in Figure 6.2 did not show clear signs of AGN activity in their spectra. Hence, 57 clear AGN LSB candidates were found. Taking into account that 22 AGN candidates are located in the AGN region above the blue line, this would lead to a total number of 79 AGN LSBs. With a total of 630 LSB galaxies examined for AGN property the fraction of AGN LSBs amounts around 10%-13%. If one assumes a value of 10%-20% (Hao et al. 2005a,b and Sparke & Gallagher 2000) as the fraction of AGN activity in HSBs, the ratio for LSBs is similar. Hence, the AGN phenomenon is clearly more common in LSBs than expected. And this does not only hold for mass-rich giant LSBs (Schombert 1998) but also for normal sized LSBs like in the present case.

6.4.2   The Environment of AGN LSBs

Since environment studies were performed on all sample LSBs it is reasonable to investigate the environment of AGN LSBs, too. For each galaxy identified as an AGN LSB the number of neighbours was looked up in the database resulting of the environment studies (Chapter 4). Therefore, the number of neighbour studies in the case of not correcting for galaxy clusters within both redshift intervals ($0.01 \leq z < 0.055$ and $0.055 \leq z < 0.1$) and with the sphere radii of $r = 0.8\,\mathrm{Mpc}$, $r = 3.2\,\mathrm{Mpc}$, $r = 5.6\,\mathrm{Mpc}$ and $r = 8.0\,\mathrm{Mpc}$ were used. In the lower redshift interval, eight AGN LSBs were found, but only two of them were contained in the environment studies. Therefore, only the higher redshift interval was probed for the environment of AGN LSBs. This redshift interval contains 53 AGN LSBs. 37 of the 53 AGN LSBs were found in the database resulting of the environment studies. The other 16 galaxies were not acquired in the environment studies due to edge correction (Chapter 4, Section 4.2.3).

Table 6.1 shows the results of the environment study of AGN LSBs. In this Table, the SDSS identifier of each AGN LSB galaxy consisting of the Plate number, the Fiber number, and the MJD, a kind of checksum calculated from the Plate and Fiber numbers, is presented. In the following individual galaxies are indicated by their SDSS Plate MJD

Fiber identifiers. Additionally, the redshift z, the central surface brightness μ_B obtained from exponential fits to the surface brightness profiles in g and r bands and the total magnitudes in g and r are listed. The last four columns of the Table show the number of neighbours for each AGN LSB on scales of $r = 0.8, 3.2, 5.6, 8.0\,\mathrm{Mpc}$.

From Table 6.1 results, that AGN LSBs are found in different environments. There exist AGN LSBs within a very low surrounding galaxy density like the galaxy SDSS 924 52409 520 or SDSS 577 52367 471. They have no neighbours on scales of $r = 0.8\,\mathrm{Mpc}$, $r = 3.2\,\mathrm{Mpc}$, only one neighbour on a scale of $r = 5.6\,\mathrm{Mpc}$ and only a few neighbours on a scale of $r = 8.0\,\mathrm{Mpc}$. On the other hand, there exist AGN LSBs which are located in very high density regions of the universe. The galaxies SDSS 306 51637 390 and SDSS 296 51984 135 possess one or two neighbours when consulting the environment study with a sphere radius of $r = 0.8\,\mathrm{Mpc}$, around 20 neighbours in the study with $r = 3.2\,\mathrm{Mpc}$, 37 or rather 55 neighbours on scales of $r = 5.6\,\mathrm{Mpc}$ and 74 or 103 galaxies in their neighbourhood on scales of $r = 8.0\,\mathrm{Mpc}$. The AGN LSB galaxy SDSS 577 5237 521 has no nearby galaxies on distances of $r \leq 0.8\,\mathrm{Mpc}$ but several tens up to more than one hundred neighbours on distance radii of $r = 3.2\,\mathrm{Mpc}$, $r = 5.6\,\mathrm{Mpc}$ and $r = 8.0\,\mathrm{Mpc}$. Hence, the individual AGN LSB can reside in low and high galaxy density environments but its number of nearby galaxies on scales below $r = 0.8\,\mathrm{Mpc}$ is low (≤ 2).

Although the AGN LSBs are found in environments of different galaxy densities, the sample was probed for an effect on the average of their galaxy density. Therefore the mean number of neighbours of the sample AGN LSBs listed in Table 6.1 separately for each scale r was calculated. The resulting values were then compared to the averaged number of neighbours of all LSB galaxies of that redshift interval. The results are presented in Table 6.2. On scales of $r = 0.8\,\mathrm{Mpc}$, $r = 3.2\,\mathrm{Mpc}$ and $r = 5.6\,\mathrm{Mpc}$ the mean numbers of neighbours are above the values of all LSBs, but the statistical significance decreases with increasing sphere radius. At the radius of $r = 8.0\,\mathrm{Mpc}$ the result is inverted. On that scale, AGN LSBs possess $\sim 4\%$ less neighbours than other LSBs, but the error margin is high ($\sim 12\%$). Therefore, this value cannot be taken into account. Hence, one can summarize the results of the AGN LSB environment, that the individual galaxy can appear in low and high density regions, but on average their environments possess a slightly increased galaxy density with respect to normal LSBs.

6.4.3 The Bulges of AGN LSBs

It was tried to perform bulge disk decompositions on the surface brightness distributions of the AGN LSBs (Trachternach, priv. comm.) with Galfit (Peng et al. 2002). For this, the SDSS DR4 images of these galaxies in the filters g and r were used. It was tried to do the decomposition by fitting Sersic (1968) profile to the bulge and an exponential profile (equation 1.1) to the disk component. The bulge disk decomposition did not work properly. However, the obtained central disk surface brightnesses were in a meaningful range, but the surface brightnesses of the bulges and their total magnitudes were useless. Therefore, the compilation of a Magorrian et al. (1998) relation for the AGN LSBs was not possible. Magorrian et al. (1998) found by constructing dynamical models for a sample of 36 nearby

galaxies, the mass of the central black hole to be $M_{BH} \simeq 0.006 M_{bulge}$ with a confidence level of 95%. If one adapts a mass to light ratio Υ for the probed objects, one can connect the bulge luminosity to the black hole masses following the Magorrian relation. Then it holds $M_{BH} \simeq 0.006 \Upsilon L_{bulge}$. Unfortunately, this was not possible for the AGN LSBs due to the failure of the bulge disk decomposition of the AGN LSB surface brightness profiles by using Galfit.

However, in the SDSS images 43 out of 57 AGN LSBs show clearly the presence of a bulge. For the center of five AGN LSBs, it can be hazarded a guess for the presence of a weak bulge structure. Taking into account all these bulge candidates, a fraction of 84% of the AGN LSBs possesses a bulge.

6.5   Conclusions

From the search for AGN LSBs in the equatorial scan region of the SDSS, it is clear that the fraction of AGNs in LSBs is as high as in HSBs. This is admirable, since LSBs are not expected to be good hosts for active nuclei. Hence, the fueling mechanisms, which are modelled for HSBs successfully, have to be revised for AGN LSBs (see also the discussion about this in Chapter 7). In the diagnostic diagram, an interesting fact appears. The LINER region of the diagnostic diagram is not populated. Hence, it seems that AGN LSBs are generally no LINERs. Nearly, all of the AGN LSBs possess a distinct bulge. However, the presence of a bulge seems to be important for AGN activity in LSBs. 84% of the AGN LSBs possesses a visible bulge. This is expected from the Magorrian relation ($M_{BH} \simeq 0.006 \Upsilon L_{bulge}$), since a supermassive black hole ($M_{BH} \sim 10^6$-$10^{10} M_{\odot}$, Sparke & Gallagher 2000) is required for AGN activity. Following the Magorrian relation such black holes would reside in the centers of prominent bulges. However, the visible bulge in AGN LSBs has not to be as pronounced as in active nuclei of HSBs due to the higher mass to light ratios which appear in LSBs in comparison to HSBs.

Table 6.1: The number of neighbours N on the scales $0.8\,\mathrm{Mpc}$, $3.2\,\mathrm{Mpc}$, $5.6\,\mathrm{Mpc}$ and $8.0\,\mathrm{Mpc}$ of each AGN galaxy found in the environment study is shown.

The Environment of AGN LSBs										
Plate	MJD	Fiber	z	μ_B [mag/"^{2}]	g [mag]	r [mag]	$N_{0.8}$	$N_{3.2}$	$N_{5.6}$	$N_{8.0}$
289	51990	535	0.0789	22.08	16.46	15.66	0	3	23	48
1002	52646	623	0.0849	22.77	17.41	16.73	0	5	9	17
1238	52761	346	0.0687	22.56	17.99	17.47	0	8	17	31
268	51633	345	0.0914	22.68	18.14	17.08	0	1	5	13
271	51883	411	0.0967	22.53	18.42	17.50	1	6	31	73
273	51957	225	0.0948	22.51	18.47	17.39	0	3	16	27
293	51994	62	0.0850	22.71	18.17	17.18	0	6	11	38
306	51637	390	0.0560	22.53	18.53	17.83	1	18	37	74
567	52252	361	0.0900	22.56	18.44	17.40	0	1	3	11
570	52266	88	0.0727	23.12	18.22	17.23	0	3	7	10
577	52367	471	0.0960	22.61	17.75	16.98	0	5	9	14
837	52642	263	0.0946	22.63	18.08	17.13	0	0	1	4
838	52378	436	0.0996	22.62	18.81	17.78	0	5	23	54
853	52374	35	0.0761	22.52	18.15	17.23	1	2	17	31
1238	52761	346	0.0687	22.56	17.99	17.47	0	8	17	31
272	51941	578	0.0562	22.50	17.71	16.74	0	2	9	17
841	52375	212	0.0978	22.62	18.53	17.68	0	0	10	24
996	52641	544	0.0778	22.53	18.50	17.72	0	5	12	32
278	51900	345	0.0674	23.08	18.28	17.29	0	12	27	32
577	52367	521	0.0694	22.66	17.79	16.87	0	17	57	114
925	52411	193	0.0782	22.99	18.68	17.95	0	5	14	21
924	52409	520	0.0977	22.54	18.71	17.84	0	0	1	2
480	51989	468	0.0623	22.61	17.74	16.90	0	10	22	56
1190	52670	240	0.0714	22.59	18.29	17.54	0	5	22	45
919	52409	338	0.0818	22.55	17.78	17.17	0	4	9	20
910	52377	461	0.0818	22.57	17.99	17.05	0	4	29	48
473	51929	386	0.0941	22.55	18.59	17.65	0	0	2	4
509	52374	402	0.0597	22.57	18.25	17.33	0	3	8	18
539	52017	455	0.0797	22.71	18.03	17.08	2	4	9	17
299	51671	536	0.0731	22.52	17.49	16.81	1	6	14	27
1221	52751	426	0.0840	22.72	18.92	17.84	0	4	8	19
1227	52733	450	0.0689	22.81	18.18	17.31	0	10	31	54
307	51663	173	0.0723	22.62	17.64	16.86	0	6	13	17
476	52314	345	0.0726	22.73	17.97	17.40	1	10	16	38
513	51989	468	0.0754	22.66	18.70	17.71	0	1	9	41
835	52326	535	0.0807	22.79	18.59	17.63	0	1	5	6
296	51984	135	0.0818	22.61	18.26	17.33	2	21	55	103

Table 6.2: The average numbers of neighbours for AGN LSBs $\overline{N}_{neighbours}$(AGN LSBs) and for all LSBs $\overline{N}_{neighbours}$(all LSBs) with the corresponding sphere radius r of the environment study (Chapter 4) are shown.

The averaged number of AGN LSB neighbours		
r [Mpc]	$\overline{N}_{neighbours}$(AGN LSBs)	$\overline{N}_{neighbours}$(all LSBs)
0.8	0.243 ± 0.085	0.181 ± 0.016
3.2	5.513 ± 0.784	4.659 ± 0.152
5.6	16.432 ± 2.050	15.834 ± 0.458
8.0	33.270 ± 4.026	34.687 ± 1.251

Chapter 7

General Discussion

With the SDSS data releases containing the spectroscopic main galaxy sample, a comprehensive data set with spectra and images of several hundred thousand galaxies including ~ 1200 LSBs was available. Therefore, it was possible to search systematically for AGN activity in LSBs. For the distinguishing between AGN LSBs and normal LSBs, a diagnostic diagram following Osterbrock (1989) plotting the logarithmic line ratios $\log([OIII]\lambda5007/H\beta)$ versus $\log([NII]\lambda6584/H\alpha)$ was used. This is not only usual, but also reasonable, since even young stars with a high energy output in a starburst galaxy cannot produce a certain degree of ionization, that would generate line ratios, which indicate AGN activity and place AGN galaxies within a certain area in the diagnostic diagram. A model from Kewley et al. (2001) which displays the limit between the area of extreme starburst galaxies and the region populated by galaxies with active nuclei in the diagnostic diagram was used for the discrimination between normal and active LSBs. Only galaxies in the AGN region beyond the error margin of the model were designated as LSBs with an active nucleus. This secures the quality of conclusions drawn on the frequency of the observed AGN LSB phenomenon. The Kewley et al. (2001) work is based on modelling the high resolution ($50\,km/s$ at $H\beta$) optical spectra of 225 warm IRAS galaxies by using their MAPPINGS III photoionization code and both the PEGASE v2.0 (Projet d'Etude des GAlaxies par Synthese Evolutive, Fioc & Rocca-Volmerange 1997) and STARBURST99 (Leitherer et al. 1999) codes for the generation of the spectral energy distribution of young star clusters. The extreme starburst classification line resulting of Kewley et al. (2001) is used for the distinction between AGN and normal LSBs. Kewley et al. (2001) checked that for realistic values of metallicity and ionization parameters continuous starburst models always fall below and to the left of this classification line in the diagnostic diagrams (where galaxies without active nuclei reside). Hence, this classification line is state of the art for the distinction between AGNs and starburst galaxies, today.

LSBs are not thought to be common hosts of AGNs. Their low stars and gas surface densities (Pickering et al. 1997) contradict the supply of enough fuel for AGN activity. It was found (Chapter 6) that the fraction of LSBs with AGN activity with respect to all LSBs is with 10%-13% similar to the values of the AGN fraction in HSBs (10%-20%, Hao et al. 2005a,b and Sparke & Gallagher 2000).

Environment does not play a major role to AGN activity in LSBs. As shown in Chapter 6, their average number of neighbours is increased compared to the one of LSBs without AGNs on scales of 0.8, 3.2 and 5.6 Mpc, but the significance of the effect is very low. Moreover, AGN LSBs were found in environments which possess a very low galaxy density.

Due to the fact that only LSBs beyond the error margins of the Kewley et al. (2001) model in the diagnostic diagram were designated as active, one can interpret the 10% fraction of AGN LSBs as a lower limit to the real fraction of active nuclei in LSBs. This interpretation as a lower limit is supported by the fact that the number of AGNs is underestimated due to a low, but present fraction of AGNs which slip into the starburst region due to obscuration effects as discussed in Kewley et al. (2001). The fraction of at least 10% AGN LSBs is a surprise. Additionally, LSBs only show a weak spiral structure (e.g.: de Blok et al. 1995, Bothun et al. 1997) if at all. However, in common theories of the feeding mechanisms of the AGN and the accretion processes, the gas and star surface densities play a major role in accretion disk physics for AGN fueling (e.g.: Duschl 1989, Duschl et al. 2000). Therefore, LSBs were neglected in the investigation of the AGN phenomenon in former times. However, it was noticed that most of the giant, Malin-like LSBs show mostly weak AGN activity (Bothun et al. 1987, Impey & Bothun 1989, Bothun et al. 1990, Sprayberry et al. 1993, 1995, Schombert 1998) and that AGN activity is possible at the faint end of the galaxy luminosity function (Hao et al. 2005a,b), but a systematic search for AGNs in all types of LSBs lacked.

The impact of low gas and star surface densities on the physics of accretion disks can be shown by an equation of Duschl (1989):

$$\frac{\partial \Sigma}{\partial t} = \frac{3}{s}\left(\sqrt{s}\frac{\partial}{\partial s}\nu\Sigma\sqrt{s}\right), \tag{7.1}$$

$$\tau_{visc} = \frac{s^2}{\nu}. \tag{7.2}$$

with $\Sigma = \int_{-\infty}^{\infty}\rho dz$ the gas surface density, ν the viscosity, s the radius of the disk and τ_{visc} the viscosity time scale. Assuming, that the time derivative of the surface density accreted for the perpetuation of AGN fueling (left side of equation 7.1) must achieve similar values for LSBs as for HSBs, then the viscosity in LSBs must be higher. This is required for a compensation of the lower surface density (right side of equation 7.1). However, it is not reasonable that gas with lower surface densities (like in LSBs) possess higher viscosities than gas at higher surface densities (found in HSBs). Moreover, the higher viscosity then would lead to a shorter life time of the AGN phenomenon in LSBs ($\tau_{visc} \propto 1/\nu$) in comparison to AGNs in HSBs. However, this contradicts the fact that the fraction of active LSBs with respect to all LSBs is the same as that of AGN HSBs with respect to all HSBs. Otherwise, one would not expect the AGN LSBs to be as frequent, as they are. Therefore, the surprisingly high fraction of AGN LSBs must have an impact on the understanding of AGN physics, since the models for fueling mechanisms have to be revised for including an explanation for AGN LSBs. Hence, the frequent occurrence of AGNs in LSBs will lead to a deeper understanding of AGNs in general, not only in

LSBs. At the same time this AGN LSB fraction supports the impression, that LSBs have a close affinity to HSBs, as they form as often AGNs as their relatives at higher surface brightness. This impression is based on the observations, that LSBs have enough gas for the sufficient production of stars in total mass (Pickering et al. 1997, McGaugh & de Blok 1997, Matthews et al. 2001a, O'Neil 2002, O'Neil et al. 2004). However, they did not since the gas appears on low surface densities (Pickering et al. 1997), below the Kennicutt (1989, 1998a) criterion for the formation of giant, star forming, molecular clouds. The fact of the AGN fraction in LSBs being similar to that in HSBs, gives another clue to the concept is found, that LSBs are similar to HSBs in general, but they evolved slowly in a less dense, and therefore quiet environment. A quiet environment means a region, where the galaxies could form and evolve undisturbed, apart from gravitational triggers, which are caused by nearby galaxies and apart from the infall of massive gas clouds. Both triggers, would disturb the gas density field and hence initiate star formation.

In Chapter 4 the environment of the LSBs, found in the spectroscopic main galaxy sample, was examined. The motivation for this study was the possibility of the low surface brightness of these galaxies being due to the fact that they formed and evolved in a quiescent region of the universe. There, gravitational triggers for star formation by nearby galaxies or the infall of massive gas clouds were improbable.

Although LSB galaxies have enough gas masses for sufficient star formation, since LSBs are generally similar to HSBs concerning the total gas content (Pickering et al. 1997, McGaugh & de Blok 1997, Matthews et al. 2001a, O'Neil 2002, O'Neil et al. 2004) they did not form as much stars as HSBs. If LSBs are located in low density environments, this could have prevented the LSB gas from lumping in the same degree like the gas in HSBs did. This is due to the absence of gravitational perturbations, which would rise the gas surface density at some regions and initiate the lumping of the gas. Hence, the gas surface density in LSBs is low (Pickering et al. 1997). First hints already exist, that on scales below $2\,\mathrm{Mpc}$, the galaxy environment of LSBs is less dense than that of HSBs (Bothun et al. 1993, Mo et al. 1994). Furthermore, a lack of nearby ($r \leq 0.5\,\mathrm{Mpc}$) companions of LSB galaxies was detected by Zaritsky & Lorrimer (1993). However, a study on the distribution of LSBs in the large scale structure on scales which correspond to the size of its substructures (galaxy cluster radii $r \sim$1-3 Mpc, size of the LSS filaments and walls $\sim 5\,\mathrm{Mpc}$) has not yet been performed.

Another possible explanation for the presence of LSBs might be found in the differences in the spin parameter λ of the Dark Matter halos between LSB and HSB galaxies. Dalcanton et al. (1997a) studied the formation of disk galaxies and used a gravitationally self-consistent model for the disk collapse in order to calculate the observable properties of disk galaxies as a function of mass and angular momentum of the initial protogalaxy. The observational properties of both normal galaxies and LSBs were reproduced. Their model generated smooth, asymptotically flat rotation curves and exponential surface brightness profiles. They found the high angular momentum halos, which also tended to be low mass, to form naturally low baryonic surface density disks or in other words low surface brightness disks. Boissier et al. (2003) found in their models for the chemical and spectrophotometric

evolution of mainly spiral galaxies and LSBs, that the models with a spin parameter of $\lambda \sim 0.04$ corresponded to spirals with Freeman values of surface brightness. Moreover, models with $\lambda > 0.06$ belonged to LSB galaxies. From these simulations follows that the Dark Matter halos of LSBs possess a higher spin parameter, than that of HSBs. Since, the spin parameter λ is linked to the structural properties of the disk, this would imply a larger scale length for the LSB disks with respect to HSB disks. Hence, the total gas mass in LSBs would be distributed over a larger scale length than in HSBs. This would explain the lower gas surface density in LSBs, too.

In Chapter 4 results were presented, which give strong evidence for the thesis that LSB galaxies are located in low density regions of the LSS. This result was found by averaging the number of neighbouring galaxies for LSBs and HSBs separately, obtained from number counting within spheres of a certain radius ($r = 0.8\,\mathrm{Mpc}$ up to $r = 8.0\,\mathrm{Mpc}$). Additionally, it could be shown that the spatial distribution of LSBs is biased against that of HSBs by more than 10% in that direction, that LSBs reside in regions of the universe which show less clustering. After removing the galaxy clusters from statistics, it could be shown that LSBs settle in a lower density environment than field galaxies. This holds for both the smaller, dwarfish LSBs which dominate the lower redshift bin ($0.01 \leq z < 0.055$) of the study and the larger LSBs, which are preferably found in the higher redshift bin ($0.055 \leq z < 0.1$). The distribution of different sized LSBs at different redshifts is due to the apparent magnitude limit of the selection function of the SDSS (Chapter 3). Although the selection function is responsible for the average size depending on redshift, it definitely cannot cause the environment effect. For only 6% of the galaxies detected in the SDSS imaging survey no spectra could have been taken by the SDSS telescope due to fiber placing constraints. The minimum distance for placing two adjacent fibers at the sky is 55" for the SDSS spectrographs (Strauss et al. 2002). On a comoving distance of $z = 0.1$ this corresponds to a minimal distance of $112\,\mathrm{kpc}$, which two adjacent galaxies must have, if for both galaxies spectra should be taken. However, the smallest scale probed in the environment studies was $800\,\mathrm{kpc}$, far beyond the minimal allowed distance. Hence, fiber placement constraints cannot be responsible for such an effect. The selection of objects for the SDSS spectroscopic galaxy sample is not against LSBs in crowded fields. It is said explicitly that in case of two galaxies with a projected distance less than 55" not necessarily the brighter object is selected, but then the selection is done by chance (Blanton et al. 2005). Hence, the observed result of the environment studies (Chapter 4), that LSBs have less neighbours than HSBs on scales of $0.8\,\mathrm{Mpc}$ to $8.0\,\mathrm{Mpc}$ cannot be mocked by selection effects.

The results of the environment of LSBs from Chapter 4 agree well with the results presented in Bothun et al. (1993) for the scales below $2\,\mathrm{Mpc}$. There, a lower galaxy density in the vicinity of LSBs in comparison to that of HSBs is seen on those scales, too, but they do not find any differences in the environment of LSB and HSBs on scales larger than $2\,\mathrm{Mpc}$. However, the statistics in Bothun et al. (1993) might be biased towards lower scales due to their two-dimensional treatment of the problem, since they measured projected distances to nearby galaxies of the scrutinized galaxy within a fixed redshift interval.

All the results fit well into the following formation scenario, which was proposed by

Bothun et al. (1997): Galaxy formation takes place due to an initial Gaussian spectrum of density perturbations with much more low-density fluctuations than high density ones. Many of these low-density perturbations are lost due to the assimilation or disruption during the evolutionary process of galaxy formation but a substantial percentage of the fluctuations survives and is expected to form LSB galaxies. Further on one can assume that the spatial distribution of the initial density contrast consists of small scale fluctuations superimposed on large-scale peaks and valleys. Small-scale peaks lead to galaxy formation, whereas the large-scale maxima induce cluster and wall formation of the LSS.

Based on the results presented in Chapter 4, it is proposed that the galaxies formed in the large-scale valleys may develop to LSB galaxies due to their isolated environments whereas HSB galaxies formed mainly on the large-scale peaks (Rosenbaum & Bomans 2004). The isolation of LSB galaxies on intermediate and small scales must have effected their evolution since tidal encounters acting as triggers for star formation would have been rarer in these LSB galaxies than for HSB galaxies. Hence, the gas surface density in these galaxies stayed low, below the Kennicutt (1989, 1998b) criterion for the formation of giant, star forming molecular clouds. Therefore, star formation in LSBs was more sporadical than organized in starbursts, like it is the case for HSBs. This kept the surface brightness of the stellar disk of LSBs low.

The results of the present work give strong evidence for this scenario, since the observed isolation of LSB galaxies takes place not only on low scales ($r \lesssim 2\,\mathrm{Mpc}$), but also on scales of $\sim$ 5-8 Mpc, which correspond to the typical size of LSS filaments (e.g.: White et al. 1987b, Doroshkevich et al. 1997). In the present case, it could be shown, that the isolation of LSBs is not only in contrast to all HSBs (including galaxy clusters), but also to field HSBs, which are located in the walls and filaments of the LSS. Therefore, it could be shown that LSBs preferably settle in the outer rims of the filaments and at the borders to the voids.

Following that scenario described above, one can conclude that LSB galaxies were formed in the low density regions of the initial universe, where the large scale density contrast was low and from which void structures formed later. However, most of the LSB galaxies have migrated to the outer rims of the LSS filaments due to gravitational infall, but some of them have still remained in the voids where they were formed.

Further evidence for this scenario was found by Haberzettl (2005). He performed a fitting of stellar population synthesis models (PEGASE) to the spectra of seven LSB galaxies found in the region of the Hubble Deep Field South. In that work it was shown that the age of the dominant stellar population of the sample LSBs was in a range of 1.4 Gyr up to 7 Gyr. Translated into redshift, this means, that the tested galaxies had their major star formation event at a redshift range of $0.2 \lesssim z \lesssim 0.5$, whereas the galaxies of the HSB comparison sample had their dominant starburst event at a redshift interval of $2 \lesssim z \lesssim 4$ (Haberzettl 2005). This value for HSBs is also consistent with the results of the simulations of the "Hierarchical Clustering" model (Springel & Hernquist 2003). Since structure formation and galaxy formation started in the overdense regions of the density contrast due to gravitation and later reached the large scale valleys of the formation scenario described above (e.g.: Springel et al. 2005), the results of (Haberzettl 2005) also give evidence to
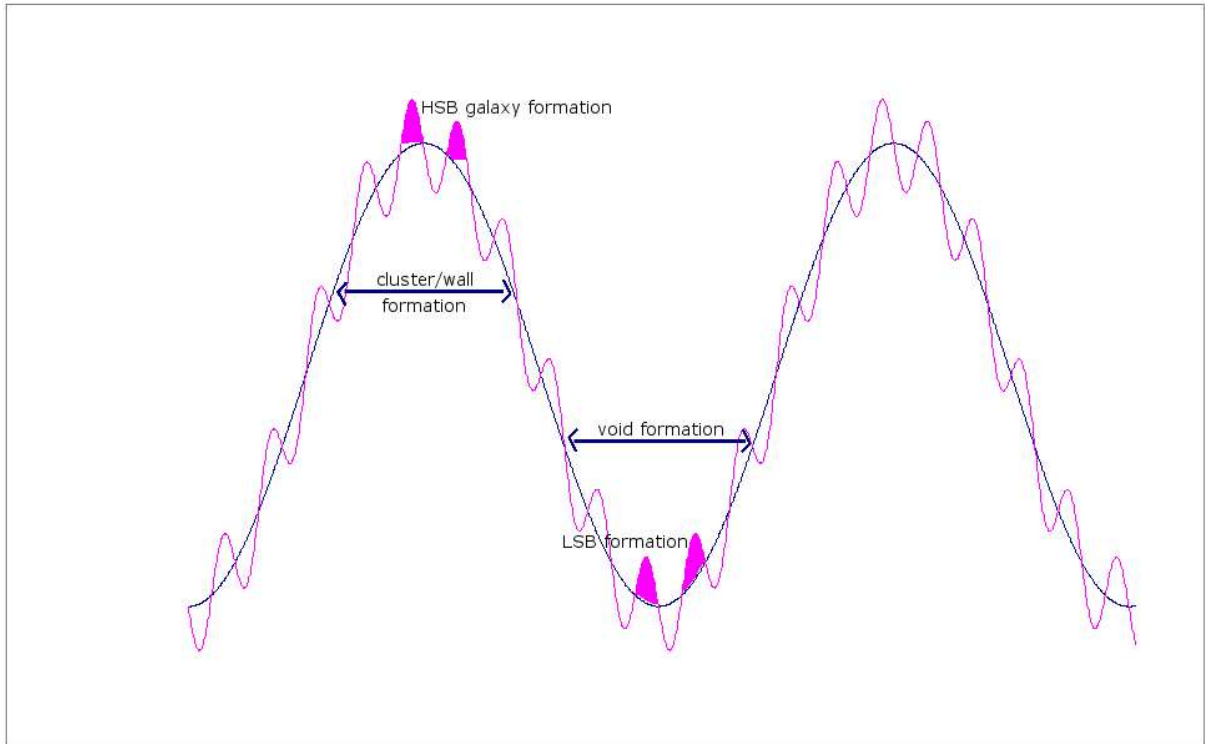
Figure 7.1: A sketch of the initial density contrast (P. Schneider, priv. comm.) for the scenario as described in Rosenbaum & Bomans (2004). It shows the density contrast in the initial universe as a superposition of large scale and small scale density fluctuations. Large scale fluctuations form the LSS, whereas small scale peaks form galaxies. According to the presented scenario, HSB galaxies were formed in large scale peaks, which later developed to clusters, walls and LSS filaments. LSBs are expected to being formed in low density regions, which developed to the voids of the LSS.

the scenario described above, which claims LSBs to be formed in large scale low density regions of the initial universe.

Moreover, with the latest results of Bailin et al. (2005) it is possible to build a causal connection between this scenario described above and the results of simulations, that the larger extents of LSB Dark Matter halos result in a higher spin parameter (Dalcanton et al. 1997a, Boissier et al. 2003) . This higher spin parameter would increase the scale lengths of the LSB disk and therefore keep the gas surface density low.

In order to explain this connection, one has to give a brief introduction to the Cold Dark Matter model (CDM). The CDM model is a kind of "pattern of thought" for the understanding of structure formation in the universe. Rotation curves of galaxy disks cannot be explained by the gravitation of baryonic matter, visible in the bands which are accessible to an astronomer (from radio to X-ray). One possible explanation is a modified law of gravitation (MOND, for further details see: Milgrom 1983). Another,

more conventional assumption is the existence of matter, of which we cannot trace any footprints except the gravitational effects. This kind of matter is called Dark Matter. Assuming Dark Matter halos around galaxies with density profiles of $\rho \propto r^\alpha$, with r the radius and $\alpha \simeq 1$, a good explanation for the inner radii of the rotation curves of galaxies in general is found. This "cuspy" behaviour of the density profiles of Dark Matter is well quantified and understood today (e.g.: Navarro et al. 1996). However, this Dark Matter profile does not hold for LSBs, which are Dark Matter dominated over all radii (e.g.: Bothun et al. 1997, McGaugh et al. 2001 and de Blok & Bosma 2002). It was found that these objects show a less rapid rise in the central rotation curves as it is found in HSB galaxies and produced in models of Dark Matter halos with cusp density profiles. Therefore, LSBs require another type of central density profile with a constant density core region or at least a shallow cuspy profile (e.g.: Flores & Primack 1994, Burkert 1995, de Blok & McGaugh 1997, de Blok et al. 2003 and de Blok 2004). Hence, the more cuspy the density profiles of Dark Matter halos are, which means that they are more concentrated in the center, the steeper is the rise of the rotation velocity with increasing radius in the central rotation curve of the scrutinized galaxy. As described before, a possible cause for the reduced surface brightness of LSB galaxies is thought to be found in the spin parameter of the Dark Matter halos (e.g.: Dalcanton et al. 1997a, Boissier et al. 2003), if the specific angular momentum of the baryons is conserved during their dissipation into a rotating disk (which is a reasonable assumption). Hence, the scale length of the disk would be related to the angular momentum of the Dark Matter halo. Therefore, a link would exist between the increased scale length (and therewith the low surface brightness) and the concentration of their Dark Matter halos. The concentration parameter of Dark Matter halos is measured as the ratio of the virial radius r_v and the scale radius r_s. If one chooses the scale radius r_s to be equal to the radius r_{200}, which encloses a spherical overdensity of 200 times the critical density ($\rho_{crit} = 3H_0^2/[8\pi G]$, with H_0 the Hubble constant and G the gravitational constant) this concentration index is called c_{200}.

Bailin et al. (2005) now performed a cosmological N-body simulation with $N = 512^3$ on a periodic $50h^{-1}$ Mpc volume using the GADGET2 code (by Springel 2005). Thereby, ΛCDM cosmology was assumed. The halos of a mass range of $10^{11} \leq M_{vir}/h^{-1} \leq 2 \cdot 10^{12}$ which are typical to be hosts of LSB and HSB galaxies were identified using a friends-of-friends algorithm and the spin parameter $\lambda' = J/[\sqrt{2}MVR]$ (with M, the total mass, J the total angular momentum, V the circular velocity at radius R) in a definition from Bullock et al. (2001) was calculated. As expected, a trend for λ' to increase with decreasing c_{200} was found. For a concentration index of $c_{200} = 10$, a median of the spin parameter $\lambda'_{med} \simeq 0.03$ and for $c_{200} = 5$ a value of $\lambda'_{med} \simeq 0.05$ was obtained. Then, assuming angular momentum conservation of the baryons during dissipation into the rotating disk, the disk angular momentum and its extent for a given mass was calculated. From that, the central surface densities were estimated and the central surface brightnesses were estimated by using the fitting equations of Mo et al. (1998). A clear trend was found that halos with lower concentrations host disks with lower central surface densities. With these results, for the first time a correlation between the spin parameter λ' and the concentration of the Dark Matter halos was found. LSBs seem to possess Dark Matter halos, which are more

diffuse and more extended than that which host HSB galaxies. Although this is not yet a refereed work, the obtained results are not only important for the theories which predict the existence of LSBs to be due to the higher spin parameter of Dark Matter halos. They are also important for the results of Chapter 4, since this could be the connection between these two scenarios. The type of diffuse, less concentrated Dark Matter halos, which preferably host LSB galaxies, one would expect to exist in lower density regions, whereas the more concentrated Dark Matter halos one would expect to be formed in high density regions of the initial universe. This is compatible to the results of Avila-Reese et al. (2005), who performed ΛCDM N-body simulations. They found the halos in clusters to have a lower median spin parameter, to be more spherical, and to possess less aligned internal angular momentum than the halos in void or field regions. Their simulations showed trends that disk galaxies which formed in halos with low spin parameters, but high concentration indices, are preferably of earlier morphological types. Furthermore, these galaxies have higher surface brightnesses, smaller scale lengths, and lower gas fractions than galaxies formed in halos which have higher spin parameters, but are low-concentrated.

If the results of Bailin et al. (2005) will be verified in future, the combination of this with the results of the environment studies (Chapter 4) and the simulations of Avila-Reese et al. (2005), would answer the following question: Are LSB galaxies due to nature or nurture? The answer would then be, that they are due to a mixture of both.

Another important point worth to be discussed in the context with present literature is the result of the LSB-HSB galaxy bias. In Section 4.3.2 of Chapter 4, it was shown that the stochastical bias generally differs with more than 10% between LSBs and HSBs in the direction that LSBs settle in less clustered environments than HSBs. These results have to be discussed in connection to common simulations for galaxy clustering and structure formation.

One usual method for simulating galaxy clustering is to perform N-body simulations without including baryonic matter (e.g.: Kauffmann et al. 1999a,b, Somerville et al. 2001). With this simplification, the problems appearing by modelling gas cooling, shocks, star formation, stellar evolution, and feedback are avoided, which would have to be integrated, if one was taking into account baryonic matter. This simplification is based on the assumption, that galaxies form within collapsed, virialized Dark Matter halos. From the simplified simulations, galaxy mock catalogues are generated. They are produced by identifying virialized Dark Matter halos from the simulations which are then populated with galaxies. Then, the clustering of the galaxies is determined by the clustering of the halos in which they condensed. These simulations show a biasing between the galaxy distribution identified by the halo distribution and the underlying Dark Matter density field in different density environments. Kauffmann et al. (1999a,b) used this technique to track the formation and merging of Dark Matter halos as a function of redshift. Then, they used semianalytic galaxy formation models additionally in order to study the evolution of the galaxy population to high redshifts and to make predictions for the spatial and redshift distribution of faint galaxies. From these simulations, they calculated the two point correlation function for galaxies and put that into a context with luminosity. However,

no dependence of the galaxy bias on luminosity was found. These results do contradict the results on the LSB-HSB galaxy bias from Chapter 4. The observed bias effect of LSB galaxies with respect to HSBs should be reproduced in a dependence of the galaxy bias on luminosity in simulations. Thus, the low luminosity objects (which are preferably LSBs) should be less biased against the underlying Dark Matter distribution, since they are antibiased against the HSB galaxy distribution. This should lead to a dependence of a galaxy/Dark Matter bias on luminosity.

Somerville et al. (2001) found the peak in the galaxy/halo overdensity distribution to occur in regions, where the matter density is close to its mean value. In the underdense regime with a density contrast of $0 < \delta \leq -1$, the galaxy bias vanishes near a density contrast of $\delta \gtrsim -1$. These results are compatible with the observations from Section 4.3.2. Since there is an opposite bias between LSBs and HSBs than that between HSB densities and the underlying Dark Matter density field, these two effects should counteract in low density regions, which are preferably populated by LSBs. Hence, the observed results of the LSB-HSB galaxy bias give some evidence that the modern cosmological N-body simulations (as presented in Somerville et al. 2001) are on the right track.

Chapter 8

Summary

In the present work, the properties of the SDSS as a survey for Low Surface Brightness (LSB) galaxies were examined first. For that the surface brightness distribution of the SDSS DR4 main galaxy sample limited to a redshift of $z \leq 0.1$ was determined. The LSB galaxies contained in the main galaxy sample were found by fitting automatically exponential profiles to the azimuthally averaged surface brightness profile of all galaxies measured by the SDSS pipelines in the bands g and r. The values for the central surface brightness obtained by the fits in g and r were converted in a Johnson-B central surface brightness $\mu_B(0)$ using the transformation equations of Smith et al. (2002). The central surface brightness value for each galaxy was corrected for Tolman-dimming corresponding to the redshift of the scrutinized galaxy. Galaxies with an undimmed (corresponding to a redshift of $z = 0$) central surface brightness in Johnson-B of $\mu_{B,corr}(0) \geq 22.5 \, \mathrm{mag/arcsec}^2$ were designated as LSBs. Otherwise, the galaxy was marked as HSB. It was shown that the LSB luminosity function is dominated by dwarf-like LSBs for a redshift range of $0.01 \leq z < 0.055$. However, the redshift interval of $0.055 \leq z < 0.1$ preferably contains larger LSBs. These galaxies have (Petrosian-r band) radii of $\sim$ 10-16 kpc, whereas the LSBs of the lower redshift interval tend to have radii of $\sim$ 2-8 kpc. This effect was caused by the apparent (Petrosian-r) magnitude limit for SDSS spectroscopy of $r \leq 17.77 \, \mathrm{mag}$ applied by the target selection algorithm of the SDSS pipeline. It is known in the literature as the Malmquist Bias.

Then, the environment of LSB galaxies was investigated by using this redshift limited spectroscopic main galaxy sample of the SDSS. Due to this redshift selection effect on the size of the galaxies, the environment studies (Chapter 4) were performed on these two symmetric redshift intervals (as described above) separately. At first, a pie slice diagram was produced showing the distribution of LSBs within the large scale structure (LSS) traced by HSBs. This diagram shows that LSBs tend to be located at the outer rims of the LSS filaments and walls, and some of them are even found in void regions. This first impression from the pie slice was examined in a statistical neighbour counting analysis. Therefore, neighbour counting within the 3-dimensional distribution of the galaxies calculated from positions and redshifts was performed for LSBs and HSBs using spheres of a certain radius. The sphere radius was varied in several runs between $r = 0.8 \, \mathrm{Mpc}$

and $r = 8.0\,\mathrm{Mpc}$ in order to probe the galaxy environment of LSBs and HSBs on different scales. It was found, that LSB galaxies have on average less neighbouring galaxies than HSBs on all scales for both redshift intervals. In a second study, galaxy clusters were excluded from statistics for probing the LSB environment with respect to that of field HSBs. The result was that LSBs have on average less neighbours than field HSBs, but the signal was not so clear as in the case of probing both cluster and field galaxies simultaneously. From the neighbour counting results, the galaxy bias between LSBs and HSBs were calculated on scales of $8.0\,\mathrm{Mpc}$, $5.6\,\mathrm{Mpc}$ and $3.2\,\mathrm{Mpc}$. It was found that LSBs are biased against all HSBs as well as against field HSBs in that direction that LSBs settle in regions which are less strongly clustered. This case is sometimes called "antibias" in the literature. And the bias difference between LSBs and HSBs amounts more than 10%. From these results it was concluded that LSBs formed and evolved in low density regions of the universe and have drifted to the outer parts of the filaments due to gravitational infall. In this context, a project with follow-up observations was introduced. For this project, Hα imaging data of a subsample containing 60 LSBs in different environments are taken. These data are used in order to measure the current Star Formation Rate (SFR) of LSBs and to link it to their environments. Although the data acquisition has not yet been finished, preliminary results deliver a first trend that the current SFR of LSBs in less dense environments is lower than that of LSBs in regions with higher galaxy densities.

The third part of the present work deals with AGNs in LSBs. The data from the equatorial scan region of the SDSS DR4 was searched for LSBs which show AGN activity. Therefore, the Hα, Hβ, [OIII]λ5007 and [NII]λ6584 line measurements of the SDSS data were used in combination with a diagnostic diagram following Osterbrock (1989) and a dividing line between AGNs and normal galaxies from Kewley et al. (2001). It was found that 57 out of 630 LSBs show clear evidence for hosting an AGN. Hence, the fraction of AGN LSBs with respect to all LSBs is similar to that of AGN activity in HSBs. The AGN LSBs and normal LSBs were checked for a correlation between AGN activity and environment. It was found that AGN LSBs can appear in low and high density environments, but a slight tendency towards regions of higher galaxy density was seen on average.

Chapter 9

Outlook

With investigations in the formation and evolution of LSBs, not only a contribution to the understanding of this class of galaxies but also clues on the formation of galaxies and structure in the universe in general are given. The study on the environment of LSBs was a first, but large step into that direction. This should be repeated on future redshift surveys which cover large areas at the sky, and which will be deeper than the SDSS. Then, it would be possible to catch LSBs at higher redshifts working against Tolman-dimming and Malmquist Bias. With those surveys also a detailed study of the current star formation and the star formation history is possible and could deliver a better understanding of LSB galaxies and galaxy formation in general.

A first candidate for the continuation of environment studies focussed on LSBs is of course the SDSS-II survey. SDSS-II will complete the observations started in the SDSS and deliver imaging and spectroscopic data of a huge contiguous region of the Northern skies by using the SDSS 2.5 m telescope. At such a survey covering a large contiguous area at the sky, the loss of objects due to edge correction when performing environment studies would become negligible. This, as well as the increased probed volume will rise the significance of environment statistics. Another suited survey may be be the Deep2 survey which is currently ongoing by using the Keck telescopes in order to study the distant universe. It is planned to obtain spectra of of ~ 50000 faint galaxies with redshifts of $z > 0.7$. A further possible candidate for those studies in the future is the survey which will be obtained with the Large Synoptic Survey Telescope (LSST) and its spectroscopic follow-up. The LSST will be a wide-field telescope facility with 8.4 m mirror diameter and a field of view of $3°$.

With those future surveys, if they are deep enough, it could be possible to perform an environment analysis of LSBs depending on redshift. From that analysis, the possible effect that LSBs were born at the regions of voids and have migrated to the outer parts of the filaments, should be observable. Especially the Deep2 survey is a good candidate to probe the redshift depending behaviour of the LSB environments, because this survey starts at a redshift of $z = 0.7$. The results obtained from that could be compared with the present results which are limited to a redshift of $z < 0.1$. Furthermore, the Deep 2 survey is focused on faint objects, which are preferably Tolman-dimmed LSB galaxies. With those deep surveys the properties of the LSBs in clusters could be studied more detailed. This

was not possible with the SDSS, since only 21 cluster LSBs were found (Chapter 4).

The completion of the study on the star formation rate of LSBs in different environments (Chapter 5.2) will contribute to a better understanding of the formation and evolution scenario discussed in Chapter 7. Furthermore, an investigation of the metallicity-luminosity relation for emission line LSBs, with metallicities obtained from the [OIII]λ4363 line using the SDSS spectroscopy is reasonable and possible.

The results obtained from the search for AGNs in LSBs (Chapter 6) are an important starting point for further investigations. Since it was shown, that AGNs in LSBs are as common as AGN activity in HSBs the results of this work encourage further studies on this topic. With the exact data of the AGN LSBs of the sample concerning surface photometry, bulge disk decomposition, spectra, measurements of the ionization parameter, H I gas distribution, one would obtain input parameters for modelling the AGN engine in these LSB objects. Those studies would include the compilation of the (Magorrian et al. 1998) relation between the black hole mass, and the (Gebhardt et al. 2000) relation between the stellar velocity dispersion and the black hole mass. Furthermore, a study on the frequency of Seyfert I and Seyfert II types in LSBs could deliver interesting results. All these follow-up studies would lead to a further understanding of AGNs as well as of LSBs in general.

Appendix A

developed C-programs

A.1   Program prepares the DR4 Data for IRAF nfit1d

```c
/*************************************************************************/
/*                      SB_extract_for_nfit1d.c V2/03                    */
/*                          Version 07/2005                             */
/*      Copyright by Dominik Rosenbaum, Astronomisches Institut, RUB     */
/*************************************************************************/


#include <stdio.h>
#include <stdlib.h>
#include <math.h>
#include <string.h>


/*compilieren  */
/*mit: gcc SB_merge_post_nfit1d_fast_DR4.c  -lm -O3 -o SB_merge_nfit1d_DR4 */


/*********************** Konstanten-Definition ***************************/


#define Maxz 1000000


/*********************** Variablendefinition ***************************/


int zae,i, j, k, l, m, n, o, p, q, length, l_id[Maxz];
FILE *cfile1, *cfile2, *cfile3;
char yes_no[10];
char dateiname1[100], dateiname2[100], dateiname3[100];
char header1[200], header2[200], stringg[100];
int plate[Maxz], MJD[Maxz], Fiber[Maxz], SpecClass[Maxz], bin[Maxz];
double ra[Maxz], dec[Maxz], Prof_G[Maxz];
double z[Maxz],zErr[Maxz],zConf[Maxz];
int zStat[Maxz];
```

```c
double utot[Maxz],gtot[Maxz],rtot[Maxz],itot[Maxz],ztot[Maxz];
int plate_out[Maxz], MJD_out[Maxz], Fiber_out[Maxz], SpecClass_out[Maxz];
int bin_out[Maxz];
double ra_out[Maxz], dec_out[Maxz];
double z_out[Maxz],zErr_out[Maxz],zConf_out[Maxz];
int zStat_out[Maxz];
double utot_out[Maxz],gtot_out[Maxz],rtot_out[Maxz],itot_out[Maxz];
double ztot_out[Maxz],petroRad_r[Maxz],petroR50_r[Maxz],petroR90_r[Maxz];
double petroRad_r_out[Maxz],petroR50_r_out[Maxz],petroR90_r_out[Maxz];
double Prof_G_Array[Maxz][15];


/****************************** Hauptprogramm **************************/

int main ( void )
{
  i=0; j=0; k=0; l=0; m=0; n=0; o=0; p=0; q=0;



  /******************************Abfrage Dateinamen******************/


  printf( "Name der Eingabedatei:\n" );
  fgets(dateiname1, 80, stdin );
  length=strlen(dateiname1);
  if (length > 0)
    {
      dateiname1[length-1]='\0';
    }
    printf("Oeffne %s ...\n", dateiname1);
    cfile1 = fopen( dateiname1,"r" );



 /********************* Kopfzeilen lesen ********************* ***/



        if( fgets(header1, 200, cfile1)== NULL)
      {
            printf("Fehler! Leere Datei\n");
                }
```

```
/*                              fgets(header2, 100, cfile1); */
/*                 printf("Header2: %s\n", header2);       */



   printf( "Name der Ausgabedatei:\n" );
  fgets(dateiname2, 80, stdin );
  length=strlen(dateiname2);
  if (length > 0)
    {
      dateiname2[length-1]='\0';
    }
   printf("Oeffne %s ... zur Ausgabe!\n", dateiname2);
   cfile2 = fopen( dateiname2,"w" );

   fprintf(cfile2, "%s", header1);

  /******** Routine zum Einlesen (Kat-File) **********/

          while ((j=fscanf(cfile1,
 "%d %d %d %d %d %lf %lf %lf %lf %lf %lf %d %lf %lf %lf %lf %lf %lf %lf %lf",
                          &plate[k],
                          &MJD[k], &Fiber[k],
                          &SpecClass[k], &bin[k],
                          &ra[k], &dec[k],
                          &Prof_G[k],
                          &z[k], &zErr[k], &zConf[k],
                          &zStat[k],
                          &utot[k],&gtot[k],&rtot[k],
                          &itot[k],&ztot[k],&petroRad_r[k],
                          &petroR50_r[k],&petroR90_r[k]))!=EOF)
            {
              l_id[k]=k;
              k++;}


          fclose(cfile1);

          printf("fertig mit Einlesen\n");

 /*********************** Array initialisieren ****************/

          for (o=0; o < Maxz; o++)
            {
              for (p=0; p< 15; p++)
```

```c
                        {
                           Prof_G_Array[o][p]=0;
                        }

                  }

   printf("fertig mit Initialisieren\n");

   /******************** Sortieren der Surface_Brightnesses in Arrays **********/




            for (j=0;j<k; j++)

              {


                if (bin[j]==0)
                 {
                plate_out[i]=plate[j];
                MJD_out[i]=MJD[j];
                Fiber_out[i]=Fiber[j];
                SpecClass_out[i]=SpecClass[j];
                bin_out[i]=bin[j];
                ra_out[i]=ra[j];
                dec_out[i]=dec[j];
                Prof_G_Array[i][0]=Prof_G[j];
                z_out[i]=z[j];
                zErr_out[i]=zErr[j];
                zConf_out[i]=zConf[j];
                zStat_out[i]=zStat[j];
                utot_out[i]=utot[j];
                gtot_out[i]=gtot[j];
                rtot_out[i]=rtot[j];
                itot_out[i]=itot[j];
                ztot_out[i]=ztot[j];
                petroRad_r_out[i]=petroRad_r[j];
                petroR50_r_out[i]=petroR50_r[j];
                petroR90_r_out[i]=petroR90_r[j];
                l_id[i]=i;
                i++;
                }
```

```
                }



            for (l=0; l<i; l++)
              {

                for (n=0; n<k; n++)
                  {
                      if(Fiber_out[l]==Fiber[n] && plate_out[l]==plate[n])
                       {
                          if (Prof_G[n] > 0)
                            {
                               Prof_G_Array[l][bin[n]]=-2.5*log10(Prof_G[n]);
                            }
                       }

                  }


              }



            for (m=0; m<i; m++)
              {
  fprintf(cfile2,
        "%d %d %d %d %d %d %.9f %.9f %.5f %.5f %.5f %.5f %.5f %.5f %.5f %.5f
%.5f %.5f %.5f %.5f %.5f %.5f %.5f %.9f %.9f %.5f %d %.5f %.5f %.5f %.5f %.5f
%.5f %.5f %.5f\n",
        l_id[m], plate_out[m], MJD_out[m], Fiber_out[m], SpecClass_out[m],
        bin_out[m],
        ra_out[m], dec_out[m], Prof_G_Array[m][0], Prof_G_Array[m][1],
      Prof_G_Array[m][2], Prof_G_Array[m][3], Prof_G_Array[m][4],
       Prof_G_Array[m][5], Prof_G_Array[m][6], Prof_G_Array[m][7],
       Prof_G_Array[m][8], Prof_G_Array[m][9], Prof_G_Array[m][10],
       Prof_G_Array[m][11], Prof_G_Array[m][12], Prof_G_Array[m][13],
       Prof_G_Array[m][14], z_out[m], zErr_out[m], zConf_out[m],
       zStat_out[m], utot_out[m], gtot_out[m], rtot_out[m], itot_out[m],
```

```c
                ztot_out[m], petroRad_r_out[m], petroR50_r_out[m], petroR90_r_out[m]);
                }

   fclose(cfile2);




   /******************** Ausgabe in Files fr Nfit1d *********************/




   while (strncmp(yes_no, "y", 1)!=0 && strncmp(yes_no,"n", 1)!=0)
     {

       printf("Sollen Files fr IRAF nfit1d erstellt werden (y/n)?\n");
       fgets(yes_no, 10, stdin);

     }



  if(strncmp(yes_no, "y", 1)==0)

 {

   for (q=0; q<i; q++)
     {
       dateiname3[0]='\0';
       sprintf(stringg, "%d", plate_out[q]);
       strcat(dateiname3,stringg);
       strcat(dateiname3,"_");
       sprintf(stringg, "%d", MJD_out[q]);
       strcat(dateiname3,stringg);
       strcat(dateiname3,"_");
       sprintf(stringg, "%d", Fiber_out[q]);
       strcat(dateiname3,stringg);
       strcat(dateiname3,".tmp");

       cfile3=fopen(dateiname3, "w");


       if( Prof_G_Array[q][0] > 0)
         { fprintf(cfile3,"0.1626345 %.9f\n", Prof_G_Array[q][0]);}

       if( Prof_G_Array[q][1] > 0)
         {fprintf(cfile3,"0.5075923 %.9f\n", Prof_G_Array[q][1]);}
```

```
        if( Prof_G_Array[q][2] > 0)
          {fprintf(cfile3,"0.8727256 %.9f\n", Prof_G_Array[q][2]);}

        if( Prof_G_Array[q][3] > 0)
          {fprintf(cfile3,"1.4419605 %.9f\n", Prof_G_Array[q][3]);}

        if( Prof_G_Array[q][4] > 0)
          {fprintf(cfile3,"2.4594308 %.9f\n", Prof_G_Array[q][4]);}

        if( Prof_G_Array[q][5] > 0)
          {fprintf(cfile3,"3.9010832 %.9f\n", Prof_G_Array[q][5]);}

        if( Prof_G_Array[q][6] > 0)
          {fprintf(cfile3,"6.1903877 %.9f\n", Prof_G_Array[q][6]);}


        fclose(cfile3);
      }
  }


 printf("Fertig!!!!\n");

 return 0;
}
```

A.2   Program for Merging the Data after nfit1d

```
/****************************************************************************/
/*                                                                        */
/*                       SB_merge_post_nfit1d                             */
/*                  needs input files sorted by plate/fiber              */
/*                          Version 07/2005                               */
/*        Copyright by Dominik Rosenbaum, Astronomisches Institut, RUB     */
/****************************************************************************/

#include <stdio.h>
#include <stdlib.h>
#include <math.h>
#include <string.h>


/********************** Konstanten-Definition ****************************/

#define Maxz 200000

/********************** Variablendefinition ****************************/

int zae,i, j, k, l, m, n, o, p, q, r, length, l_id[Maxz];
int kleq_gr;
double mag, progress;
char smag[20], skleq_gr[20], header1[200];
FILE *cfile1, *cfile2, *cfile3, *cfile4;

char dateiname1[100], dateiname2[100], dateiname3[100], dateiname4[100];
int plate[Maxz], MJD[Maxz], Fiber[Maxz], SpecClass[Maxz], bin[Maxz];
double ra[Maxz], dec[Maxz], Prof_G_Array[Maxz][15], z[Maxz], zErr[Maxz];
double zConf[Maxz];
int zStat[Maxz];
double utot[Maxz],gtot[Maxz],rtot[Maxz],itot[Maxz],ztot[Maxz];

int plateG[Maxz], MJDG[Maxz], FiberG[Maxz];
double shisqG[Maxz], errG[Maxz], mueG[Maxz], scalelengthG[Maxz];
int plateR[Maxz], MJDR[Maxz], FiberR[Maxz];
double shisqR[Maxz], errR[Maxz], mueR[Maxz], scalelengthR[Maxz];

int l_id_out[Maxz], plate_out[Maxz], MJD_out[Maxz], Fiber_out[Maxz];
int  SpecClass_out[Maxz], bin_out[Maxz];
double ra_out[Maxz], dec_out[Maxz], Prof_G_Array_out[Maxz][15];
double z_out[Maxz], zErr_out[Maxz];
double zConf_out[Maxz];
int zStat_out[Maxz];
```

```
double mueB_out[Maxz];
double utot_out[Maxz],gtot_out[Maxz],rtot_out[Maxz],itot_out[Maxz];
double ztot_out[Maxz];
double petroRad_r_out[Maxz],petroR50_r_out[Maxz],petroR90_r_out[Maxz];
double petroRad_r[Maxz],petroR50_r[Maxz],petroR90_r[Maxz];

/****************************** Hauptprogramm **************************/

int main ( void )
{
  i=0; j=0; k=0; l=0; m=0; n=0; o=0; p=0; q=0; r=0;



  /*****************************Abfrage Dateinamen*******************/


  printf( "Name der Eingabedatei mit ra dec (G-Filter):\n" );
  fgets(dateiname1, 80, stdin );
  length=strlen(dateiname1);
  if (length > 0)
    {
      dateiname1[length-1]='\0';
    }
     printf("Oeffne %s ...\n", dateiname1);
     cfile1 = fopen( dateiname1,"r" );


    printf( "Name der Eingabedatei (IRAF nfit1d, G-Filter):\n" );
  fgets(dateiname2, 80, stdin );
  length=strlen(dateiname2);
  if (length > 0)
    {
      dateiname2[length-1]='\0';
    }
     printf("Oeffne %s ...\n", dateiname2);
     cfile2 = fopen( dateiname2,"r" );

       printf( "Name der Eingabedatei (IRAF nfit1d, R-Filter):\n" );
  fgets(dateiname3, 80, stdin );
  length=strlen(dateiname3);
  if (length > 0)
    {
      dateiname3[length-1]='\0';
    }
```

```c
    printf("Oeffne %s ...\n", dateiname3);
    cfile3 = fopen( dateiname3,"r" );


      printf( "Name der Ausgabedatei:\n" );
 fgets(dateiname4, 80, stdin );
 length=strlen(dateiname4);
 if (length > 0)
   {
     dateiname4[length-1]='\0';
   }
    printf("Oeffne %s ...\n", dateiname4);
    cfile4 = fopen( dateiname4,"w" );




  printf("Welche Grenz-Surface Brightness?\n");

 fgets ( smag, 10, stdin);

 mag=atof(smag);

 printf("Welche Selektion (1) oder (2)?\n");

 printf("(Zur Selektion von Galaxien heller als Grenz-SB: '1' eingeben)\n");


printf("(Zur Selektion von Galaxien dunkler als Grenz-SB: '2' eingeben\n)");

printf("Also welche Selektion (1) oder (2)?\n");

fgets ( skleq_gr, 2, stdin);

kleq_gr=atoi(skleq_gr);

printf ("Seletion: %d\n",kleq_gr);
```

```
/*********************** Kopfzeilen lesen *********************** ***/



        if( fgets(header1, 200, cfile1)== NULL)
      {
       printf("Fehler! Leere Datei\n"); }



  /******** Routine zum Einlesen (Kat-File) **********/

        while ((j=fscanf(cfile1,
  "%d %d %d %d %d %d %lf %lf %lf %lf %lf %lf %lf %lf %lf %lf %lf %lf %lf %lf
%lf %lf %lf %lf %lf %lf %d %lf %lf %lf %lf %lf %lf %lf %lf",
                        &l_id[k],
                        &plate[k],
                        &MJD[k], &Fiber[k],
                        &SpecClass[k], &bin[k],
                        &ra[k], &dec[k],
                        &Prof_G_Array[k][0],
                        &Prof_G_Array[k][1],
                        &Prof_G_Array[k][2],
                        &Prof_G_Array[k][3],
                        &Prof_G_Array[k][4],
                        &Prof_G_Array[k][5],
                        &Prof_G_Array[k][6],
                        &Prof_G_Array[k][7],
                        &Prof_G_Array[k][8],
                        &Prof_G_Array[k][9],
                        &Prof_G_Array[k][10],
                        &Prof_G_Array[k][11],
                        &Prof_G_Array[k][12],
                        &Prof_G_Array[k][13],
                        &Prof_G_Array[k][14],
                        &z[k], &zErr[k], &zConf[k],
                        &zStat[k],&utot[k],
                        &gtot[k],&rtot[k],
                        &itot[k],&ztot[k],
                        &petroRad_r[k], &petroR50_r[k],
                        &petroR90_r[k]))!=EOF)
            {
```

```
      k++;}


fclose(cfile1);

while ((j=fscanf(cfile2,
                 "%d  %d %d %lf %lf %lf %lf",
                 &plateG[l], &MJDG[l], &FiberG[l],
                 &shisqG[l], &errG[l], &mueG[l],
                 &scalelengthG[l]))!=EOF)
  {

    l++;}


fclose(cfile2);


while ((j=fscanf(cfile3,
                 "%d  %d %d %lf %lf %lf %lf",
                 &plateR[m], &MJDR[m], &FiberR[m],
                 &shisqR[m], &errR[m], &mueR[m],
                 &scalelengthR[m]))!=EOF)
  {

    m++;}


fclose(cfile3);




printf("fertig mit Einlesen\n");




printf("Bearbeite Daten\n");
```

```
          o=0;
          p=0;
          for(n=0; n < k; n++)
            {
              while ((plate[n]>plateG[o] || (plate[n]==plateG[o]
&& Fiber[n]>FiberG[o]) || (plate[n]==plateG[o] && Fiber[n]==FiberG[o]
&& MJD[n]>MJDG[o])) && o<l) o++;
              if (plate[n]<plateG[o] || (plate[n]==plateG[o]
&& Fiber[n]<FiberG[o]) || ((plate[n]==plateG[o] && Fiber[n]==FiberG[o]
&& MJD[n]<MJDG[o]))) continue;


              while ((plateG[o]>plateR[p] || (plateG[o]==plateR[p]
&& FiberG[o]>FiberR[p]) ||(plateG[o]==plateR[p] && FiberG[o]==FiberR[p]
&&  MJDG[o]>MJDR[p])) && p<m) p++;
              if (plateG[o]<plateR[p] ||
(plateG[o]==plateR[p] && FiberG[o]<FiberR[p]) ||
((plateG[o]==plateR[p] && FiberG[o]==FiberR[p] && MJDG[o]<MJDR[p]))) continue;


                        l_id_out[q]= l_id[n];
                        plate_out[q] = plate[n];
                        MJD_out[q] = MJD[n];
                        Fiber_out[q] = Fiber[n];
                        SpecClass_out[q]=SpecClass[n];
                        bin_out[q]=bin[n];
                        ra_out[q]=ra[n];
                        dec_out[q]=dec[n];
                        Prof_G_Array_out[q][0]=mueG[o];
                        Prof_G_Array_out[q][1]=mueR[p];
                        z_out[q]=z[n];
                        zErr_out[q]=zErr[n];
                        zConf_out[q]=zConf[n];
                        zStat_out[q]=zStat[n];
                        mueB_out[q]=mueG[o]+0.47*(mueG[o]-mueR[p])+0.17;
                        utot_out[q]=utot[n];
                        gtot_out[q]=gtot[n];
                        rtot_out[q]=rtot[n];
                        itot_out[q]=itot[n];
                        ztot_out[q]=ztot[n];
                        petroRad_r_out[q]=petroRad_r[n];
                        petroR50_r_out[q]=petroR50_r[n];
                        petroR90_r_out[q]=petroR90_r[n];
                        q++;
```

```c
            progress=(n*1.000)/(k*1.000)*100;
            printf("Progress: %.2f Prozent \n", progress);
          }
         printf(" %d %d Prozent \n", o,p);
         printf("Schreibe Ausgabedatei\n");


         /********************* Ausgabe in Datei *************************/
  if (kleq_gr==1)
    {


         for (r=0; r < q; r++)
           {


             if(  mueB_out[r] <= mag )
               {

                 fprintf(cfile4,
   "%d %d %d %d %d %d %.9f %.9f %.9f %.9f %.9f %.9f %.9f %d %.9f %.9f %.9f
%.5f %.5f %.5f %.5f %.5f %.5f %.5f %.5f\n",
                     l_id_out[r], plate_out[r], MJD_out[r], Fiber_out[r],
                     SpecClass_out[r], bin_out[r], ra_out[r], dec_out[r],
                     Prof_G_Array_out[r][0], Prof_G_Array_out[r][1],
                     z_out[r], zErr_out[r], zConf_out[r], zStat_out[r],
                     Prof_G_Array_out[r][0], Prof_G_Array_out[r][1],
                     mueB_out[r], utot_out[r], gtot_out[r], rtot_out[r],
                     itot_out[r], ztot_out[r], petroRad_r_out[r],
                     petroR50_r_out[r], petroR90_r_out[r]);
               }
           }
    }


  if (kleq_gr==2)
    {


         for (r=0; r < q; r++)
```

```
               {


           if(  mueB_out[r] > mag )
             {

               fprintf(cfile4,
    "%d %d %d %d %d %d %.9f %.9f %.9f %.9f %.9f %.9f %.9f %d %.9f %.9f %.9f
  %.5f %.5f %.5f %.5f %.5f %.5f %.5f %.5f\n",
                       l_id_out[r], plate_out[r], MJD_out[r], Fiber_out[r],
                       SpecClass_out[r], bin_out[r], ra_out[r], dec_out[r],
                       Prof_G_Array_out[r][0], Prof_G_Array_out[r][1],
                       z_out[r], zErr_out[r], zConf_out[r], zStat_out[r],
                       Prof_G_Array_out[r][0], Prof_G_Array_out[r][1],
                       mueB_out[r], utot_out[r], gtot_out[r], rtot_out[r],
                       itot_out[r], ztot_out[r], petroRad_r_out[r],
                       petroR50_r_out[r], petroR90_r_out[r]);
             }
           }
     }

         fclose(cfile4);


         printf("fertig ;-)\n");

         return 0;
  }
```

A.3   Program for Neighbour Counting with Spheres

```
/****************************************************************************/
/*                          Gal_Kugel_Vol                               */
/*                        Version 8/2005 (DR4)                          */
/*      Copyright by Dominik Rosenbaum, Astronomisches Institut, RUB    */
/****************************************************************************/


/* zaehlt die Anzahl der Nachbargalaxien innerhalb eines Kugelvolumens    */

#include <stdio.h>
#include <stdlib.h>
#include <math.h>
#include <string.h>



/*********************** Konstanten-Definition ***************************/

#define Maxz 300000


/*********************** Variablendefinition ***************************/
int zae,i, j, k, l, m, n, o, p, length, nr[Maxz], n_nachbar[Maxz];
/* long specobj_ID[Maxz]; */
FILE *cfile1, *cfile2, *cselektion;
char dateiname1[100], dateiname2[100], header1[100], header2[100];
char sk_vol[10], skleq_gr[2];
int l_id[Maxz], pobj_field_seg_run[Maxz], pobj_field_seg_rerun[Maxz];
int pobj_field_seg_camCol[Maxz],pobj_field_field[Maxz];
int pobj_objid[Maxz],zStatus[Maxz],kleq_gr;
double ra[Maxz], dec[Maxz], SFB[Maxz], SFB_r[Maxz], SFB_B[Maxz], k_vol;
double Prof_G1[Maxz],Prof_G2[Maxz],Prof_G3[Maxz],Prof_G4[Maxz],Prof_G5[Maxz];
double Prof_G6[Maxz],Prof_G7[Maxz],Prof_G8[Maxz],Prof_G9[Maxz],Prof_G10[Maxz];
double Prof_G11[Maxz],Prof_G12[Maxz],Prof_G13[Maxz],Prof_G14[Maxz];
double Prof_G15[Maxz],z[Maxz],zErr[Maxz],zConf[Maxz];
double xk[Maxz], yk[Maxz], zk[Maxz], dx, dy, dz;
double hubble, lichtg,pi;
double decmin, decmax;
double deltamin[Maxz], deltamax[Maxz], arg_arctan;
double utot[Maxz], gtot[Maxz], rtot[Maxz], itot[Maxz], ztot[Maxz];
double petroRad_r[Maxz], petroR50_r[Maxz], petroR90_r[Maxz];
double progress;
/*********************** Hauptprogramm ***************************/

int main ( void )
```

```
{
  i=0; j=0; k=0; l=0; m=0; n=0;
  pi=3.14159265358;
  hubble=71.0;
  lichtg=300000.0;

  /* Deklinationsbereich */

  decmin=-1.2;


  decmax=+1.2;

  /*******************************Abfrage Dateinamen*******************/


  printf( "Name der Eingabedatei:\n" );
  fgets(dateiname1, 80, stdin );
  length=strlen(dateiname1);
  if (length > 0)
    {
      dateiname1[length-1]='\0';
    }
    printf("Oeffne %s ...\n", dateiname1);
    cfile1 = fopen( dateiname1,"r" );

  printf( "Name der Ausgabedatei:\n" );
  fgets(dateiname2, 80, stdin );
  length=strlen(dateiname2);
  if (length > 0)
    {
      dateiname2[length-1]='\0';
    }
    printf("Oeffne %s ... zur Ausgabe!\n", dateiname2);
    cfile2 = fopen( dateiname2,"w" );

 printf("Radius zu welchem Volumen? [Mpc]\n");

  fgets ( sk_vol, 10, stdin);

  k_vol=atof(sk_vol);

  printf("Kugelvolumen: 4/3*PI* %.3f  Mpc\n",  k_vol);

  /******** Routine zum Einlesen (Kat-File) **********/
```

```
            while ((j=fscanf(cfile1,
"%d %d %d %d %d %d %lf %lf %lf %lf %lf %lf %lf %d %lf %lf %lf %lf %lf %lf %lf
%lf %lf %lf %lf",
                              &l_id[k],
                              &pobj_field_seg_run[k],
                              &pobj_field_seg_rerun[k], &pobj_field_seg_camCol[k],
                              &pobj_field_field[k], &pobj_objid[k],
                              &ra[k], &dec[k],
                              &Prof_G1[k], &Prof_G2[k],
                              &z[k], &zErr[k], &zConf[k],
                              &zStatus[k], &SFB[k], &SFB_r[k], &SFB_B[k],
                              &utot[k], &gtot[k], &rtot[k], &itot[k],
                              &ztot[k],
                              &petroRad_r[k], &petroR50_r[k],
                              &petroR90_r[k]))!=EOF)
            {

              k++;


            }


    fclose (cfile1);


    /******************* Daten in karth Koord umrechnen *******************/



    for (m=0; m < k; m++)

      {
        xk[m]=(((z[m]+1)*(z[m]+1)-1)/((z[m]+1)*(z[m]+1)+1))*(lichtg/hubble)
*cos(pi*ra[m]/180.0)*sin(pi*(90.0-dec[m])/180.0);
        yk[m]=(((z[m]+1)*(z[m]+1)-1)/((z[m]+1)*(z[m]+1)+1))*(lichtg/hubble)
*sin(pi*ra[m]/180.0)*sin(pi*(90.0-dec[m])/180.0);
        zk[m]=(((z[m]+1)*(z[m]+1)-1)/((z[m]+1)*(z[m]+1)+1))*(lichtg/hubble)
*cos(pi*(90.0-dec[m])/180.0);


    /* printf("%d %.5f %.5f %.5f %.5f %.5f %.5f\n", l_id[m], ra[m], dec[m],
            z[m], xk[m], yk[m], zk[m]);
    */
```

```
        }


    /************* Abstaende berechnen *************/


    printf("Berechne Koordinaten und suche nach Nachbarn\n");

    for (p=0; p < k; p++)
      {
        n_nachbar[p]=0;
      }


    for (n=0; n < k; n++)



      {


        for (o=0; o < k; o++)

          {
            if(o!=n)
              {
                dx=xk[n]-xk[o];
                dy=yk[n]-yk[o];
                dz=zk[n]-zk[o];
                if (sqrt((dx*dx)+(dy*dy)+(dz*dz)) <= k_vol)
                {
                  n_nachbar[n]++;
                }

              }

          }
        /*
        printf ("%d %d\n", l_id[n], n_nachbar[n]);
        */

                progress=(n*1.0)/(k*1.0)*100;
                printf("Progr.: %.2f Prozent \n", progress);
      }
```

```
/******************** Ausgabe der Galaxien ********************/

    for (m=0; m < k; m++)


         {


              arg_arctan=(k_vol /(((z[m]+1)*(z[m]+1)-1)/((z[m]+1)*(z[m]+1)+1)
*lichtg/hubble));
              /*
              arg_arctan=(3.9 /(((z[m]+1)*(z[m]+1)-1)/((z[m]+1)*(z[m]+1)+1)
*lichtg/hubble));
              */
              deltamin[m] = decmin + 0.1 + (180.0*atan(arg_arctan)/pi);
              deltamax[m] = decmax - 0.1 - (180.0*atan(arg_arctan)/pi);

              /* Ausgabe in Selektion.dat; * = Selektion fuer Datei */
              printf("%d %d %0.5f %0.5f %0.5f %0.5f %0.5f", l_id[m],
n_nachbar[m], ra[m], dec[m], z[m], deltamin[m], deltamax[m]);

              /*      cselektion=fopen("Selektion.dat", "w");

              fprintf(cselektion,"%d %d %0.5f %0.5f %0.5f %0.5f %0.5f",
              l_id[m], n_nachbar[m], ra[m], dec[m], z[m], deltamin[m],
              deltamax[m]);
              */


              if ((0.01 <= z[m] && z[m] <= 0.1) && ((144.0 <= ra[m] && ra[m]
<= 197.0) || (144.0 <= ra[m] && ra[m] <= 197.0)) && (deltamin[m] <= dec[m] &&
dec[m] <= deltamax[m])) { printf(" *");}

              printf("\n");


    /*  Ende Ausgabe in Selektion.dat */


              /*  Anfang Ausgabe in Datei */


              /*  if ((0.055 <= z[m] && z[m] <= 0.1) && */
  if ((0.01 <= z[m] && z[m] <= 0.055) &&
```

```
     ((175.0 < ra[m] && ra[m] < 202.0 &&  -3.2 < dec[m] && dec[m]<-0.2)||
      (132.0 < ra[m] && ra[m] < 226.0 && -0.2 < dec[m] && dec[m]< 4.2)||
      (130.0 < ra[m] && ra[m]  < 166.0 && 4.2 < dec[m] && dec[m]< 9.0)||
      (166.0 < ra[m] && ra[m]  < 184.0 && 4.2 < dec[m] && dec[m]< 5.7)||
      (189.0 < ra[m] && ra[m]  < 210.0 && 4.2 < dec[m] && dec[m]< 5.4)||
      (144.0 < ra[m] && ra[m]  < 159.0 && 9.0 < dec[m] && dec[m]< 12.0)||
      (166.0 < ra[m] && ra[m]  < 186.0 && 9.0 < dec[m] && dec[m]< 13.0)||
      (202.0 < ra[m] && ra[m]  < 235.0 && -2.2 < dec[m] && dec[m]< -0.2)||
      (118.0 < ra[m] && ra[m]  < 125.5 && 24.0 < dec[m] && dec[m]<49.5)||
      (125.5 < ra[m] && ra[m]  < 141 && 32.2 < dec[m] && dec[m]< 52.5)||
      (141.0 < ra[m] && ra[m]  < 168.0 && 40.0 < dec[m] && dec[m]< 61.5)||
      (168.0 < ra[m] && ra[m]  < 196.0 && 42.0 < dec[m] && dec[m]< 68.0)||
      (196.0 < ra[m] && ra[m]  < 220.0 && 53.0 < dec[m] && dec[m]< 64.0)||
      (196.0 < ra[m] && ra[m]  < 223.0 && 41.0 < dec[m] && dec[m]< 45.0)||
      (220.0 < ra[m] && ra[m]  < 237.0 && 48.0 < dec[m] && dec[m]< 57.0)||
      (223.0 < ra[m] && ra[m]  < 248.0 && 34.0 < dec[m] && dec[m]< 48.0)||
      (311.8 < ra[m] && ra[m]  < 360.0 &&
    deltamin[m] < dec[m] && dec[m] < deltamax[m])||
   (0.0 < ra[m] && ra[m]  < 53.9 &&
    deltamin[m] < dec[m] && dec[m] < deltamax[m])))


              {

     fprintf(cfile2,
"%d %d %d %d %d %d %.9f %.9f %.3f %.3f %.5f %.5f %.5f %d %.5f %.5f %.6f %.5f
%.5f %.5f %.5f %.5f %.5f %.5f %.5f\n",
                         l_id[m], pobj_field_seg_run[m],
                         pobj_field_seg_rerun[m], pobj_field_seg_camCol[m],
                         pobj_field_field[m], n_nachbar[m],
                         ra[m], dec[m], SFB[m], SFB_r[m], z[m],
                         zErr[m], zConf[m],
                         zStatus[m], SFB[m], SFB_r[m], SFB_B[m],
                         utot[m],gtot[m],rtot[m],itot[m],ztot[m],
                         petroRad_r[m], petroR50_r[m], petroR90_r[m]);

                }
            }

     fclose (cfile2);

     printf("fertig ;-)\n");

     return 0;
  }
```

A.4   Cluster Finding Algorithm

```
/**************************************************************************/
/*                       Search_Clusters_DR4.c                         */
/*                         Version 10/2005                             */
/*       Copyright by Dominik Rosenbaum, Astronomisches Institut, RUB   */
/**************************************************************************/


/*                 sucht nach Clustern / fingers of God in der DR4       */

#include <stdio.h>
#include <stdlib.h>
#include <math.h>
#include <string.h>



/*********************** Konstanten-Definition ***************************/

#define Maxz 300000



/*********************** Variablendefinition ***************************/
int zae,i, j, k, l, m, n, o, p, length, nr[Maxz], n_nachbar[Maxz];
/* long specobj_ID[Maxz]; */
FILE *cfile1, *cfile2, *cselektion;
char dateiname1[100], dateiname2[100], header1[100], header2[100];
char sk_vol[10], ssearch_dispersion[10],scluster_members[10];
int l_id[Maxz], pobj_field_seg_run[Maxz], pobj_field_seg_rerun[Maxz];
int pobj_field_seg_camCol[Maxz],pobj_field_field[Maxz];
int pobj_objid[Maxz],zStatus[Maxz],kleq_gr;
double ra[Maxz], dec[Maxz], SFB[Maxz], SFB_r[Maxz], SFB_B[Maxz], k_vol;
double Prof_G1[Maxz],Prof_G2[Maxz],Prof_G3[Maxz],Prof_G4[Maxz],Prof_G5[Maxz];
double Prof_G6[Maxz],Prof_G7[Maxz],Prof_G8[Maxz],Prof_G9[Maxz],Prof_G10[Maxz];
double Prof_G11[Maxz],Prof_G12[Maxz],Prof_G13[Maxz],Prof_G14[Maxz];
double Prof_G15[Maxz],z[Maxz],zErr[Maxz],zConf[Maxz];
double xk[Maxz], yk[Maxz], zk[Maxz], dalpha, ddelta, dz;
double hubble, lichtg,pi;
double decmin, decmax;
double deltamin[Maxz], deltamax[Maxz], arg_arctan;
double utot[Maxz], gtot[Maxz], rtot[Maxz], itot[Maxz], ztot[Maxz];
double petroRad_r[Maxz],petroR50_r[Maxz],petroR90_r[Maxz];
double search_dispersion;
int cluster_members;
double progress;
char dateiname3[100];
```

```
/***************************** Hauptprogramm *************************/

int main ( void )
{
  i=0; j=0; k=0; l=0; m=0; n=0;
  pi=3.14159265358;
  hubble=71.0;
  lichtg=300000.0;

  /* Deklinationsbereich */

  decmin=-0.8;


  decmax=3.6;

  /*****************************Abfrage Dateinamen*******************/


  printf( "Name der Eingabedatei:\n" );
  fgets(dateiname1, 80, stdin );
  length=strlen(dateiname1);
  if (length > 0)
    {
      dateiname1[length-1]='\0';
    }
     printf("Oeffne %s ...\n", dateiname1);
     cfile1 = fopen( dateiname1,"r" );

  printf( "Name der Ausgabedatei ohne Clusters:\n" );
  fgets(dateiname2, 80, stdin );
  length=strlen(dateiname2);
  if (length > 0)
    {
      dateiname2[length-1]='\0';
    }
     printf("Oeffne %s ... zur Ausgabe!\n", dateiname2);
    cfile2 = fopen( dateiname2,"w" );

  printf( "Name der Ausgabedatei mit Clusters:\n" );
  fgets(dateiname3, 80, stdin );
  length=strlen(dateiname3);
  if (length > 0)
    {
      dateiname3[length-1]='\0';
```

```
    }
     printf("Oeffne %s ... zur Ausgabe!\n", dateiname3);



  printf("Welcher Radius fuer den Suchkonus? [Mpc]\n");

   fgets ( sk_vol, 10, stdin);

   k_vol=atof(sk_vol);

   printf("Radius: %.3f\n",  k_vol);


  printf("Welche Geschwindigkeitsdispersion? [km/s]\n");

   fgets (ssearch_dispersion, 10, stdin);

   search_dispersion=atof(ssearch_dispersion)/lichtg;


  printf("Dispersionsbereich: %.3f\n", search_dispersion);

  printf("Wieviele Cluster Members?\n");


  fgets (scluster_members, 10, stdin);

  cluster_members=atoi(scluster_members);


  printf("Cluster Members: %d\n", cluster_members);



   /******** Routine zum Einlesen (Kat-File) **********/

          while ((j=fscanf(cfile1,
"%d %d %d %d %d %d %lf %lf %lf %lf %lf %lf %lf %d %lf %lf %lf %lf %lf %lf %lf
%lf %lf %lf %lf",
                           &l_id[k],
                           &pobj_field_seg_run[k],
                           &pobj_field_seg_rerun[k], &pobj_field_seg_camCol[k],
```

```
                                  &pobj_field_field[k], &pobj_objid[k],
                                  &ra[k], &dec[k],
                                  &Prof_G1[k], &Prof_G2[k],
                                  &z[k], &zErr[k], &zConf[k],
                                  &zStatus[k], &SFB[k], &SFB_r[k], &SFB_B[k],
                                  &utot[k], &gtot[k], &rtot[k], &itot[k],
                                  &ztot[k], &petroRad_r[k], &petroR50_r[k],
                                  &petroR90_r[k]))!=EOF)
            {

               k++;


            }


     fclose (cfile1);


     /****************** Daten in karth Koord umrechnen ******************/



     //   for (m=0; m < k; m++)

     //     {
     //        xk[m]=(((z[m]+1)*(z[m]+1)-1)/((z[m]+1)*(z[m]+1)+1))*(lichtg/hubble)
*cos(pi*ra[m]/180.0)*sin(pi*(90.0-dec[m]))/180.0);
     //        yk[m]=(((z[m]+1)*(z[m]+1)-1)/((z[m]+1)*(z[m]+1)+1))*(lichtg/hubble)
*sin(pi*ra[m]/180.0)*sin(pi*(90.0-dec[m]))/180.0);
     //     zk[m]=(((z[m]+1)*(z[m]+1)-1)/((z[m]+1)*(z[m]+1)+1))*(lichtg/hubble)
*cos(pi*(90.0-dec[m])/180.0);


        /*        printf("%d %.5f %.5f %.5f %.5f %.5f %.5f\n", l_id[m], ra[m],
dec[m],
                 z[m], xk[m], yk[m], zk[m]);
        */

     // }


     /************ Abstaende berechnen ************/
```

```
   printf("Berechne Koordinaten und suche nach Nachbarn\n");

   for (p=0; p < k; p++)
     {
       n_nachbar[p]=0;
     }


   for (n=0; n < k; n++)



     {


       for (o=0; o < k; o++)

         {
           if(o!=n)
             {
 dalpha=2*((z[n]+1)*(z[n]+1)-1)/((z[n]+1)*(z[n]+1)+1)*lichtg/hubble
*sin(pi/180*(ra[n]-ra[o])/2);
 ddelta=2*((z[n]+1)*(z[n]+1)-1)/((z[n]+1)*(z[n]+1)+1)*lichtg/hubble*sin(pi/180
*(dec[n]-dec[o])/2);
 dz=((z[n]+1)*(z[n]+1)-1)/((z[n]+1)*(z[n]+1)+1)-((z[o]+1)*(z[o]+1)-1)/((z[o]+1)
*(z[o]+1)+1);
               if (sqrt((dalpha*dalpha)+(ddelta*ddelta)) <= k_vol &&
                  dz < search_dispersion && dz > (-1.0)*search_dispersion)
               {
                 n_nachbar[n]++;
               }

             }
         }

       progress=(n*1.000)/(k*1.000)*100;

   printf ("Galaxie: %d Nachbarn: %d  Progress: %.3f\n", l_id[n], n_nachbar[n],
             progress);

     }

   /******************** Ausgabe der Galaxien ********************/
```

```
   cselektion=fopen(dateiname3, "w");


     for (m=0; m < k; m++)



         {




           /* Ausgabe in Selektion.dat; * = Selektion fuer Datei */
           /*     printf("%d %d %0.5f %0.5f %0.5f %0.5f %0.5f", l_id[m],
n_nachbar[m], ra[m], dec[m], z[m], deltamin[m], deltamax[m]); */

           /*     cselektion=fopen("Selektion.dat", "w");

           fprintf(cselektion,"%d %d %0.5f %0.5f %0.5f %0.5f %0.5f",
           l_id[m], n_nachbar[m], ra[m], dec[m], z[m], deltamin[m],
           deltamax[m]);
           */



   if ( n_nachbar[m]>= cluster_members)
     {
     fprintf(cselektion, "%d %d %d %d %d %d %.9f %.9f %.5f %d %.9f %.5f %.5f %d
%.5f %.5f %.6f %.5f %.5f %.5f %.5f %.5f %.5f %.5f %.5f\n",
                         l_id[m], pobj_field_seg_run[m],
                         pobj_field_seg_rerun[m], pobj_field_seg_camCol[m],
                         pobj_field_field[m], pobj_objid[m],
                         ra[m], dec[m], Prof_G1[m], n_nachbar[m],
                         z[m], zErr[m], zConf[m],
                         zStatus[m], SFB[m], SFB_r[m], SFB_B[m],
                         utot[m],gtot[m],rtot[m],itot[m],ztot[m],
                         petroRad_r[m], petroR50_r[m], petroR90_r[m]);
     }

   //   printf("\n");



     /*  Ende Ausgabe in Selektion.dat */
```

```c
                  /*  Anfang Ausgabe in Datei */


               if ( n_nachbar[m] < cluster_members )
                 {

               fprintf(cfile2,
 "%d %d %d %d %d %d %.9f %.9f %.5f %d %.9f %.5f %.5f %d %.5f %.5f %.6f %.5f
%.5f %.5f %.5f %.5f %.5f %.5f %.5f\n",
                            l_id[m], pobj_field_seg_run[m],
                            pobj_field_seg_rerun[m], pobj_field_seg_camCol[m],
                            pobj_field_field[m], pobj_objid[m],
                            ra[m], dec[m], Prof_G1[m], n_nachbar[m],
                            z[m], zErr[m], zConf[m],
                            zStatus[m], SFB[m], SFB_r[m], SFB_B[m],
                            utot[m],gtot[m],rtot[m],itot[m],ztot[m],
                            petroRad_r[m], petroR50_r[m], petroR90_r[m]);


                 }

           }
   fclose (cfile2);

   printf("fertig ;-)\n");

   return 0;
}
```

Appendix B

Parameter Study for the Cluster Finding Code

In order to find the best parameters for the cluster finding algorithm, the parameter space containing the three adjustable parameters of radius r velocity dispersion σ and minimum number of cluster members $N_{Members}$ was varied within reasonable borders. Then the results were plotted. As the best compromise between the sensitivity for detecting clusters and the non detection of other structures the values $r = 2.5\,\mathrm{Mpc}$, $\sigma = 1000\,\mathrm{km/s}$ and $N_{Members} = 50$ were chosen. The diagrams at the following pages show the graphical results of this parameter study.
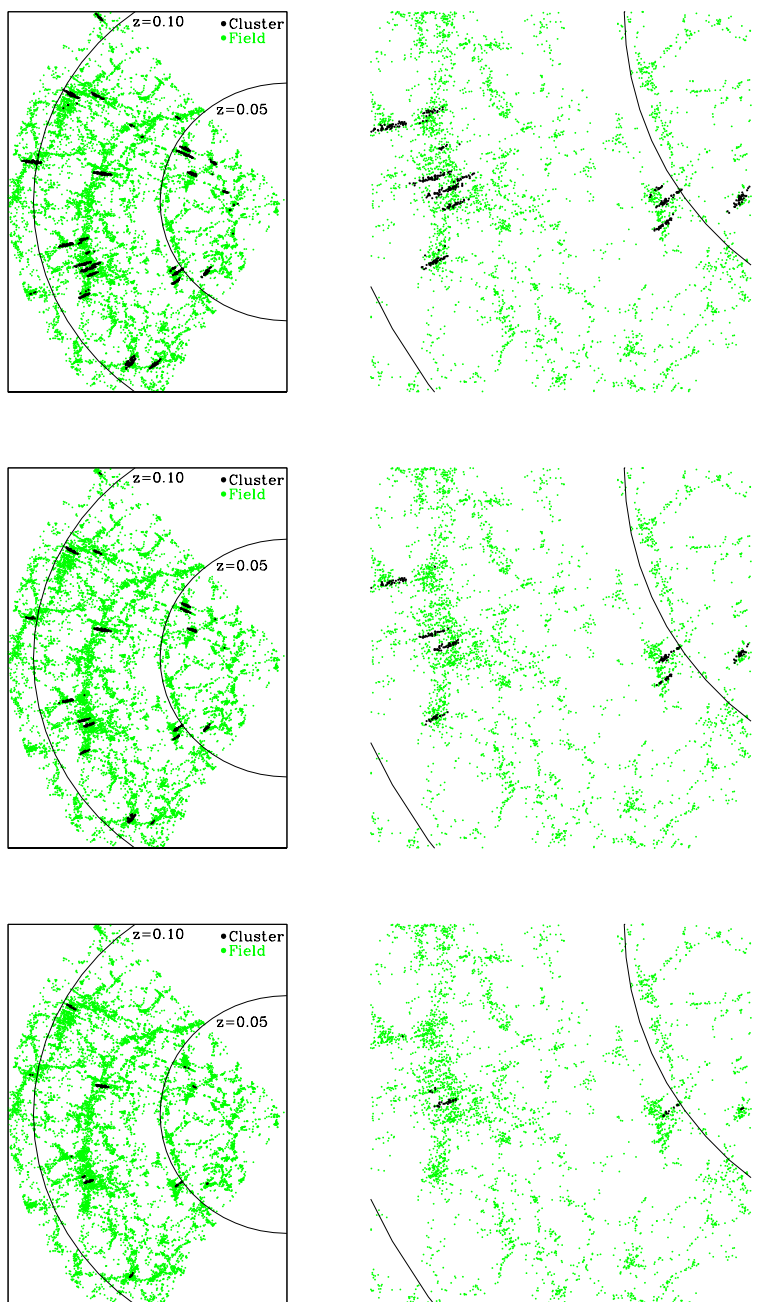
Figure B.1: Cluster search parameter study: Right panel is a zoom into left panel. Parameters (from top to bottom):

r (Mpc)	σ (km/s)	$N_{Members}$
2.0	1000	40
2.0	1000	50
2.0	1000	60
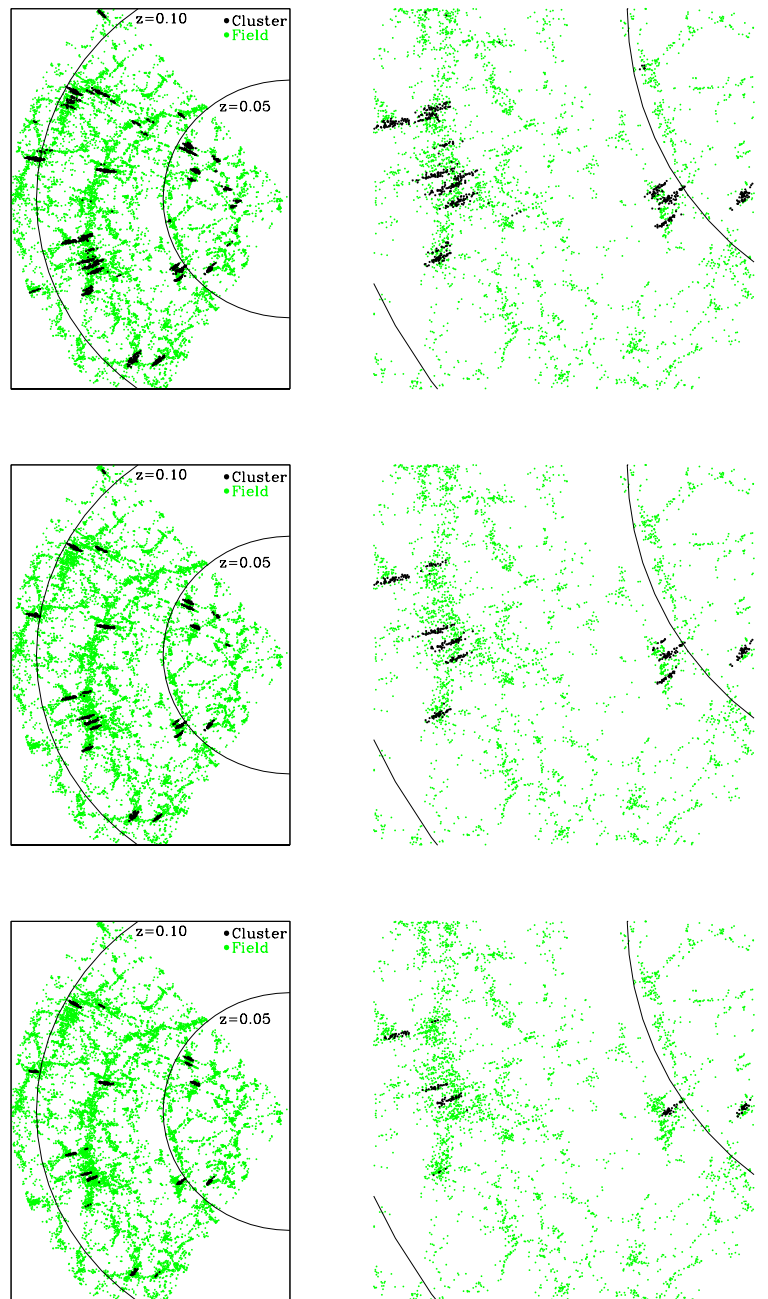
Figure B.2: Cluster search parameter study continued.
Parameters (from top to bottom):

r [Mpc]	σ [km/s]	$N_{Members}$
2.5	1000	40
2.5	1000	50
2.5	1000	60
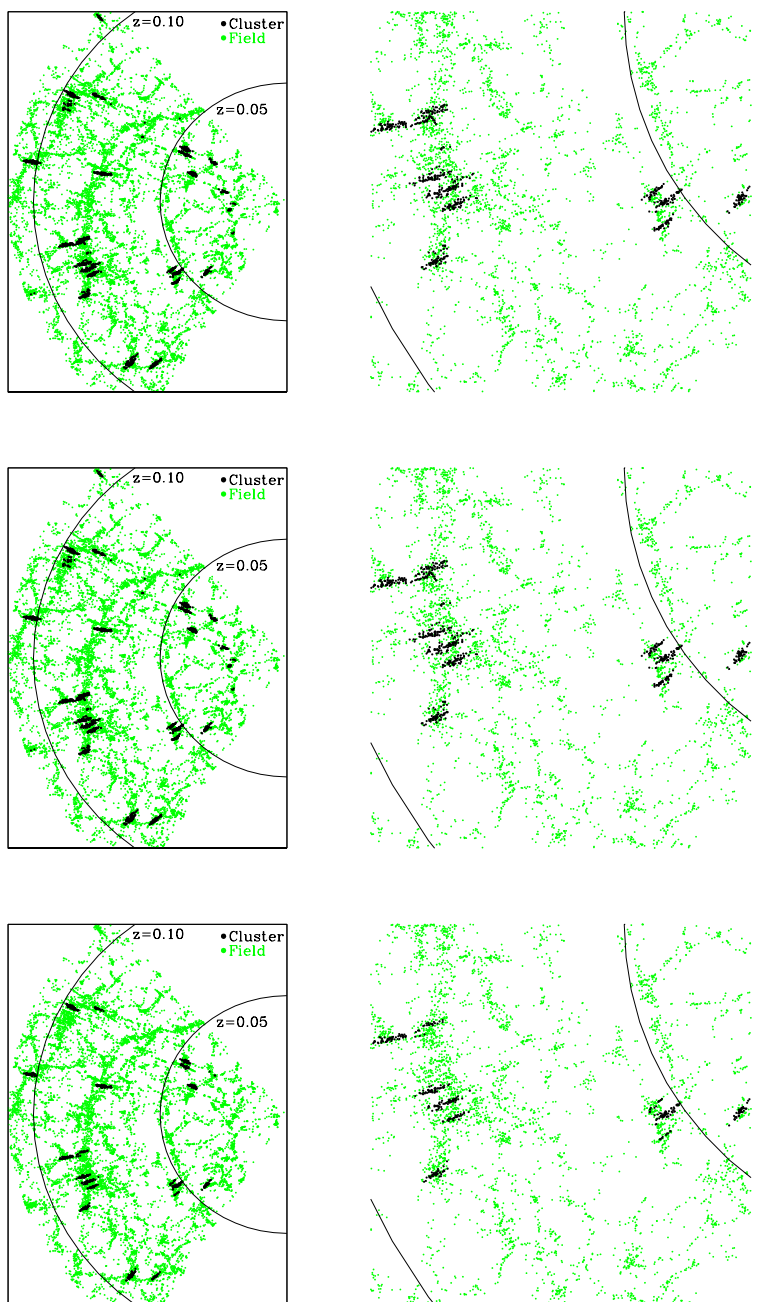
Figure B.3: Cluster search parameter study continued.
Parameters (from top to bottom):

r [Mpc]	σ [km/s]	$N_{Members}$
3.0	1000	40
3.0	1000	50
3.0	1000	60
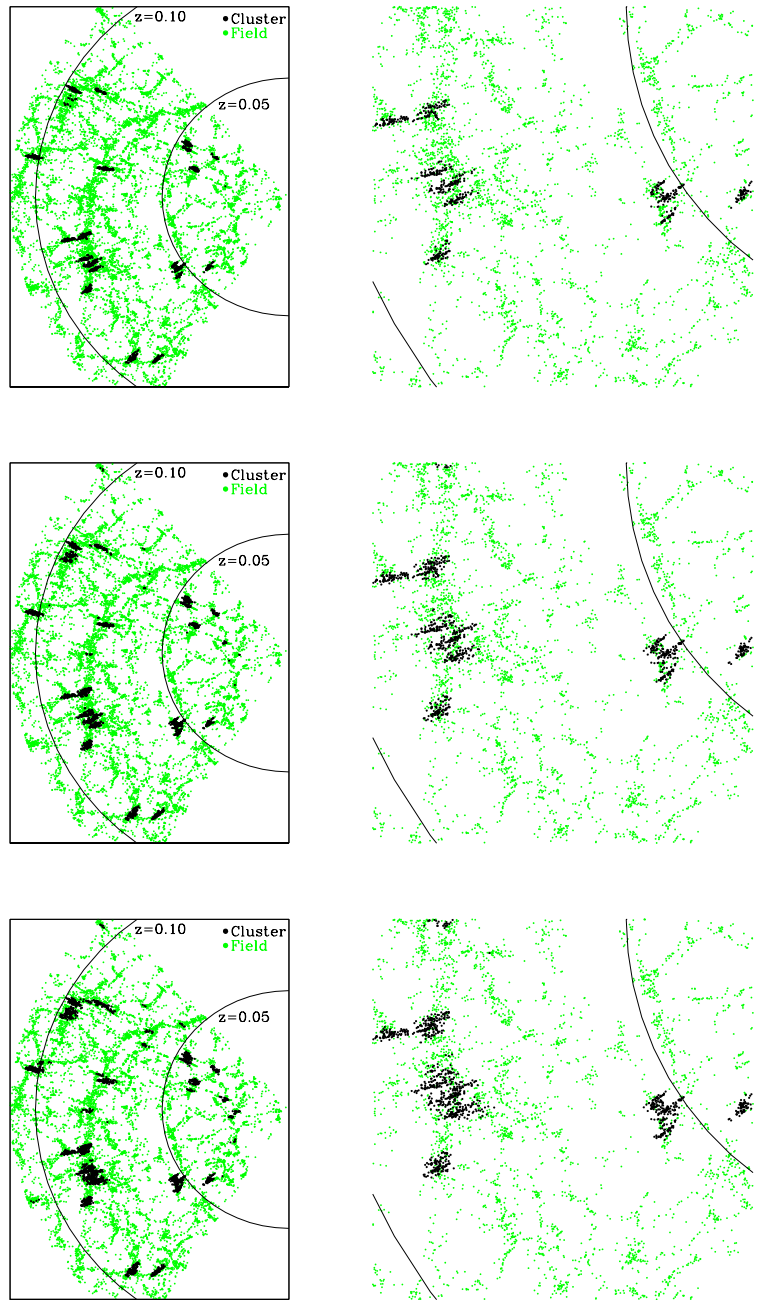
Figure B.4: Cluster search parameter study continued.
Parameters (from top to bottom):

r [Mpc]	σ [km/s]	$N_{Members}$
3.5	1000	50
4.0	1000	50
4.5	1000	50
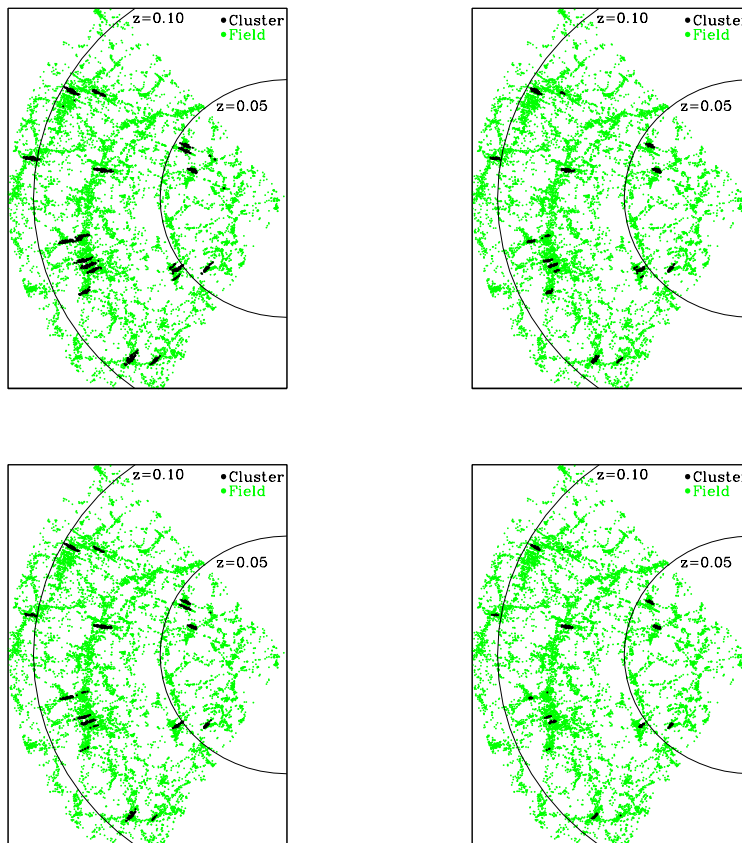
Figure B.5: Cluster search parameter study continued.
Parameters (from top left to bottom right):
r [Mpc] σ [km/s] $N_{Members}$
3.0   1200   50
3.0   800   50
2.5   1200   50
2.5   800   50

Bibliography

Abazajian, K., Adelman-McCarthy, J. K., Agüeros, M. A. & 150 co-authors, 2004: The Second Data Release of the Sloan Digital Sky Survey; AJ 128, 502–512

Abazajian, K., Adelman-McCarthy, J. K., Agüeros, M. A. & 186 co-authors, 2003: The First Data Release of the Sloan Digital Sky Survey; AJ 126, 2081–2086

Abell, G. O., 1958: The Distribution of Rich Clusters of Galaxies.; ApJS 3, 211+

Abell, G. O., Corwin, H. G. & Olowin, R. P., 1989: A catalog of rich clusters of galaxies; ApJS 70, 1–138

Adelman-McCarthy, J. K., Agüeros, M. A., Allam, S. S. & 151 co-authors, 2005: The Fourth Data Release of the Sloan Digital Sky Survey; ArXiv Astrophysics e-prints, arXiv:astro-ph/0507711

Arp, H., 1965: A Very Small, Condensed Galaxy.; ApJ 142, 402–406

Avila-Reese, V., Colin, P., Gottloeber, S., Firmani, C. & Maulbetsch, C., 2005: The dependence on environment of Cold Dark Matter Halo properties; ArXiv Astrophysics e-prints, arXiv:astro-ph/0508053

Bailin, J., Power, C., Gibson, B. K. & Steinmetz, M., 2005: How Concentrated Are The Haloes Of Low Surface Brightness Galaxies In The Cold Dark Matter Model; ArXiv Astrophysics e-prints, arXiv:astro-ph/0502231

Becker, R. H., White, R. L. & Helfand, D. J., 1995: The FIRST Survey: Faint Images of the Radio Sky at Twenty Centimeters; ApJ 450, 559+

Bertin, E. & Arnouts, S., 1996: SExtractor: Software for source extraction.; A&AS 117, 393–404

Blanton, M., 2004: Discussion at workshop: "Science with LSST and Other Large Surveys"; University of Washington, Seattle, 20.-22.9.2004

Blanton, M., Lupton, R., Schlegel, D., Strauss, M., Brinkmann, J., Fukugita, M. & Loveday, J., 2005: The properties and luminosity function of extremely low luminosity galaxies; ArXiv Astrophysics e-prints, arXiv:astro-ph/0410164 v2

Boissier, S., Monnier Ragaigne, D., van Driel, W., Balkowski, C. & Prantzos, N., 2003: From spirals to low surface brightness galaxies; ApSS 284, 913–916

Bothun, G., Impey, C. & McGaugh, S., 1997: Low-Surface-Brightness Galaxies: Hidden Galaxies Revealed; PASP 109, 745–758

Bothun, G. D., Impey, C. D. & Malin, D. F., 1991: Extremely low surface brightness galaxies in the Fornax Cluster - Properties, stability, and luminosity fluctuations; ApJ 376, 404–423

Bothun, G. D., Impey, C. D., Malin, D. F. & Mould, J. R., 1987: Discovery of a huge low-surface-brightness galaxy - A protodisk galaxy at low redshift?; AJ 94, 23–29

Bothun, G. D., Schombert, J. M., Impey, C. D. & Schneider, S. E., 1990: Discovery of a second giant low surface brightness galaxy - Further confirmation of slowly evolving disk galaxies; ApJ 360, 427–435

Bothun, G. D., Schombert, J. M., Impey, C. D., Sprayberry, D. & McGaugh, S. S., 1993: The small scale environment of low surface brightness disk galaxies; AJ 106, 530–547

Bowen, D. V., Tripp, T. M. & Jenkins, E. B., 2001: Damped Lyα Absorption from a Nearby Low Surface Brightness Galaxy; AJ 121, 1456–1460

Braine, J., Herpin, F. & Radford, S. J. E., 2000: Deep search for CO emission in the Low Surface Brightness galaxy Malin 1; AAP 358, 494–498

Bullock, J. S., Dekel, A., Kolatt, T. S., Kravtsov, A. V., Klypin, A. A., Porciani, C. & Primack, J. R., 2001: A Universal Angular Momentum Profile for Galactic Halos; ApJ 555, 240–257

Burkert, A., 1995: The Structure of Dark Matter Halos in Dwarf Galaxies; ApJ-Letter 447, L25+

Cabanela, J., Womack, M. & Dickey, J. M., 2001: Deep CO Observations of Four LSBs; Bulletin of the American Astronomical Society 33, 1315+

Chakravarti, I. M., Laha, R. G. & Roy, J., 1967: *Handbook of Methods of Applied Statistics, Volume I*; John Wiley and Sons

Cole, S., Lacey, C. G., Baugh, C. M. & Frenk, C. S., 2000: Hierarchical galaxy formation; MNRAS 319, 168–204

Coles, P., 1993: Galaxy formation with a local bias; MNRAS 262, 1065–1075

Colless, M., Dalton, G., Maddox, S. & 26 co-authors, 2001: The 2dF Galaxy Redshift Survey: spectra and redshifts; MNRAS 328, 1039–1063

Condon, J. J., Cotton, W. D., Yin, Q. F., Shupe, D. L., Storrie-Lombardi, L. J., Helou, G., Soifer, B. T. & Werner, M. W., 2003: The SIRTF First-Look Survey. I. VLA Image and Source Catalog; AJ 125, 2411–2426

Cox, A., 2000: *Allens's Astrophysical Quantities*; ed., 2000, Springer Verlag, ISBN 0–387–98746–0

Dalcanton, J., Spergel, D. N., Gunn, J. E., Schmidt, M. & Schneider, D. P., 1997a: The Number Density of Low-Surface Brightness Galaxies with $23 < \mu_0 < 25$ V mag/arcsec^2; AJ 114, 2178+

Dalcanton, J. J., Spergel, D. N. & Summers, F. J., 1997b: The Formation of Disk Galaxies; ApJ 482, 659+

Davies, J. I., 1990: Visibility and the selection of galaxies; MNRAS 244, 8–24

Davies, J. I., Phillipps, S., Cawson, M. G. M., Disney, M. J. & Kibblewhite, E. J., 1988: Low surface brightness galaxies in the Fornax Cluster - Automated galaxy surface photometry. III; MNRAS 232, 239–258

Davies, J. I., Phillipps, S. & Disney, M. J., 1990: B and R CCD surface photometry of selected low surface brightness galaxies in the region of the Fornax cluster; MNRAS 244, 385–407

de Blok, W. J. G., 2004: CDM in LSB Galaxies: Toward the Optimal Halo Profile; in *IAU Symposium*; S. 69+

de Blok, W. J. G. & Bosma, A., 2002: High-resolution rotation curves of low surface brightness galaxies; AAP 385, 816–846

de Blok, W. J. G., Bosma, A. & McGaugh, S., 2003: Simulating observations of dark matter dominated galaxies: towards the optimal halo profile; MNRAS 340, 657–678

de Blok, W. J. G. & McGaugh, S. S., 1997: The dark and visible matter content of low surface brightness disc galaxies; MNRAS 290, 533–552

de Blok, W. J. G., McGaugh, S. S. & Rubin, V. C., 2001: High-Resolution Rotation Curves of Low Surface Brightness Galaxies. II. Mass Models; AJ 122, 2396–2427

de Blok, W. J. G. & van der Hulst, J. M., 1998: Star formation and the interstellar medium in low surface brightness galaxies. II. Deep CO observations of low surface brightness disk galaxies; AAP 336, 49–56

de Blok, W. J. G., van der Hulst, J. M. & Bothun, G. D., 1995: Surface photometry of low surface brightness galaxies; MNRAS 274, 235–255

de Jong, R. S., 1996: Near-infrared and optical broadband surface photometry of 86 face-on disk dominated galaxies. III. The statistics of the disk and bulge parameters.; A&A 313, 45–64

Disney, M. J., 1976: Visibility of galaxies; Nature 263, 573–575

Doroshkevich, A. G., Fong, R., Gottlöber, S., Mücket, J. P. & Müller, V., 1997: The formation and evolution of large- and superlarge-scale structure in the Universe - II. N-body simulations; MNRAS 284, 633–654

Duschl, W. J., 1989: Accretion disk models with a self-consistent viscosity parameter alpha in convective zones; A&A 225, 105–111

Duschl, W. J., Strittmatter, P. A. & Biermann, P. L., 2000: A note on hydrodynamic viscosity and selfgravitation in accretion disks; A&A 357, 1123–1132

Fan, X., Narayanan, V. K., Lupton, R. H. & 31 co-authors, 2001: A Survey of z>5.8 Quasars in the Sloan Digital Sky Survey. I. Discovery of Three New Quasars and the Spatial Density of Luminous Quasars at z~6; AJ 122, 2833–2849

Fath, E. A., 1908: Bulletin Number 149 - The spectra of some spiral nebulae and globular star clusters.; Lick Observatory Bulletin 5, 71–77

Fioc, M. & Rocca-Volmerange, B., 1997: PEGASE: a UV to NIR spectral evolution model of galaxies. Application to the calibration of bright galaxy counts.; A&A 326, 950–962

Fish, R. A., 1964: A Mass-Potential Relationship in Elliptical Galaxies and Some Inferences Concerning the Formation and Evolution of Galaxies.; ApJ 139, 284+

Fisher, J. R. & Tully, R. B., 1981: Neutral hydrogen observations of a large sample of galaxies; ApJS 47, 139–200

Flores, R. A. & Primack, J. R., 1994: Observational and theoretical constraints on singular dark matter halos; ApJ-Letter 427, L1–L4

Freeman, K. C., 1970: On the Disks of Spiral and so Galaxies; ApJ 160, 811+

Fuchs, B., 2002: Dim matter in the disks of low surface brightness galaxies; in *Dark matter in astro- and particle physics. Proceedings of the International Conference DARK 2002, Cape Town, South Africa, 4 - 9 February 2002. H. V. Klapdor-Kleingrothaus, R. D. Viollier (eds.). Physics and astronomy online library. Berlin: Springer, ISBN 3-540-44257-X, 2002, p. 28 - 35*; S. 28–35

Fukugita, M., Ichikawa, T., Gunn, J. E., Doi, M., Shimasaku, K. & Schneider, D. P., 1996: The Sloan Digital Sky Survey Photometric System; AJ 111, 1748+

Gebhardt, K., Bender, R., Bower, G., Dressler, A., Faber, S. M., Filippenko, A. V., Green, R., Grillmair, C., Ho, L. C., Kormendy, J., Lauer, T. R., Magorrian, J., Pinkney, J., Richstone, D. & Tremaine, S., 2000: A Relationship between Nuclear Black Hole Mass and Galaxy Velocity Dispersion; ApJ 539, L13–L16

Gomez, P., Nichol, R., Miller, C., Balogh, M., Goto, T., Zabludoff, A., Romer, K. & 10 co-authors, 2003: Galaxy Star Formation as a Function of Environment in the Early Data Release of the Sloan Digital Sky; ApJ 584, 210–227

Goto, T., 2005: Do star formation rates of galaxy clusters depend on mass? Blue/late-type fractions and total star formation rates of 115 galaxy clusters as a function of cluster virial mass; MNRAS 356, L6–L10

Gunn, J. E., Carr, M., Rockosi, C. & 37 co-authors, 1998: The Sloan Digital Sky Survey Photometric Camera; AJ 116, 3040–3081

Haberzettl, L. G., 2005: Star Formation History of Low Surface Brightness Galaxies in the HDF-S; PhD-thesis

Hanisch, R. J., 1989: STSDAS - the Space Telescope Science Data Analysis System; in *Data Analysis in Astronomy*; S. 129+

Hao, L., Strauss, M. A., Fan, X., Tremonti, C. A., Schlegel, D. J., Heckman, T. M., Kauffmann, G., Blanton, M. R., Gunn, J. E., Hall, P. B., Ivezić, Ž., Knapp, G. R., Krolik, J. H., Lupton, R. H., Richards, G. T., Schneider, D. P., Strateva, I. V., Zakamska, N. L., Brinkmann, J. & Szokoly, G. P., 2005a: Active Galactic Nuclei in the Sloan Digital Sky Survey. II. Emission-Line Luminosity Function; AJ 129, 1795–1808

Hao, L., Strauss, M. A., Tremonti, C. A., Schlegel, D. J., Heckman, T. M., Kauffmann, G., Blanton, M. R., Fan, X., Gunn, J. E., Hall, P. B., Ivezić, Ž., Knapp, G. R., Krolik, J. H., Lupton, R. H., Richards, G. T., Schneider, D. P., Strateva, I. V., Zakamska, N. L., Brinkmann, J., Brunner, R. J. & Szokoly, G. P., 2005b: Active Galactic Nuclei in the Sloan Digital Sky Survey. I. Sample Selection; AJ 129, 1783–1794

Høg, E., Fabricius, C., Makarov, V. V., Urban, S., Corbin, T., Wycoff, G., Bastian, U., Schwekendiek, P. & Wicenec, A., 2000: The Tycho-2 catalogue of the 2.5 million brightest stars; A&A 355, L27–L30

Hopkins, A. M., Miller, C. J., Nichol, R. C., Connolly, A. J., Bernardi, M., Gómez, P. L., Goto, T., Tremonti, C. A., Brinkmann, J., Ivezić, Ž. & Lamb, D. Q., 2003: Star Formation Rate Indicators in the Sloan Digital Sky Survey; ApJ 599, 971–991

Hubble, E. P., 1936: Realm of the Nebulae; Yale University Press

Huchra, J. P., Geller, M. J., Clemens, C. M., Tokarz, S. P. & Michel, A., 1993: The CfA Redshift Catalogue, Version Nov. 1993 (Huchra+, 1993); VizieR Online Data Catalog 7164, 0+

Humason, M. L., Mayall, N. U. & Sandage, A. R., 1956: Redshifts and magnitudes of extragalactic nebulae.; AJ 61, 97–162

Impey, C. & Bothun, G., 1989: Malin 1 - A quiescent disk galaxy; ApJ 341, 89–104

Impey, C. & Bothun, G., 1997: Low Surface Brightness Galaxies; ARAA 35, 267–307

Impey, C. D., Sprayberry, D., Irwin, M. J. & Bothun, G. D., 1996: Low Surface Brightness Galaxies in the Local Universe. I. The Catalog; ApJS 105, 209+

Kauffmann, G., Colberg, J. M., Diaferio, A. & White, S. D. M., 1999a: Clustering of galaxies in a hierarchical universe - I. Methods and results at z=0; MNRAS 303, 188–206

Kauffmann, G., Colberg, J. M., Diaferio, A. & White, S. D. M., 1999b: Clustering of galaxies in a hierarchical universe - II. Evolution to high redshift; MNRAS 307, 529–536

Kennicutt, R. C., 1989: The star formation law in galactic disks; ApJ 344, 685–703

Kennicutt, R. C., 1998a: Star Formation in Galaxies Along the Hubble Sequence; ARAA 36, 189–232

Kennicutt, R. C., 1998b: The Global Schmidt Law in Star-forming Galaxies; ApJ 498, 541+

Kennicutt, R. C., Armus, L., Bendo, G., Calzetti, D., Dale, D. A., Draine, B. T., Engelbracht, C. W., Gordon, K. D., Grauer, A. D., Helou, G., Hollenbach, D. J., Jarrett, T. H., Kewley, L. J., Leitherer, C., Li, A., Malhotra, S., Regan, M. W., Rieke, G. H., Rieke, M. J., Roussel, H., Smith, J.-D. T., Thornley, M. D. & Walter, F., 2003: SINGS: The SIRTF Nearby Galaxies Survey; PASP 115, 928–952

Kent, S. M. & Gunn, J. E., 1982: The dynamics of rich clusters of galaxies. I - The Coma cluster; AJ 87, 945–971

Kewley, L. J., Dopita, M. A., Sutherland, R. S., Heisler, C. A. & Trevena, J., 2001: Theoretical Modeling of Starburst Galaxies; ApJ 556, 121–140

King, I., 1962: Density Law in Spherical Stellar Systems.; AJ 67, 274–275

Knezek, P. & Schombert, J., 1993: Low Intensity AGN Activity in Giant LSB Galaxies; Bulletin of the American Astronomical Society 25, 1363+

Knezek, P. M., 1993: The stellar and gaseous content of massive low surface brightness disk galaxies; PhD-thesis

Krusch, E., 2003: Investigation of the dwarf galaxy population in Hickson Compact Groups; PhD-thesis

Lacey, C. & Silk, J., 1991: Tidally triggered galaxy formation. I - Evolution of the galaxy luminosity function; ApJ 381, 14–32

Lee, H.-c., Gibson, B. K., Flynn, C., Kawata, D. & Beasley, M. A., 2004: Is the initial mass function of low surface brightness galaxies dominated by low-mass stars?; MNRAS 353, 113–117

Leitherer, C., Schaerer, D., Goldader, J. D., Delgado, R. M. G., Robert, C., Kune, D. F., de Mello, D. F., Devost, D. & Heckman, T. M., 1999: Starburst99: Synthesis Models for Galaxies with Active Star Formation; ApJs 123, 3–40

Lupton, R. H., Gunn, J. E. & Szalay, A. S., 1999: A Modified Magnitude System that Produces Well-Behaved Magnitudes, Colors, and Errors Even for Low Signal-to-Noise Ratio Measurements; AJ 118, 1406–1410

Magorrian, J., Tremaine, S., Richstone, D., Bender, R., Bower, G., Dressler, A., Faber, S. M., Gebhardt, K., Green, R., Grillmair, C., Kormendy, J. & Lauer, T., 1998: The Demography of Massive Dark Objects in Galaxy Centers; AJ 115, 2285–2305

Malin, D. F., 1978: Photographic amplification of faint astronomical images; Nature 276, 591–593

Malmquist, K. G., 1922: Introduction of Malmquist Bias; journMedd. Lund. Astron. Obs. Ser. II, 32

Matsubara, T., Szalay, A. S. & Landy, S. D., 2000: Cosmological Parameters from the Eigenmode Analysis of the Las Campanas Redshift Survey; ApJL 535, L1–L4

Matthews, L. D. & Gao, Y., 2001: CO Detections of Edge-on Low Surface Brightness Galaxies; ApJL 549, L191–L194

Matthews, L. D., van Driel, W. & Monnier-Ragaigne, D., 2001a: H I observations of giant low surface brightness galaxies; AAP 365, 1–10

Matthews, L. D. & Wood, K., 2001: Modeling the Interstellar Medium of Low Surface Brightness Galaxies: Constraining Internal Extinction, Disk Color Gradients, and Intrinsic Rotation Curve Shapes; ApJ 548, 150–171

Matthews, L. D., Wood, K. & Gao, Y., 2001b: Dust and Molecular Gas in LSB Galaxies; in *ASP Conf. Ser. 230: Galaxy Disks and Disk Galaxies*; S. 381–382

Matthews, T. A. & Sandage, A. R., 1963: Optical Identification of 3c 48, 3c 196, and 3c 286 with Stellar Objects.; ApJ 138, 30+

McGaugh, S. S., 1994: Oxygen abundances in low surface brightness disk galaxies; ApJ 426, 135–149

McGaugh, S. S., Barker, M. K. & de Blok, W. J. G., 2003: A Limit on the Cosmological Mass Density and Power Spectrum from the Rotation Curves of Low Surface Brightness Galaxies; ApJ 584, 566–576

McGaugh, S. S. & Bothun, G. D., 1994: Structural characteristics and stellar composition of low surface brightness disk galaxies; AJ 107, 530–542

McGaugh, S. S., Bothun, G. D. & Schombert, J. M., 1995a: Galaxy Selection and the Surface Brightness Distribution; AJ 110, 573+

McGaugh, S. S. & de Blok, W. J. G., 1997: Gas Mass Fractions and the Evolution of Spiral Galaxies; ApJ 481, 689+

McGaugh, S. S., Rubin, V. C. & de Blok, W. J. G., 2001: High-Resolution Rotation Curves of Low Surface Brightness Galaxies. I. Data; AJ 122, 2381–2395

McGaugh, S. S., Schombert, J. M. & Bothun, G. D., 1995b: The Morphology of Low Surface Brightness Disk Galaxies; AJ 109, 2019+

Meurer, G. R., Hanish, D., Ferguson, H. C., Drinkwater, M., Webster, R. L., Meyer, M., Freeman, K. C., Kennicutt, R. C., Kilborn, V. A., Knezek, P., Koribalski, B., Staveley-Smith, L., Putman, M. & Smith, R. C., 2001: The Survey for Ionization in Neutral Gas Galaxies: Public Data Release; Bulletin of the American Astronomical Society 33, 1315+

Meusinger, H., Brunzendorf, J. & Krieg, R., 1999: LSB galaxies in the Perseus cluster region; in *Astronomische Gesellschaft Meeting Abstracts*; S. 101+

Milgrom, M., 1983: A modification of the Newtonian dynamics as a possible alternative to the hidden mass hypothesis; ApJ 270, 365–370

Miller, C. J., Nichol, R. C., Reichart, D., Wechsler, R. H., Evrard, A. E., Annis, J., McKay, T. A., Bahcall, N. A., Bernardi, M., Boehringer, H., Connolly, A. J., Goto, T., Kniazev, A., Lamb, D., Postman, M., Schneider, D. P., Sheth, R. K. & Voges, W., 2005: The C4 Clustering Algorithm: Clusters of Galaxies in the Sloan Digital Sky Survey; AJ 130, 968–1001

Minchin, R., Davies, J., Disney, M., Boyce, P., Garcia, D., Jordan, C., Kilborn, V., Lang, R., Roberts, S., Sabatini, S. & van Driel, W., 2005: A Dark Hydrogen Cloud in the Virgo Cluster; ApJL 622, L21–L24

Mo, H. J., Mao, S. & White, S. D. M., 1998: The formation of galactic discs; MNRAS 295, 319–336

Mo, H. J., McGaugh, S. S. & Bothun, G. D., 1994: Spatial distribution of low-surface-brightness galaxies; MNRAS 267, 129+

Morshidi-Esslinger, Z., Davies, J. I. & Smith, R. M., 1999: An automated search for nearby low-surface-brightness galaxies - I. The catalogue; MNRAS 304, 297–310

Navarro, J. F., Frenk, C. S. & White, S. D. M., 1996: The Structure of Cold Dark Matter Halos; ApJ 462, 563+

Navarro, J. F., Frenk, C. S. & White, S. D. M., 1997: A Universal Density Profile from Hierarchical Clustering; ApJ 490, 493+

Newberg, H. J. & Sloan Digital Sky Survey Collaboration, 2003: Sloan Extension for Galactic Underpinnings and Evolution (SEGUE); American Astronomical Society Meeting Abstracts 203, 0+

Nilson, P., 1973: *Uppsala general catalogue of galaxies*; Acta Universitatis Upsaliensis. Nova Acta Regiae Societatis Scientiarum Upsaliensis - Uppsala Astronomiska Observatoriums Annaler, Uppsala: Astronomiska Observatorium, 1973

Oke, J. B. & Sandage, A., 1968: Energy Distributions, K Corrections, and the Stebbins-Whitford Effect for Giant Elliptical Galaxies; ApJ 154, 21+

O'Neil, K., 2000a: The First Optical Spectroscopy of Red LSB Galaxies, and the Possible Discovery of the Largest Galaxy Known; Bulletin of the American Astronomical Society 32, 1501+

O'Neil, K., 2000b: The Morphology, Color, and Gas Content of Low Surface Brightness Galaxies; in *ASP Conf. Ser. 215: Cosmic Evolution and Galaxy Formation: Structure, Interactions, and Feedback*; S. 178+

O'Neil, K., 2001: Optical Spectroscopy of Red LSB Galaxies; Bulletin of the American Astronomical Society 33, 909+

O'Neil, K., 2002: The HI Content and Extent of Low Surface Brightness Galaxies: Could LSB Galaxies be Responsible for Damped Ly-α Absorption?; in *ASP Conf. Ser. 254: Extragalactic Gas at Low Redshift*; S. 202+

O'Neil, K., Andreon, S. & Cuillandre, J.-C., 2003: The z¡0.1 surface brightness distribution; AAP 399, L35–L38

O'Neil, K. & Bothun, G., 2000: The Space Density of Galaxies through $\mu_B(0)$=25.0 Magnitudes per Inverse Arcsecond Squared; ApJ 529, 811–815

O'Neil, K., Bothun, G., van Driel, W. & Monnier Ragaigne, D., 2004: A new H I catalog of Low Surface Brightness galaxies out to z = 0.1. Tripling the number of massive LSB galaxies known; AAP 428, 823–835

O'Neil, K., Bothun, G. D. & Cornell, M. E., 1997a: A Wide Field CCD Survey for Low Surface Brightness Galaxies:I.Data Acquisition, Description, and Initial Results; AJ 113, 1212+

O'Neil, K., Bothun, G. D., Schombert, J., Cornell, M. E. & Impey, C. D., 1997b: A Wide Field CCD Survey for Low Surface Brightness Galaxies.II.Color Distributions, Stellar Populations, and Missing Baryons; AJ 114, 2448+

O'Neil, K., Hofner, P. & Schinnerer, E., 2000: First Detection of CO in a Low Surface Brightness Galaxy; ApJL 545, L99–L102

Osterbrock, D. E., 1989: *Astrophysics of gaseous nebulae and active galactic nuclei*; Research supported by the University of California, John Simon Guggenheim Memorial Foundation, University of Minnesota, et al. Mill Valley, CA, University Science Books, 1989, 422 p.

Peebles, P. J. E., 1969: Origin of the Angular Momentum of Galaxies; ApJ 155, 393+

Peng, C. Y., Ho, L. C., Impey, C. D. & Rix, H.-W., 2002: Detailed Structural Decomposition of Galaxy Images; AJ 124, 266–293

Petrosian, V., 1976: Surface brightness and evolution of galaxies; ApJ 209, L1–L5

Phillipps, S., Disney, M. J., Kibblewhite, E. J. & Cawson, M. G. M., 1987: The surface brightness of 1550 galaxies in Fornax. II - Automated galaxy surface photometry; MNRAS 229, 505–515

Pickering, T. E. & Impey, C. D., 1995: Chemical Abundances in Giant LSB Disk Galaxies; Bulletin of the American Astronomical Society 27, 868+

Pickering, T. E., Impey, C. D., van Gorkom, J. H. & Bothun, G. D., 1997: Neutral Hydrogen Distributions and Kinematics of Giant Low Surface=20 Brightness Disk Galaxies; AJ 114, 1858+

Pickles, A. J., 1998: A Stellar Spectral Flux Library: 1150-25000 Å; PASP 110, 863–878

Pier, J. R., Munn, J. A., Hindsley, R. B., Hennessy, G. S., Kent, S. M., Lupton, R. H. & Ivezić, Ž., 2003: Astrometric Calibration of the Sloan Digital Sky Survey; AJ 125, 1559–1579

Reaves, G., 1956: Dwarf galaxies in the Virgo cluster.; AJ 61, 69–76

Reid, I. N., Brewer, C., Brucato, R. J., McKinley, W. R., Maury, A., Mendenhall, D., Mould, J. R., Mueller, J., Neugebauer, G., Phinney, J., Sargent, W. L. W., Schombert, J. & Thicksten, R., 1991: The second Palomar Sky Survey; PASP 103, 661–674

Romanishin, W., Krumm, N., Salpeter, E., Knapp, G., Strom, K. M. & Strom, S. E., 1982: Low surface brightness spiral galaxies. I - Neutral hydrogen content and location in the infrared Fisher-Tully diagram; ApJ 263, 94–100

Romanishin, W., Strom, K. M. & Strom, S. E., 1983: A study of low surface brightness spiral galaxies. II Optical surface photometry, infrared photometry, and H II region spectrophotometry; ApJS 53, 105–128

Rosenbaum, S. D. & Bomans, D. J., 2004: The environment of Low Surface Brightness galaxies; A&A 422, L5–L8

Roukema, B. F. & Peterson, B. A., 1995: A survey for low surface brightness galaxies in the field.; A&AS 109, 511–521

Rowan-Robinson, M., Saunders, W., Lawrence, A. & Leech, K., 1991: The QMW IRAS galaxy catalogue - A highly complete and reliable IRAS 60-micron galaxy catalogue; MNRAS 253, 485–495

Salpeter, E. E., 1955: The Luminosity Function and Stellar Evolution.; APJ 121, 161+

Sandage, A. & Binggeli, B., 1984: Studies of the Virgo cluster. III - A classification system and an illustrated atlas of Virgo cluster dwarf galaxies; AJ 89, 919–931

Schmidt, M., 1963: 3C 273: a star-like object with large red-shift.; Nature 197, 1040–1040

Schombert, J., 1998: Active Galactic Nucleus Activity in Giant, Low Surface Brightness Galaxies; AJ 116, 1650–1656

Schombert, J. M. & Bothun, G. D., 1988: A catalog of low-surface-brightness objects - Declination zone + 20 deg; AJ 95, 1389–1399

Schombert, J. M., Bothun, G. D., Impey, C. D. & Mundy, L. G., 1990: CO deficiency in LSB galaxies - Clues to their star-formation history; AJ 100, 1523–1531

Schombert, J. M., Bothun, G. D., Schneider, S. E. & McGaugh, S. S., 1992: A catalog of low surface brightness galaxies - List II; AJ 103, 1107–1133

Sersic, J. L., 1968: *Atlas de galaxias australes*; Cordoba, Argentina: Observatorio Astronomico, 1968

Seyfert, C. K., 1943: Nuclear Emission in Spiral Nebulae.; ApJ 97, 28+

Shapley, H., 1938: Two stellar systems of a new kind; Nature 142, 715+

Shectman, S. A., Landy, S. D., Oemler, A., Tucker, D. L., Lin, H., Kirshner, R. P. & Schechter, P. L., 1996: The Las Campanas Redshift Survey; ApJ 470, 172+

Smith, J. A., Tucker, D. L., Kent, S., Richmond, M. W., Fukugita, M., Ichikawa, T., Ichikawa, S.-i., Jorgensen, A. M., Uomoto, A., Gunn, J. E., Hamabe, M., Watanabe, M., Tolea, A., Henden, A., Annis, J., Pier, J. R., McKay, T. A., Brinkmann, J., Chen, B., Holtzman, J., Shimasaku, K. & York, D. G., 2002: The u'g'r'i'z' Standard-Star System; AJ 123, 2121–2144

Somerville, R. S., Lemson, G., Sigad, Y., Dekel, A., Kauffmann, G. & White, S. D. M., 2001: Non-linear stochastic galaxy biasing in cosmological simulations; MNRAS 320, 289–306

Sparke, L. S. & Gallagher, J. S., 2000: *Galaxies in the universe : an introduction*; Galaxies in the Universe, by Linda S. Sparke and John S. Gallagher, III, pp. 416. ISBN 0521592410. Cambridge, UK: Cambridge University Press, September 2000.

Spergel, D. N., Verde, L., Peiris, H. V., Komatsu, E., Nolta, M. R., Bennett, C. L., Halpern, M., Hinshaw, G., Jarosik, N., Kogut, A., Limon, M., Meyer, S. S., Page, L., Tucker, G. S., Weiland, J. L., Wollack, E. & Wright, E. L., 2003: First-Year Wilkinson Microwave Anisotropy Probe (WMAP) Observations: Determination of Cosmological Parameters; ApJS 148, 175–194

Sprayberry, D., 1994: Cosmological Implications of Low Surface Brightness Galaxies; PhD-thesis

Sprayberry, D., Impey, C. D., Bothun, G. D. & Irwin, M. J., 1995: Properties of the class of giant low surface brightness spiral galaxies; AJ 109, 558–571

Sprayberry, D., Impey, C. D., Irwin, M. J., McMahon, R. G. & Bothun, G. D., 1993: Discovery of a Third Giant Low Surface Brightness Disk Galaxy; ApJ 417, 114+

Springel, V., 2005: The cosmological simulation code GADGET-2; MNRAS 364, 1105–1134

Springel, V. & Hernquist, L., 2003: The history of star formation in a Λ cold dark matter universe; MNRAS 339, 312–334

Springel, V., White, S. D. M., Jenkins, A., Frenk, C. S., Yoshida, N., Gao, L., Navarro, J., Thacker, R., Croton, D., Helly, J., Peacock, J. A., Cole, S., Thomas, P., Couchman, H., Evrard, A., Colberg, J. & Pearce, F., 2005: Simulations of the formation, evolution and clustering of galaxies and quasars; Nature 435, 629–636

Stoughton, C., Lupton, R. H., Bernardi, M. & 188 co-authors, 2002: Sloan Digital Sky Survey: Early Data Release; AJ 123, 485–548

Strauss, M. A., Weinberg, D. H., Lupton, R. H. & 33 co-authors, 2002: Spectroscopic Target Selection in the Sloan Digital Sky Survey: The Main Galaxy Sample; AJ 124, 1810–1824

Swaters, R. A., Verheijen, M. A. W., Bershady, M. A. & Andersen, D. R., 2004: The Kinematics in the Cores of Low Surface Brightness Galaxies; in *IAU Symposium*; S. 77+

Tody, D., 1986: The IRAF Data Reduction and Analysis System; in *Instrumentation in astronomy VI; Proceedings of the Meeting, Tucson, AZ, Mar. 4-8, 1986. Part 2 (A87-36376 15-35). Bellingham, WA, Society of Photo-Optical Instrumentation Engineers, 1986, p. 733.*; S. 733+

Tolman, R. C., 1934: *Relativity, Thermodynamics, and Cosmology*; Relativity, Thermodynamics, and Cosmology, Oxford: Clarendon Press, 1934

Tonry, J. & Davis, M., 1979: A survey of galaxy redshifts. I - Data reduction techniques; AJ 84, 1511–1525

Turnshek, D. A., Rao, S., Nestor, D., Lane, W., Monier, E., Bergeron, J. & Smette, A., 2001: The z=0.0912 and z=0.2212 Damped Lyα Galaxies along the Sight Line toward the Quasar OI 363; ApJ 553, 288–298

Ulmer, M. P., Bernstein, G. M., Martin, D. R., Nichol, R. C., Pendleton, J. L. & Tyson, J. A., 1996: Low Surface Brightness Galaxies in the Core of the Coma Cluster; AJ 112, 2517+

van den Bergh, S., 2000: *The Galaxies of the Local Group*; The galaxies of the Local Group, by Sidney Van den Bergh. Published by Cambridge, UK: Cambridge University Press, 2000 Cambridge Astrophysics Series Series, vol no: 35, ISBN: 0521651816.

van den Hoek, L. B., de Blok, W. J. G., van der Hulst, J. M. & de Jong, T., 2000: The evolution of the stellar populations in low surface brightness galaxies; AAP 357, 397–413

van der Hulst, J. M., Skillman, E. D., Smith, T. R., Bothun, G. D., McGaugh, S. S. & de Blok, W. J. G., 1993: Star formation thresholds in Low Surface Brightness galaxies; AJ 106, 548–559

van Dokkum, P. G., 2001: Cosmic-Ray Rejection by Laplacian Edge Detection; PASP 113, 1420–1427

Waddell, P., Mannery, E. J., Gunn, J. E. & Kent, S. M., 1998: Sloan digital sky survey 2.5-meter telescope: optics; in *Proc. SPIE Vol. 3352, p. 742-753, Advanced Technology Optical/IR Telescopes VI, Larry M. Stepp; Ed.*; S. 742–753

White, S. D. M., Briel, U. G. & Henry, J. P., 1993: X-ray archaeology in the Coma cluster; MNRAS 261, L8–L12

White, S. D. M., Davis, M., Efstathiou, G. & Frenk, C. S., 1987a: Galaxy distribution in a cold dark matter universe; Nature 330, 451–453

White, S. D. M. & Frenk, C. S., 1991: Galaxy formation through hierarchical clustering; ApJ 379, 52–79

White, S. D. M., Frenk, C. S., Davis, M. & Efstathiou, G., 1987b: Clusters, filaments, and voids in a universe dominated by cold dark matter; ApJ 313, 505–516

Wolfe, A. M., Turnshek, D. A., Smith, H. E. & Cohen, R. D., 1986: Damped Lyman-alpha absorption by disk galaxies with large redshifts. I - The Lick survey; ApJS 61, 249–304

York, D. G., Adelman, J., Anderson, J. E. & 141 co-authors, 2000: The Sloan Digital Sky Survey: Technical Summary; AJ 120, 1579–1587

Zabludoff, A. I. & Mulchaey, J. S., 1998: Hierarchical Evolution in Poor Groups of Galaxies; ApJ 498, L5+

Zabludoff, A. I. & Zaritsky, D., 1995: A Collision of Subclusters in Abell 754; ApJ 447, L21+

Zacharias, N., Urban, S. E., Zacharias, M. I., Hall, D. M., Wycoff, G. L., Rafferty, T. J., Germain, M. E., Holdenried, E. R., Pohlman, J. W., Gauss, F. S., Monet, D. G. & Winter, L., 2000: The First US Naval Observatory CCD Astrograph Catalog; AJ 120, 2131–2147

Zackrisson, E., Bergvall, N. & Östlin, G., 2005: The stellar populations of the bluest low surface brightness galaxies; AAP 435, 29–41

Zaritsky, D. & Lorrimer, S. J., 1993: Low surface brightness galaxies and tidally triggered star formation; in *Evolution of Galaxies and their Environment*; S. 82–83

Zwicky, F., Herzog, E., Wild, P., Karpowicz, M. & Kowal, C. T., 1968: *Catalogue of galaxies and of clusters of galaxies*; Vols. 1-6, 1961-1968 (Pasadena: California Institute of Technology)

Acknowledgements

Curriculum Vitae

Personal data:

Name	Stefan <u>Dominik</u> Rosenbaum
Day of birth	08/20/1975
Place of birth	Neuwied, Germany
Nationality	German
Address	Buchenstr. 6, 56727 Mayen, Germany

Education:

08/1982 - 06/1986	primary school: Grundschule Hinter Burg, Mayen
08/1986 - 06/1995	secondary school: Megina-Gymnasium, Mayen
Foreign Languages	English, Latin
06/23/1995	university qualification: Abitur

Alternative Civilian Service:

09/1995 - 09/1996	at the rescue station of the German Red Cross in Brodenbach, Germany with education to a certified Emergency Medical Technician (EMT)
01/26/1996	statutory audit for EMT

Studies:

10/1996 - 09/2002	study of physics at the Rheinische Friedrich-Wilhelms-Universität Bonn
09/04/2002	degree completed with diploma
since 02/2003	PhD student of physics at the Ruhr-Universität Bochum

Employment:

10/2000 - 02/2001 and 10/2001 - 02/2002	research assistant at the Institut für Strahlen- und Kernphysik, Bonn as tutor for the practical courses
06/2002 - 09/2002	research assistant at the Physikalisches Institut, Universität Bonn as tutor for the exercises of the lecture Exp.-Physik II
02/2003 - 01/2006	graduate scholarship holder of the GRK 787 at the Astronomisches Institut der Ruhr-Universität Bochum

Erklärung

Hiermit versichere ich, dass ich die vorliegende Dissertation eigenständig und ohne andere als die angegebenen Hilfsmittel angefertigt und die Zitate kenntlich gemacht habe.

Dominik Rosenbaum   Bochum, den 13.01.2006